

MODELLING OF DROPWISE CONDENSATION ON A CYLINDRICAL
SURFACE INCLUDING THE SWEEPING EFFECT

A THESIS SUBMITTED TO
THE GRADUATE SCHOOL OF NATURAL AND APPLIED SCIENCES
OF
MIDDLE EAST TECHNICAL UNIVERSITY

BY

TALİP EMRAH ÖZLER

IN PARTIAL FULFILLMENT OF THE REQUIREMENTS
FOR
THE DEGREE OF MASTER OF SCIENCE
IN
MECHANICAL ENGINEERING

MAY 2007

Approval of the Graduate School of Natural and Applied Sciences

Prof. Dr. Canan ÖZGEN
Director

I certify that this thesis satisfies all the requirements as a thesis for the degree of Master of Science.

Prof. Dr. Kemal İDER
Head of the Department

This is to certify that we have read this thesis and that in our opinion it is fully adequate, in scope and quality, as a thesis for the degree of Master of Science.

Assoc. Prof. Dr. Cemil YAMALI
Supervisor

Examining Committee Members

Prof. Dr. Kahraman ALBAYRAK (METU, ME) _____

Assoc. Prof. Dr. Cemil YAMALI (METU, ME) _____

Asst. Prof. Dr. İlker TARI (METU, ME) _____

Asst. Prof. Dr. Tahsin ÇETİNKAYA (METU, ME) _____

Prof. Dr. Ercan ATAER (GAZİ UNV., ME) _____

I here declare that all information in this document has been obtained and presented in accordance with academic rules and ethical conduct. I also declare that, as required by these rules and conduct, I have fully cited and referenced all material and the results that are not original to this work.

TALİP EMRAH ÖZLER

Signature:

ABSTRACT

MODELLING OF DROPWISE CONDENSATION ON A CYLINDRICAL SURFACE INCLUDING THE SWEEPING EFFECT

Özler, Talip Emrah

M.S., Department of Mechanical Engineering

Supervisor: Assoc. Prof. Dr. Cemil YAMALI

May 2007, 111 pages

The purpose of this study was to analyze the dropwise condensation on a cylindrical surface including the sweeping effect theoretically. For this purpose, first the problem of the equilibrium shape and departure size of drops on the outer surface of a cylinder was formulated. The equations of the surface of the drop were obtained by minimizing (for a given volume) the total energy of the drop which consists of surface and gravitational energy by using the techniques of variational calculus. The departure size of the droplets on a surface at varies angle of inclinations were also determined experimentally. Drop departure size is observed to decrease up to as the surface inclination was decreased up to 90 degree and then it increased up to 180 degree.

Mean base heat flux, drop departure rate, sweeping frequency, fraction of covered area, sweeping period, local heat flux and average heat flux for the dropwise condensation on a cylindrical surface including the sweeping effect is formulated and the resulting integral equation was solved by using the finite difference techniques.

The results show that drop departure rate and sweeping frequency was strongly affected by the angular position and reached asymptotic value at large angular positions.

Comparing the results of the average heat flux values at different diameters show that at larger diameters the average heat flux becomes larger. This is due to the increased sweeping effect at larger diameters.

Keywords: Departure Size, Dropwise Condensation, Average Heat Flux, Departure Rate, Sweeping Effect

ÖZ

DAMLACIĞIN SÜPÜRME ETKİSİ DİKKATE ALINARAK DAMLACIK YOĞUŞMASININ SİLİNDİR YÜZEY ÜZERİNDE MODELLENMESİ

Özler, Talip Emrah

Yüksek Lisans, Makina Mühendisliği Bölümü

Tez Yöneticisi: Doç. Dr. Cemil YAMALI

Mayıs 2007, 111 Sayfa

Bu çalışmanın amacı damlacığın süpürme etkisini dikkate alarak silindir yüzey üzerindeki Damlacık Yoğuşması'nı analiz etmektir. Bu amaç doğrultusunda, silindirin dış yüzeyindeki iki boyutlu damlacık yoğuşmasına tabi olan damlaların yüzeyden kopma (harekete geçme) boyutlarının ve denge durumundaki şekillerinin problemi tanımlanmıştır. Variational Calculus metodu kullanılarak damlacık yüzeyinin denklemleri, yüzey ve yer çekimi enerjisini içine alan toplam enerjinin minimize edilmesiyle (belirlenmiş bir hacimde) elde edilmiştir. Değişik açılarda yüzeydeki damlacıkların yüzeyden kopma boyutları deneysel olarak belirlenmiştir. Damlacığın yüzeyden kopma boyutu yüzey eğimi 90° olana kadar azalış göstermekte, daha sonra 180° 'ye kadar artış göstermektedir.

Silindir yüzeydeki damlacık yoğuşmasında süpürme etkisi dikkate alınarak ortalama temel ısı akısı, damlacığın yüzeyden kopma sıklığı, damlacığın süpürme sıklığı, damlacığın kapladığı alan, local ısı akısı ve ortalama ısı akısı formüle edilmiş, bulunan integraller finite difference method kullanılarak çözülmüştür.

Farklı silindir aplarında ortalama ısı akı deęerlerinin sonuları karşılařtırıldıęında yksek aplarda ortalama ısı akısı daha fazla olmaktadır. Bu yksek aplarda sprme etkisinin artmasından kaynaklanmaktadır.

Sonular, damlacık kopma sıklıęının ve sprme sıklıęının aısal pozisyondan gl bir Őekilde etkilendięini ve yksek aısal pozisyonlarda asimptotik bir deęere ulařtıęını gstermektedir.

Anahtar Kelimeler: Yzeyden Kopma Boyutu, Damlacık Yoęuřması, Ortalama Isı Akısı, Sprme Sıklıęı, Sprme Etkisi

To my parents,
Who always support me in all aspects of my life,
And to Miss. Özgül ACAR,

ACKNOWLEDGMENTS

I would like to express my sincere appreciation to Assoc. Prof. Dr. Cemil Yamalı for his guidance, support, understating and valuable contributions throughout the research. I am also grateful to the jury members for their valuable contributions.

I am thankful to my parents, not only because they supported me throughout my education life, as well as during this study, but also they provided me good living and working conditions.

I am also thankful to my brother. I completed two master programs at METU (Engineering Management and Mechanical Engineering). He supported me all the time. Really, my educational life is a real project of my brother.

Finally, if my girlfriend hasn't supported me, it was not possible to complete this master program. She helped me when I was distressed, hence I would like to give the biggest thanks to her whose name is Özgül ACAR.

TABLE OF CONTENTS

ABSTRACT	iv
ÖZ	vi
ACKNOWLEDGMENTS	ix
TABLE OF CONTENTS	x
LIST OF TABLES	xii
LIST OF FIGURES	xiii
NOMENCLATURE.....	xvii
CHAPTER	
1. INTRODUCTION	1
1.1 Condensation.....	1
1.1.1 Filmwise Condensation.....	3
1.1.2 Dropwise Condensation	4
2. LITARATURE REVIEW	6
2.1 Drop size Distribution.....	8
2.2 Heat Conduction Through The Droplets.....	11
2.3 Departure Size.....	13
2.4 Influence of Non-condensable Gases on Dropwise Condensation	16
2.5 Promoting Dropwise Condensation	18
2.6 The Effect of Sweeping on Dropwise Condensation	22
3. MATHEMATICAL ANALYSES	24
3.1 Calculating the Departure Size of Drops	25
3.1.1 Work of Adhesion Between The Liquid Drop And The Surrounding Vapor.....	29
3.1.2 Work of Adhesion between the Drop and the Solid Surface	31
3.1.3 Gravitational Potential Energy.....	32
3.1.4 Making the Variable Dimensionless	34

3.1.5 Finding the Equation for the Interface Profile of Droplet by Using Calculus of Variations	35
3.1.7 Finding Departure Size Experimentally.....	39
3.2 Calculating the Local Heat Transfer Including Sweeping Effect on the Cylindrical Surface	42
3.2.1 Conduction Through A Single Droplet.....	42
3.2.2 Heat Flux in Direct Condensation Range.....	44
3.2.3 Heat Flux in Coalescences Range.....	45
3.2.4 Heat Flux in Dropwise Condensation Including the Sweeping Effect	47
4. RESULTS AND DISCUSSION	63
4.1 Calculation of Departure Size	64
4.2 Mean Heat Flux through a Single Droplet	67
4.3 Drop Departure Rate	69
4.4 Drop Sweeping Frequency	79
4.5 Fraction of Condenser Area Covered By Falling Drops.....	82
4.6 Sweeping Period of The Falling Drops.....	84
4.7 Local Heat Flux.....	86
4.8 Average Heat Flux	89
5. CONCLUSIONS.....	91
6.1 Recommendations for Future Work.....	92
REFERENCES.....	93
APPENDICES	
A. MATCAD SOURCE PROGRAM I.....	100
B. MATCAD SOURCE PROGRAM II.....	105
C. MATCAD SOURCE PROGRAM III.....	107
D. MATCAD SOURCE PROGRAM IV.....	108

LIST OF TABLES

TABLES

Table 2.1 Steam side heat transfer coefficients [51].....	21
Table 4.1 Experimental results of departure size for cylindrical condenser surface at β (angle) between 0 and π	65
Table 4.2 The parameters of Eq. 3.28.....	67
Table 4.3 The mass of the droplets.....	71
Table 4.4 The velocity of the droplets.....	72
Table 4.5 Departure Size Heat Flux of the Drops.....	73
Table 4.6 The time elapsed between the sweepings (τ).....	75
Table 4.7 Drop Departure Rate at $\Delta T=10$ K.....	76
Table 4.8 Drop Departure Rate at $\Delta T=50$ K.....	78
Table 4.9 Drop Sweeping Frequency.....	80

LIST OF FIGURES

FIGURES

Fig. 1.1 Classification of Condensation Phenomena	2
Fig. 1.2 Schematic of filmwise condensation on a horizontal condenser tube	3
Fig 1.3 Photograph of filmwise condensation on plain horizontal surface [2]	4
Fig.1.4 Schematic of dropwise condensation on a horizontal condenser tube [2].....	5
Fig.1.5 Photograph of dropwise condensation on plain horizontal surface.	5
Fig. 2.1 Variation of time-averaged heat transfer coefficient with departing drop diameter [30].....	14
Fig. 2.2 Chronological order of the year for different techniques used for promoting dropwise condensation [2].....	22
Fig. 3.1 Coordinate system for drop on a flat surface.....	25
Fig. 3.2 Surface inclination is zero.	26
Fig. 3.3 Surface inclination is between 0 and $\pi/2$	26
Fig. 3.4 Surface inclination is between $\pi/2$ and π	27
Fig. 3.5 Surface inclination is π	28
Fig. 3.6 The surface of work of adhesion.....	29
Fig. 3.7 The centroid of the semicircle	30
Fig. 3.8 The surface of work of adhesion.....	31
Fig. 3.9 The height equation of drop.....	33

Fig. 3.10 Schematic of solution procedure.....	36
Fig. 3.11 Variation of departure size on the condenser surface.....	39
Fig. 3.12 Experimental Procedure.....	40
Fig. 3.13 Model for heat conduction through a droplet	44
Fig. 3.14 Model for Determining the Local Number of Departing Drops on a Vertical Surface	49
Fig. 3.15 Model for Sweeping Frequency [1].....	53
Fig. 3.16 Bare Surface.....	54
Fig. 3.17 The Drops Which is affected only by direct condensation.....	54
Fig. 3.18 Coalescences Range.....	55
Fig. 3.19 Drops Distribution Where some of them are about to depart.....	55
Fig. 3.20 Another Drops Distribution Where some of them are about to depart.....	55
Fig. 3.21 Variation of Maximum Drop Radius Between Two Sweepings	60
Fig. 4.1 An example of experimental calculation of departure size.....	64
Fig. 4.2 The profiles of droplets between 0° and 90°.....	65
Fig. 4.3 The profiles of droplets between 90° and 180°.....	66
Fig. 4.4 Variation of departure size with angle β	66
Fig. 4.5 Heat Flux versus Droplet Size at $\Delta T_t = 1$ °C.....	68
Fig. 4.6 Heat Flux versus Drop Radius at $\Delta T_t = 10$ °C	68
Fig.4.7 Heat Flux versus Droplet Size at $\Delta T_t = 100$ °C.....	69
Fig. 4.8 Method used to calculate the mass of the droplet.....	70
Fig. 4.9 Departure Size Heat Flux of Droplets.....	73
Fig 4.10 The equation of maximum drop size at $\Delta T = 10$ K	74
Fig 4.11 The equation of maximum drop size at $\Delta T = 50$ K	75
Fig 4.12 Drop Departure Rate at $\Delta T = 10$ K.....	77

Fig 4.13 Drop Departure Rate at $\Delta T=50$ K.....	78
Fig 4.14 Variation of drop departure rate with angular position at $D =2.3$ cm.....	79
Fig. 4.15 Variation of the Sweeping Period of Falling Drops with Different Surface Angles where the cylinder diameter is 2.3 cm.....	80
Fig. 4.16 Variation of the Sweeping Period of Falling Drops with Different Surface Angles where the cylinder diameter is 5 cm.....	81
Fig. 4.17 Variation of the Sweeping Period of Falling Drops with Different Surface Angles where the cylinder diameter is 10 cm.....	81
Fig. 4.18 Fraction of Condenser Area Covered by Falling Droplets Versus Angle where the cylinder diameter is 2,3 cm.....	82
Fig. 4.19 Fraction of Condenser Area Covered by Falling Droplets Versus Angle where the cylinder diameter is 5 cm.....	83
Fig. 4.20 Fraction of Condenser Area Covered by Falling Droplets Versus Angle where the cylinder diameter is 10 cm.....	83
Fig. 4.21 Fraction of Condenser Area Covered by Falling Droplets Versus Angle where the cylinder diameter is 10 cm.....	84
Fig. 4.22 Fraction of Condenser Area Covered by Falling Droplets Versus Angle where the cylinder diameter is 10 cm.....	85
Fig. 4.23 Fraction of Condenser Area Covered by Falling Droplets Versus Angle where the cylinder diameter is 10 cm.....	85
Fig 4.24 Local Heat Flux as a Function of Angle of Inclination for $D=2,3$ cm.....	86
Fig 4.25 Local Heat Flux as a Function of Angle of Inclination for $D=5$ cm.....	87
Fig 4.26 Local Heat Flux as a Function of Angle of Inclination for $D=10$ cm.....	87
Fig 4.27 Local Heat Flux as a Function of Angle of Inclination for all diameters at $\Delta T=10K$	88

Fig 4.28 Average Heat Flux as a Function of Angle of Inclination for all diameters at $\Delta T=10K$	89
Fig 4.29 Average Heat Flux as a Function of Angle of Inclination for all diameters at $\Delta T=50K$	89

NOMENCLATURE

		UNIT
D	Diameter	[m]
D_{dep}	Departure diameter of drop	[m]
f_{co}	Fraction of area occupied by droplets	
f_d	Departing frequency of the droplets	
f_s	Sweeping frequency of the droplets	
g	Acceleration due to the gravity	[m/s ²]
G	Gas constant	[J/kgK]
h	Height of the drop	[m]
h_e	Equivalent heat transfer coefficient for the liquid-vapor interface at the point of interest.	[W/(m ² K)]
h_{fg}	Latent heat of vaporization	[J/kg]
k	Thermal conductivity	[W/(m.K)]
L	Lenght of the drop	[m]
m_d	Mass of the drop	[kg]
n	Exponent used in Eq. 2.1	
p	Time period between two successive sweeping	
P_v^*	Saturation pressure corresponding to vapor temperature	[N/m ²]
q	Total heat transfer	
q''_{av}	Average heat flux over the condenser surface	
q''_{co}	Contribution of the coalescing droplets to dropwise condensation heat flux without sweeping	[W/m ²]
q_d	The total heat transfer rate through the droplet	[W]
q''_d	Mean heat flux over the solid surface contact area of the droplet	[W/m ²]
q''_{loc}	Local heat flux on the condenser surface	
q''_T	Dropwise condensation heat flux without sweeping	[W/m ²]

ΔP	Pressure difference across the interface at a particular location	
R_i	Radii of curvature at the interface	
r	Drop base radius	[m]
r^*	Nondimensional drop base radius	
r_{co}	Mean radius at which droplets start coalescing	[m]
r^*_{co}	Nondimensional mean drop radius at which drops start coalescing	
r_{dep}	Departure size of droplets	[m]
r_{max}	Maximum drop size in the distribution	[m]
R	The radius of curvature of the interface at the point of interest	[m]
t	Time	[sn]
ΔT_t	Difference between the vapor and the interface temperatures	[K]
T	Temperature	[K]
T_{sat}	Vapor saturation temperature	[K]
T_i	Temperature of liquid-vapor interface	[K]
T_s	Condenser surface temperature	[K]
U	Energy	
v	Velocity of the falling Droplet	[m/s]
V	Volume of drop	[m ³]
σ	Surface tension	[N/m]
θ	Contact angle	[rad]
β	Plate inclination	[degree]
ρ_l	Liquid density	[kg/m ³]
λ	Lagrange multiplier	
γ	Condensation coefficient	
w	Width	[m]
ξ	Height	[m]

Subscripts

co	Coalescence
dep	Departure
g	Gravity
I	Interface
l	Liquid
max	maximum
s	Solid
sat	Saturation
T	Total
v	Vapor
*	Dimensionless

CHAPTER 1

INTRODUCTION

1.1 Condensation

Condensation is a phase-change process in which vapor converts into liquid when the temperature of the vapor is reduced below the saturation temperature, corresponding to its pressure or on a solid surface whose temperature is below the saturation temperature of the vapor. In the latter case the vapor temperature may be either at saturation or superheated. But, in both condition, condensation requires a certain amount of subcooling. Everywhere in nature can be frequently encountered with condensation. Hence it is still one of the most important heat transfer processes in many energy conversion systems all over the world which are widely used in power generation, chemical process, air-conditioning, automotive and many other industries.

The latent heat forming the energy must be removed from the region of condensation during the phase change process, either by convection, diffusion or radiation. In the region of condensation taking place, a pressure decrease occurs, and as a result mass diffuses toward this region. The combined mass and heat transfer characterizes the condensation phenomena. The precise beginning of condensation has not been clearly identified, but it is believed that the process is initiated with a nucleus formed by a group of vapor molecules within the vapor bulk or on a solid surface. In this sense it is a nucleation phenomenon [1].

Generally, the condensation phenomenon can be classified as bulk condensation, and surface condensation.

Bulk condensation can occur in the bulk vapor, if vapor temperature falls below its saturation temperature. This phenomenon is also called homogeneous condensation and is facilitated by foreign particles such as dust. The formation of fog is an example of this type of condensation.

Surface condensation takes place on a subcooled solid surface when exposed to vapor. This type of condensation has an efficient heat transfer process and is utilized in various industrial applications. Because of its wide application in industry, it is the most important condensation type for engineering applications. Surface condensation is subdivided into two groups as condensation onto liquid surfaces and condensation onto solid surfaces. Solid surface condensation occurs on a solid surface at low temperatures. For form of the liquid phase on the solid surface, we can distinguish surface condensation as dropwise condensation and filmwise condensation. Depending upon the characteristics of the condenser surface employed, either one or both of these can take place on a surface.

The classification of condensation phenomena as mentioned above is illustrated in Fig. 1.1.

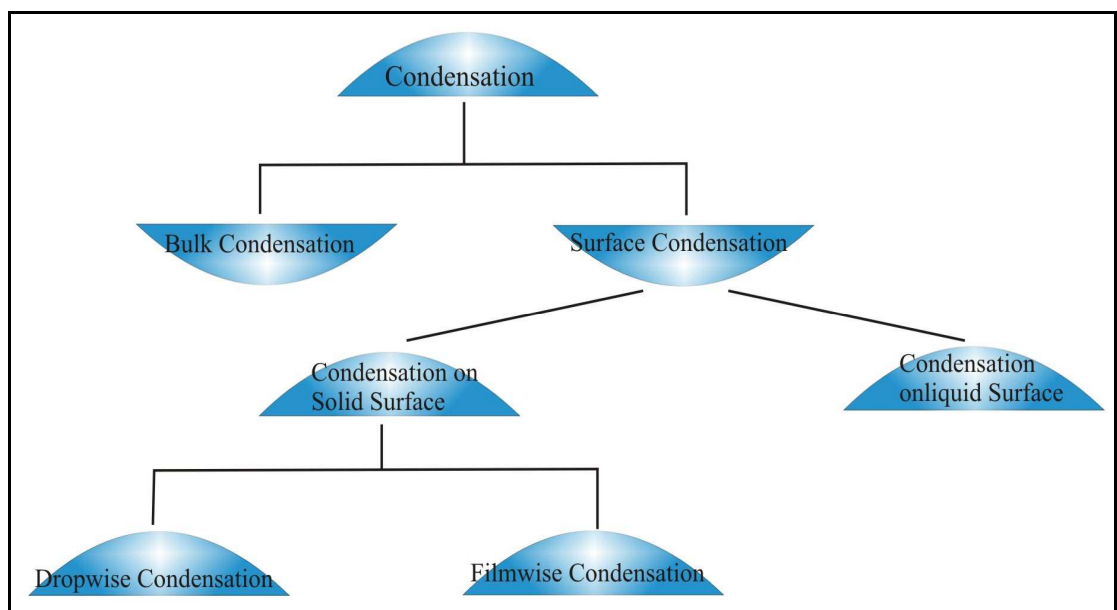


Fig. 1.1 Classification of Condensation Phenomena

1.1.1 Filmwise Condensation

Filmwise condensation occurs when the condensate wets the surface and forms a liquid film on the surface. Liquid film on the surface slides down under the influence of gravity. The filmwise condensation is illustrated on a smooth horizontal tube in Fig. 1.2 [2]. Continuous film of liquid flows around the tube due to both gravity and vapor shear forces. The film is thinnest at the top of the tube and grows to its thickest at the bottom of the tube.

The physical processes of filmwise condensation is relatively simple, hence it is convenient to analytical treatment. The first attempt to analyze and to formulate the filmwise condensation was made by Nusselt [2]. And Nusselt [2] made some assumptions as the flow of the condensate in the film is laminar, the fluid properties are constant, sub-cooling of the condensate may be neglected, momentum changes through the film are negligible, the vapor is stationary and exerts no drag on the downward motion of the condensate, heat transfer is by conduction only surface is isothermal and as a result derived a set of correlations for different tube configurations.

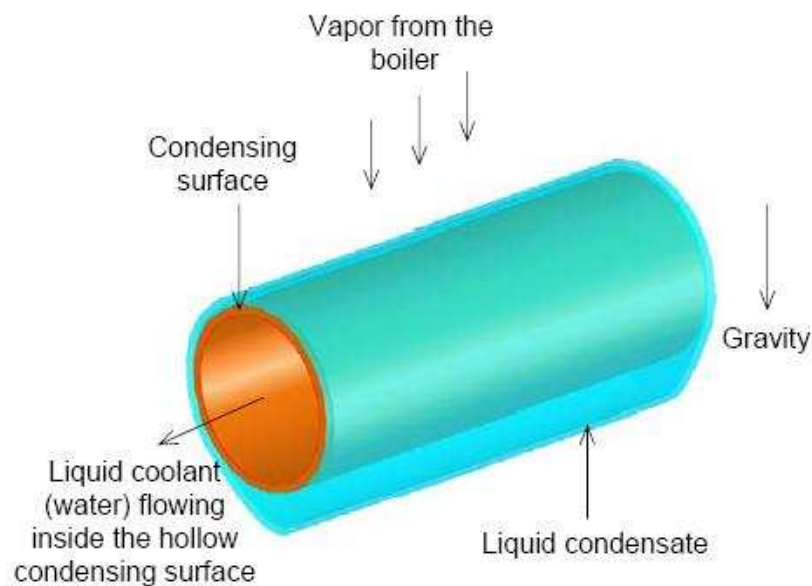


Fig. 1.2 Schematic of filmwise condensation on a horizontal condenser tube

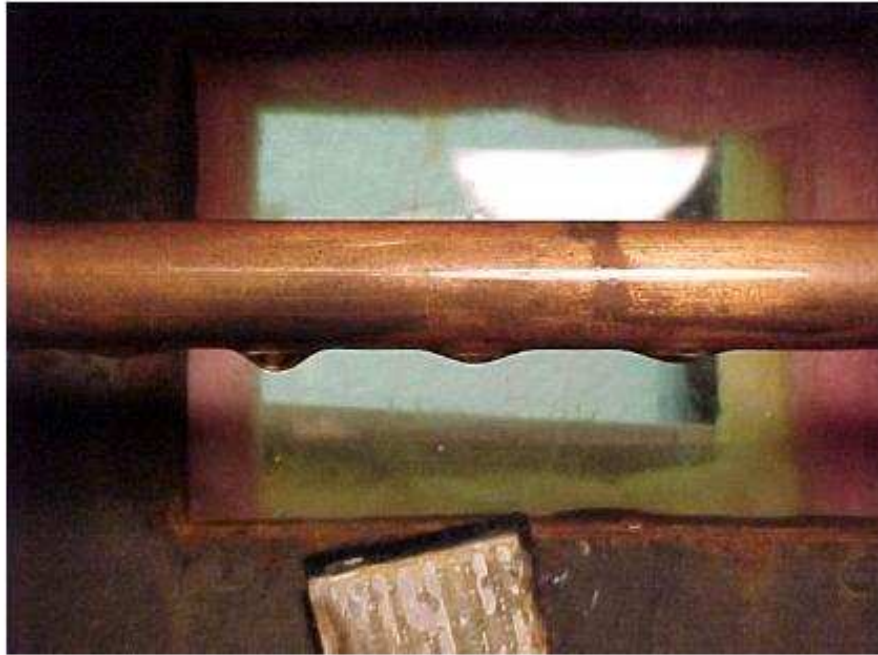


Fig 1.3 Photograph of filmwise condensation on plain horizontal surface [2]

1.1.2 Dropwise Condensation

Dropwise condensation takes place when the liquid condensate does not wet the solid surface and the condensed vapor forms droplets on the surface instead of a continuous film, countless droplets of varying diameter cover the condensing surface as shown in Fig. 1.4. These drops grow by direct condensation and by coalescences between droplets until reached certain size. The drops then leave the surface by the action of body forces and/or vapor shear.

There is no liquid film in this case to resist heat transfer. Because of that situation, heat transfer coefficient with dropwise condensation is an order of magnitude larger than with filmwise condensation. Therefore, in heat transfer applications, dropwise condensation is preferred. Hence, people have tried to achieve sustainable dropwise condensation by using various types of vapor additives and surface coatings. But until now, it couldn't have been possible to sustain dropwise

condensation. To be efficient on condensers, the filmwise condensation must take place entirely.

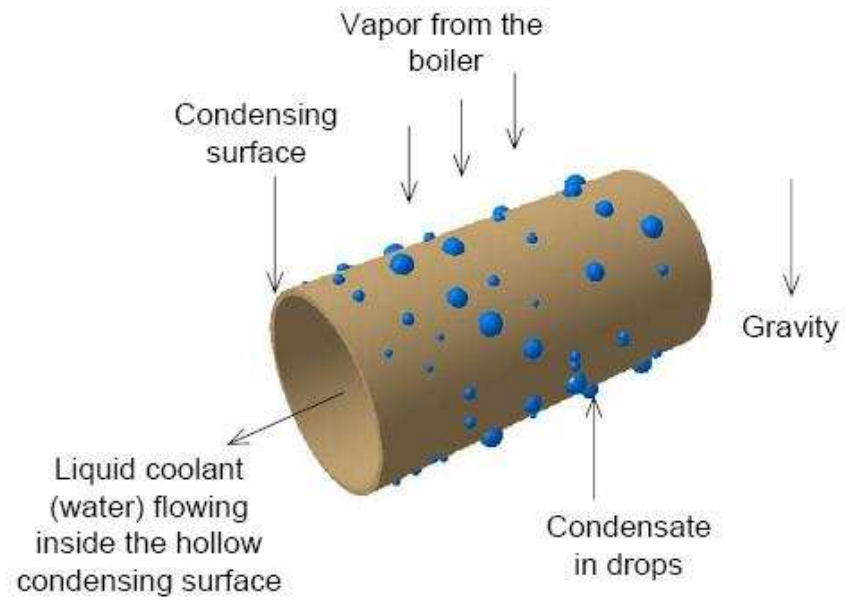


Fig.1.4 Schematic of dropwise condensation on a horizontal condenser tube [2].

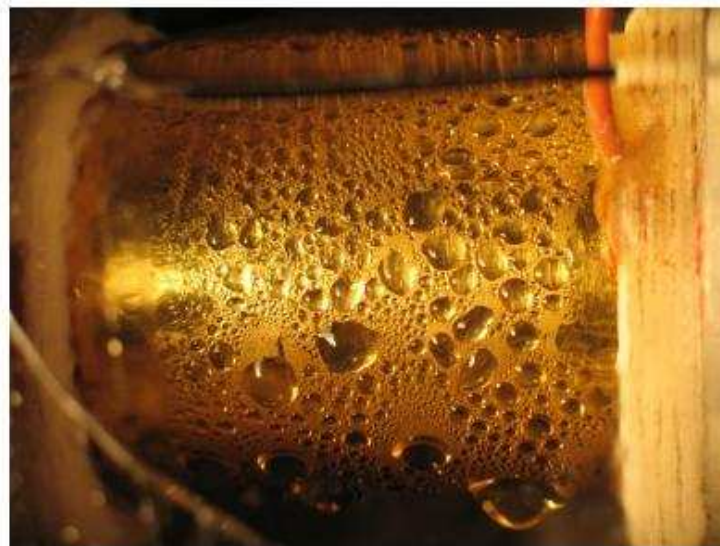


Fig.1.5 Photograph of dropwise condensation on plain horizontal surface.

CHAPTER 2

LITARATURE REVIEW

In this section the review of literature about dropwise condensation will be presented. This review is mainly based on the mechanism of dropwise condensation, formation of droplets, drop size distribution, heat conduction through the droplets, departure size, effects of non-condensable gases, promoting dropwise condensation especially by gold coating and the effect of sweeping.

Dropwise condensation was first recognized by Schmidt [3] in 1930. By this article, it is found that the heat transfer coefficient with dropwise condensation is substantially higher than with filmwise condensation. By the way, the interest on dropwise condensation is launched.

Basically, the dropwise condensation is a cyclic process which begins with the nucleation of droplet, continuous with growth and seemingly random coalescences and than ends with drop departing and sweeping the front path on surface. Hence, understanding of mechanisms of dropwise condensation requires knowledge of how the drops form and grow. Relating to the mechanism for the nucleation process the earliest models which is called film fracture model is presented by Jakob [4]. He defined that the process begins with formation of a very thin layer of condensate on the bare surface. Until forming a droplet, the film grows quickly from zero thickness to critical thickness. And new layer begins to grow in the bare area left by fractured film. Nevertheless, he described that the critical thickness of the film has a certain value which doesn't depend on the vapor and condensation conditions. This article was supported by Baer and McKelvey [5].

With the reevaporation process between droplets, Emmons [6] attempted to account large heat transfer rates with dropwise condensation. According to this process, condensing and reevaporating vapor molecules form a superheated vapor and when this superheated vapor contacts with the drop, condensation occurs. This reevaporation process model is modified by Erb and Thelen [7]. Both Emmons and Erb and Thelen attributed the large heat transfer rates in dropwise condensation in the vapor between droplets.

Diffusion mechanism is firstly proposed by Eucken [8]. In this mechanism, an absorbed layer of vapor molecules is assumed to exist on the bare surface between the droplets. All the above descriptions about mechanism of dropwise condensation are not based on the experimental results. The first experimental analysis is made by Welch and Westwater [9] to describe the mechanism of dropwise condensation. They made high speed motion pictures through a microscope. It was observed from the films that numerous coalescences took place between the extremely small droplets.

The first experimental evidence on the nucleation character of dropwise condensation was made by McCormick and Baer [10]. They formed a test which repeated continuously on a given surface where drop were condensed, then evaporated and condensed again. From this test, it is observed that after some repetitions drops appeared to grow from the same site.

Umur and Griffith [11] showed that a film does not grow on the surface as the surface is cooled to below the vapor temperature and also that condensate film can not form thicker than a monolayer. The film behind the drops rolling over the surface does not happen. Rolling drops leave behind them at most a monolayer. They concluded that no film greater than a monolayer in thickness exists on the area between the drops and that no net condensation takes place on this area. Also the results of Umur and Griffith's work don't support the film-fracture hypothesis, but this work doesn't prove that the area between the droplets is inactive.

Based on photographic study of dropwise condensation, McCormick and Westwater [12] confirmed that the dropwise condensation is a nucleation phenomenon. These

photographs showed that the droplets nucleate and grow, and then coalesce with neighboring large droplets. Also they observed that new drops occur on surface left by coalescing droplets.

As a result, it is proven from above articles that firstly primary drops occur at nucleation sites as a result of nucleation. Then they grow by direct condensation of vapor on various nucleation sites on the condensing surface and then coalescence starts between neighboring drops because of the small distance between neighboring drops by the action of the surface tension force. These coalesced drops continue to grow by again direct condensation and coalescing the neighboring drops. As the process continues, after coalescences, a largest drop present continues to increase until reaching the departure size. At that point, the largest drop starts to sweep and clear the surface.

2.1 Drop size Distribution

It is essential to know drop size distribution on condensing surface for the analytic formulation of the dropwise condensation phenomena. Because of obtaining a thorough understanding of the mechanism of dropwise condensation, it is necessary to be able to predict the heat transfer coefficient. To calculate the average heat transfer for the entire surface, the distribution of drops by sizes from the smallest primary drops to the largest departing drops must be known.

Some kinds of different theory were satisfied by the researchers for drop size distribution. Early attempts made by Fatica and Katz [13] and Sugawara and Michiyoshi [14] at calculating the heat transfer coefficient assumed all the drops on the surface were uniform in size and spacing. Wenzel [15] assumed that drops grow in uniform square array and that coalescences occur between four neighboring drops to form a larger drop in a new uniform square.

Graham and Griffith [16] and Kodali [17] proposed that surface area is much larger than the largest drops. Hence, they define the averaged size distribution over this entire area. They satisfied this definition by measurements of drop size distributions with random photographs and the effects of the sweeping process were included.

On the other hand, Tanaka [18] defined transient development to the drop size distribution, starting with a newly swept region and continuing to an arbitrary time corresponding to a maximum size. At this maximum size local distribution becomes a steady distribution when averaged over a large area, but does not incorporate the sweeping effect. This distribution is called as uniform size distribution in recent study. Tanaka studied both analytically and experimentally. In this study, the growth of droplets, transient formation and development of a drop size distribution on swept area was evaluated.

Glicksman and Rose [19] found a universal form a distribution function for large drops which grow primarily by coalescence with smaller drops. The predicted distribution is not valid for small drops which grow by direct condensation.

Gose, Mucciardi and Baer [20] and Tanasawa and Tachibana [21] have attempted to model the drop growth and coalescence process by computer. Both works modeled drops of entire range of sizes on a fixed area. The computer facility limited their investigations to artificially low site densities on the order of 10^4 sites per cm^2 .

P. Griffith and C. Graham [16] determined also the drop distributions at atmospheric and low pressure for dropwise condensation on a smooth vertical copper surface promoted with di-octadecyl disulphide by using Polaroid microscope camera at variety of magnifications. And nucleation site densities of 200×10^6 sites/ cm^2 were found.

Glicksman and Hunt [22] made the analytical studies. They divided the dropwise condensation cycle into a number of stages, starting with values of nucleation site density up to $10^8 / \text{cm}^2$, but they also omitted the effects of non-uniform conduction.

The study showed that the drop size distributions are quite different at very small sizes.

Le Fevre and Rose [23] proposed the Eq. 2.1 to calculate the fraction of surface covered by the droplets in the size range r to r_{\max} . They assumed a form for the time averaged distribution which had the correct behavior for the limiting cases of very large and very small drops. Except n , the below equation contains no parameters for the fluid or solid surface properties. Hence, this equation may be suitable only for the unsteady drop size distribution.

$$f_{co} \left(\frac{r}{r_{\max}} \right) = 1 - \left(\frac{r}{r_{\max}} \right)^n \quad (2.1)$$

Where:

- f_{co} : Fraction of area occupied by droplets
 r : Radius

This equation can also be used for a surface swept by departing droplets as well as for unswept surfaces. The effect of sweeping can be introduced into the equation above by choosing a suitable value for n . about Tanaka [24] made a theoretical study to show that the value of n is around 1/3 for the unsteady drop size distribution.

Maa and Wu [25] used the population balance model. By using the model, they derived the drop size distribution of small drops which grow mainly by direct condensation based on the assumption of steady size distribution. Later, Maa [26] also used the population balance model to derive a drop size distribution considering both small and large drops on the condensing surface. He solved the resulting equation numerically. The number of nucleation sites was varied so that the result would fit the experimental data.

And the recent investigation about drop size distribution was made by Wu, Yang and Yuan [27]. They made a theoretical study about dropwise condensation. They proposed that the condensing surface temperature varies periodically and the transient dropwise condensation occurs repeatedly on the tracks left by the departing drops. This confirms that heat transfer of a drop would be influenced by the neighbor drops. In the process, primary drops are formed at nucleation sites, and then coalescence occurs between neighboring drops with the drops growth. A new generation of drops is formed at sites exposed by coalescence. These again grow to be followed by a third generation and so on until a falling drop sweeps the entire field and the process restarts. They simulated random fractal model, drop size and spatial distributions. They find the photographs of dropwise condensation taken at different instants or in different scales are similar and a whole photograph can be obtained by enlarging properly a local photograph. This characteristic indicates that dropwise condensation appears self-similar, which is one of the most important features of fractals. In addition, drop spatial distribution also possesses randomness.

2.2 Heat Conduction Through The Droplets

As mentioned above that the heat transfer rates associated with dropwise condensation are more than 10 times larger than associated with filmwise condensation. Large heat transfer coefficients enable designers to achieve a specified heat transfer rate with a smaller surface area, and thus smaller condenser. Therefore, dropwise condensation is the preferred condensation in heat transfer applications.

We explained the importance of drop size distribution on heat transfer calculations. In order to calculate the heat flux with dropwise condensation, the drop size distribution and also the heat transfer through the individual droplets must be known. There are many kinds of variables which effect heat transfer through the dropwise condensation. Some of these variables are pressure, promoter, noncondensable gas concentration, surface orientation, departure radius vs.

There are some points which are shown below to be considered for complete analyses of the heat transfer through a droplet.

- Heat transfer through a drop
- Heat transfer through the substrate material
- The existence and the variation of the interfacial heat transfer coefficient at the vapor-liquid interface.
- Interference of heat conduction through a single droplet with the heat conduction in the neighboring droplets.

Since heat transfer is an important aspect of dropwise condensation, various attempts have been made to estimate and/or correlate the heat transfer rate in this process.

Fatica and Katz [13] were the first to propose a model to compute the rate of heat transfer by assuming that on a given area all drops are the same size, are uniformly spaced and grow by condensation at their surfaces. Their model is based on the assumption that at steady state, all drops have one representative diameter and one contact angle. The base of the drop is at a constant temperature (T_s), the liquid – vapor interface and bare condensing surface are taken to be at a different constant temperature (T_v), the difference between these two temperatures is the driving potential of condensation. The rate of conduction between two surfaces is computed graphically using an orthogonal mapping technique. Suguwara and Michiyoshi [14] proposed a model as an extension of Fatica and Katz's model. They attempted to take into account the periods when the surface is being swept off by a falling droplet, but their model didn't be successful.

P. Griffith and C. Graham [16] made an assumption that the spherical droplet surface is at the vapor temperature has been removed and the base of the droplet has a uniform temperature. An approach based on kinetic theory of gases was used to determine equivalent heat transfer rates and thus temperature along the boundary of the droplet. While eliminating the infinite heat flow rates at the edge of the droplet, too little weight to heat flow rates in the center of the droplet was given. In their study a solution has been obtained for a droplet of fixed diameter in the steady state temperature.

Sadhal and Plesset [28] studied effect of the thermal conductivity of the substrate material by solving for the temperature distribution in the substrate using the differential inequalities technique. In this study, a constant interfacial heat transfer coefficient on the drop surface was assumed, thus the results were not applicable for small droplets close to the critical size. And they also studied the effect of condenser material by solving the steady heat conduction equation for a geometry consisting of a droplet in the form of a spherical segment on a semi infinite solid.

Abu-Orabi [29] developed a population balance concept to predict the dropwise distribution for small drops that grow by direct condensation. All the resistances to heat transfer due to the drop (conduction through the drop, vapor-liquid interfacial resistance, and drop curvature) and due to the promoter layer and also the sweeping effect of falling drops are incorporated into the model. The total heat flux is calculated from the drop size distributions and the heat transfer rate through a single drop. The work in this paper proposed that to adequately calculate the heat flux, all the resistances to heat transfer due to the drop and the promoter layer have to be included.

2.3 Departure Size

The size at which drops are removed from the surface is called the departure size. The departure size is an important parameter in dropwise condensation. Because, decrease in the departure size results in an increase in heat transfer coefficients. And also the departure size is related to the drop size distribution and the sweeping rate.

Tower and Westwater [30] measured average heat transfer coefficient and the cycle time for a plate inclined at various angles. The experiments were conducted with total temperature differences in the approximate range of 2-3 °F. The departing drop diameter varied from 1900 to 2500 μ with cycle times from less than 1-1(1/2) sec, respectively. The results demonstrated that the calculated heat transfer coefficient decreases as the departing drop size is increased, as shown on Fig. 2.1.

NUMERICAL SIMULATION OF DROPWISE CONDENSATION

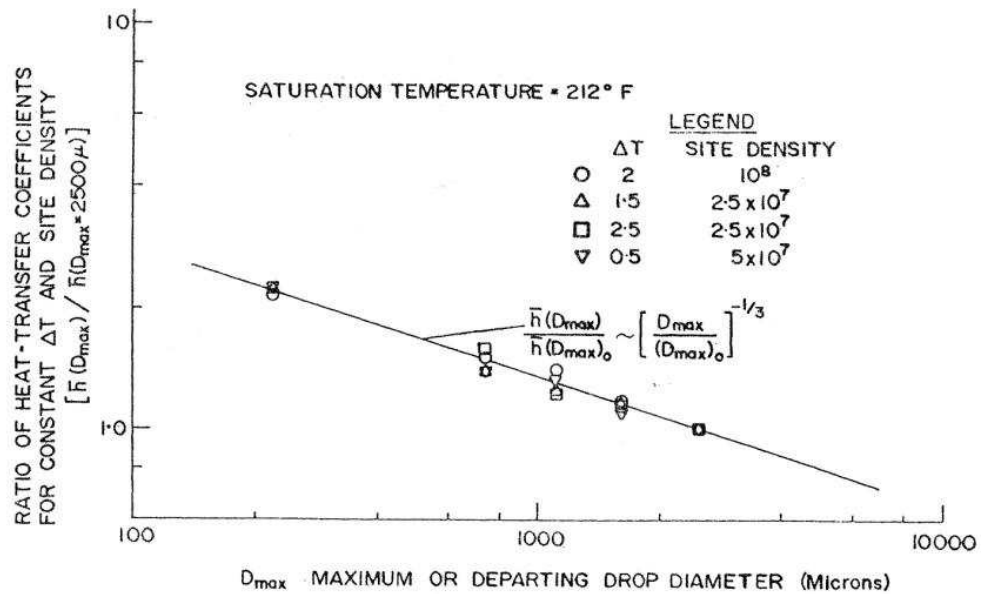


Fig. 2.1 Variation of time-averaged heat transfer coefficient with departing drop diameter [30].

Shape of the interface is defined by the solution of the general Laplace equation of capillarity described by Laplace [31]:

$$\Delta P = \sigma \left(\frac{1}{R_1} + \frac{1}{R_2} \right) \quad (2.2)$$

Where:

ΔP : Pressure difference across the interface at a particular location

σ : Interfacial tension

R_i : Radii of curvature at the interface

In a gravitational field, the pressure difference across a two-fluid interface will vary with position relative to the gravitational potential, and R_1 and R_2 must adjust

themselves appropriately. The number of different forms of Eq. 2.2 could be given, depending on the appropriate coordinate system.

In the case of solid surface, the balance of forces at the triple interface is commonly expressed in terms of an equilibrium contact angle, given by Young's Equation defined by Young [32]:

$$\sigma_{sv} - \sigma_{sl} = \sigma_{lv} \cos \theta \quad (2.3)$$

Where:

σ : Surface tension

θ : Contact angle

For homogeneous fluids and smooth solid surfaces all the surface tensions take on singular values. On the other hand, the θ should itself have a unique value.

Neumann and Good [33] demonstrated that contact angle hysteresis is due to surface heterogeneity, and is consistent with treating the contact angle as a thermodynamic variable.

A liquid drop resting on or suspended from a horizontal surface, a vapor/gas bubble under or above a horizontal surface, and a liquid/vapor interface in a vertical circular tube, all of them produce an interface with axial symmetry. Firstly, Bashfort and Adams [34] presented the computation of the shapes of these two dimensional drops in 1883. They obtained the results by laborious numerical integration. In 1970s, several other solution techniques applied to this problem. Hartfard and Hartley [35] used high speed computers to perform numerical integration required. Chesters [36] used perturbation technique for small drops or bubbles, while the stability of pendant drops was studied using variational methods by Pitts [37].

When the horizontal surface on which a drop rests is tilted, the shape is no longer axially-symmetric. Larkin [38] obtained the profiles and the definition of contact angle for interfaces on an inclined plane for this case by numerical integration.

From the balancing of surface forces by gravity, it is also possible to compute the critical angle of inclination of the surface at which a drop of given size would begin to slide. Integration of the two dimensional cylindrical form of the Laplace equation of capillarity was also used as a means of computing contact angles from precise measurements of meniscus rise on a flat plate by Neumann [39].

Pitts [40] used variation calculus to solve the profile of the two dimensional cylindrical drop hanging from the underside of a horizontal surface.

2.4 Influence of Non-condensable Gases on Dropwise Condensation

Many early investigators conducted their experiments without paying any attention to the presence of inert gases in their vapor of condensation. Some noticed their existence and called the attention to their influence. The systems which uses in industrial application usually contain some amount of non-condensable gases and also both filmwise condensation and dropwise condensation are affected by non-condensable gases. The source of this gas is usually air leakage in a vacuum apparatus, or dissolved gases in feed water.

The condensing vapor carries non-condensable gases to the condenser surface. Non-condensable gases accumulate and cause a reduction in heat transfer coefficient by reducing the vapor partial pressure. This reduction might be large enough to offset the gains of dropwise condensation. Therefore, the removal of non-condensable gases may become necessary to improve the heat transfer coefficient.

The first study to the effect of non-condensable gases on heat transfer was made by Othmer [41] who proposed that significant decrease in heat transfer coefficient

occurs with an increase in the amount of non-condensable gases present in filmwise condensation. Also Sparrow and Lin [42] demonstrated that the case of a filmwise condensation in the presence of non-condensable gases. A theory devised for predicting condensation heat transfer coefficient in the presence of non-condensable gases on a cooled vertical surface immersed in a large body of vapor containing non-condensable gases.

Some workers commented on the need for adequate venting of the condensing chamber. LeFevre and Rose [23] observed a sort of surface temperature fluctuations in their experimental work and they attributed this phenomenon to the presence of non-condensable gases in the condensing steam.

Hampson [43] investigated of the effect of non-condensable gases in the case of filmwise and dropwise condensations. He reported that the heat transfer steam-side coefficient decreases with the increase of steam-nitrogen concentration. He also reported that the presence of non-condensable gases may be expected to reduce the very large difference between dropwise and filmwise condensations. He obtained variable heat loadings by varying either the cooling water temperature or the cooling water velocity.

Potter, Tanner, Pope and West [44] found in the procedure of their investigation on the effect of non-condensable gases on dropwise condensation that the value of the steam-side heat transfer coefficient decreases with the increase of heat flux and the increase of non-condensable gases. They also reported that the reduction of the coefficient is greater with CO₂ than with N₂. They demonstrated that this reduction is more pronounced with the;

- a) Increase of the heat flux, and as a result of the increase in steam-gas concentration.
- b) With the decrease of steam velocity.

In their work the non-condensable gas was nitrogen and carbon dioxide.

McCormick and Westwater [45] have carried out some experiments to investigate the effect of non-condensable gases on dropwise condensation in the unsteady state conditions. They found that the heat flux decreases with the increase of steam-air concentrations. They investigated the effect for two steam-air concentrations namely 4400 ppm and 6500 ppm. They reported that the heat flux decreases remarkably with the slightest increase of the steam-air concentration.

2.5 Promoting Dropwise Condensation

Dropwise condensation has a significantly higher heat transfer coefficient than filmwise condensation. But, up to now there are still few literature reports on the industrial application of dropwise condensation. The reason is that filmwise condensation is a very common situation whereas dropwise condensation requires long life surface.

Dropwise condensation can be promoted by:

- a. Applying a suitable organic promoter to the condenser surface before operation.
- b. Injection of non-wetting agent periodically (or continuously) into the vapor
- c. Coating the condenser surface with a thin layer of an inorganic compound such as metal sulfide.
- d. Using a thin layer of special (noble) metal (such as gold, chromium. etc) or metal compounds
- e. Coating the condensing surface with a thin layer of an organic polymer.

For dropwise condensation the promoting types are given above, nevertheless, a good promoter should be long lasting, easy to apply, nontoxic and must be compatible with

the system in which it is used, i.e., it should not impair the proper functioning of the other parts of the system.

In laboratory, the first method was used to obtain dropwise condensation with organic promoter whose solution may be wiped, brushed, or painted on the surface, or it can be sprayed directly on the surface. Sometimes, the solution of organic promoter immersed into the surface. But in every case, the promoter chemisorbs on the substrate in question. It seems there is little evidence indicating that one method is more effective than another. It is proven that the absorbed layer obtained must be non-wetting as long as it is thicker than a few molecular layers. Hence, the amount of promoter needed to produce dropwise condensation is very minute. What matters is how long such a surface can sustain dropwise condensation. Tests carried out for a number of such substances. The most systematic study among them was done by Blackman, Dewar and Hampson [46, 47]. They obtained the necessary characteristics as detailed that the promoters should possess 37 compounds which are synthesized that would serve the purpose. All the compounds were used in condensation tests and it was proved that a compound called glycerol tri-[11 ethoxy (thiocarbonyl) thiundecanoate] performed the longest lifetime for maintaining perfect dropwise condensation.

Das, Kilty, Marto, Andeen, and Kumar [48] used self-assembled monolayer coating to promote dropwise condensation of steam on various tube substrates (such as, horizontal). They showed that SAM coating increased the condensation heat transfer coefficient by factors of 4 for gold coated aluminum, and by about 5 for copper, the durability of the bonding was not determined. As a result, they showed larger increase of dropwise condensation heat transfer coefficient compared with the filmwise condensation by using this technique.

The second method, injection of non-wetting agent periodically (or continuously) into the vapor is also a useful technique. The non-wetting property can be attained by replenishing the surface layer by injection of a suitable material into the steam entering the condensation steam. Blackman, Dewar and Hampson [46] reported that the minimum amount of promoter needed for injection method is about 0.002 – 0.1% of the vapor, though it depends on the substrate and the promoter. This amount will

not matter economically, if some fraction of it is recovered afterward. Problems with the injection method are possible contamination and corrosion of the surface.

For the method of coating the condenser surface with a thin layer of an inorganic compound such as metal sulfide, Erb and Thelen [49] presented the result of their systematic test. They noticed that sulfide of copper and silver exhibit extremely low solubility in water. The hydrophobic nature of these mineral sulfides has also been known. For a number of sulfated metal surfaces, tests were done. One of them is sulfated silver on mild steel showed perfect dropwise condensation. But, they found that silver surface had better dropwise condensation than the sulfated silver sample. By comparison of the position in the periodic table (Cu – Ag – Au), they predicted that gold also would produce dropwise condensation.

Thin layer of a noble metal (such as gold, chromium. etc) or metal compounds on surfaces produce dropwise condensation. It is proven by researchers that the most important one is gold-plated surfaces. Experiments carried out using gold-plated condenser surfaces without any organic promoter. Erb and Thelen [49] made lots of condensation studies on silver, gold, rhodium, palladium, chromium and platinum surfaces. Three of these surfaces (gold, palladium and rhodium) exhibited good dropwise condensation. It was found that, of the three, gold was the most reliable because it was not adversely affected by a period of shutdown in air as the other two for a period of time.

Wilkins, Bromley and Read [50] reported that the steam condenses as a film on a very carefully cleaned gold surface. They also concluded that, in Erb and Thelen's experiment, some organic compounds adsorbed onto to the gold surface must have prompted dropwise condensation.

Previous studies observed that coating the condensing surface with a thin layer of an organic polymer can sustain dropwise condensation for the longest time. Haraguchi, Shimada and Kumagia (51) found that a coating of polyvinylidene chloride 10 μm thick provided perfect dropwise condensation of steam for over 21,586 hours and its processing cost was much cheaper than other methods used previously even for a

large area coating surface. The result showed that the dropwise condensation heat transfer coefficient was more than 20 times that for filmwise condensation. Holden, Wanniarachchi, Marto and Rose (52) evaluated 14 kinds of organic coatings for their ability to promote and sustain dropwise condensation of steam at atmospheric pressure for 22,000 hours, but failed to find that a thin polymer coating of less than 1 μm can adhere well to a metal substrate (i.e., copper and its alloys) in an air steam milieu. The results for these coatings are shown in Table 2.1. It is clearly seen in Table 2.1 that Nedox produced the best thermal performance. Nedox is a commercially available coating developed by the General Magnaplate Corporation for use as a corrosion resistant mold release.

Table 2.1 Steam side heat transfer coefficients [51]

Coating Type	$h_0 / (\text{kW}/\text{m}^2.\text{K})$
Uncoated	10 ± 0.5
No-Stik	4 ± 0.5
Nedox	86 ± 13
NRL C-6 Fluoroepoxy	20 ± 1
NRL Fluoroacrylic	53 ± 7
Parylene-N, 0.5 μm	67 ± 10
Parylene-N, 1.0 μm	52 ± 8

Marto, Looney and Rose [53] found that an organic coating 1 μm thick could sustain dropwise condensation for more than 12,000 hours. O'Neill and Westwater's [54] lifetime test on electroplated silver surfaces maintained dropwise condensation for about 24,000 hours.

Some of highly polymerized compounds have very low surface energies and cannot be wetted by liquids such as water. The most typical of them is PTFE (Teflon). Many researchers attempted to produce long-term dropwise condensation using PTFE-coated surfaces. Guo, Bai, Cai, and Lin [55] coated PTFE on an electrochemically eroded porous surface and tested steam dropwise condensation on the surface. Yang and Cheng [56] investigated dropwise condensation of steam on Ni-PTFE composite plated surfaces.

The chronological order of the year for different techniques used for promoting dropwise condensation is shown in Fig. 2.3 [2].

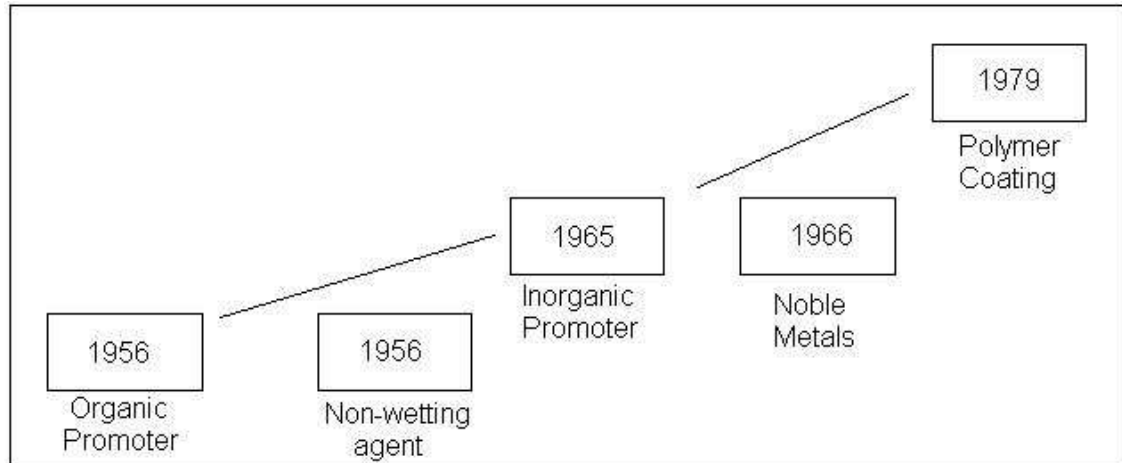


Fig. 2.2 Chronological order of the year for different techniques used for promoting dropwise condensation [2]

2.6 The Effect of Sweeping on Dropwise Condensation

The dropwise condensation begins with the nucleation of droplet, continuous with growth and seemingly random coalescences and than ends with drop departing and sweeping on surface. This cycle continues repetitively. Sweeping effect is also in this cycle, hence must be paid attention of this effect to understand the mechanism of dropwise condensation.

Three parameters affect the sweeping rate:

- I. The vapor to surface temperature difference

If the temperature difference is increased, the heat flux increases and the number of departing droplets per unit time increase; consequently the surface is swept frequently.

II. Body forces acting on the droplets

Increasing the body forces causes the droplets to depart at smaller sizes, and the sweeping rate thereby also increases.

III. The physical size of the condensing surface

Increasing the dimension of the condensing surface in the direction of the sweeping frequency because of the increased the heat transfer rate.

Sweeping by departing drops was considered to have a significant effect on heat transfer rate, even in the earliest works on dropwise condensation. Fatica and Katz [13] obtained that departing droplets originate in a region confined to within $\frac{1}{4}$ inch to $\frac{1}{2}$ inch from the top of the condensing surface. Therefore, as one moves downward on a condenser surface, the surface will be swept faster because of the increasing number of droplets. They presented that the dropwise condensation heat transfer coefficient would be low in a region close to the top of the condenser surface, then will increase further down as a result of faster sweeping, then level off, and finally, as one proceeds sufficiently far down the surface, the surface will be flooded by falling droplets, and the heat transfer coefficient would decrease. Also Shea and Krase [57] showed that the local heat transfer coefficient decreases beyond 4 inches from the top of a vertical cooling surface. Main studies about sweeping effect of drops on dropwise condensation made by Yamali. In this thesis, main help will be taken by Yamali's articles and his doctoral thesis. Hence, what he did about sweeping effect will be explained in further chapters.

CHAPTER 3

MATHEMATICAL ANALYSES

In this study, the dropwise condensation on cylindrical surface will be analyzed by analytically. The mathematical analyses are divided into two parts.

At the first part of this study, the problem of equilibrium shape and departure size of two-dimensional dropwise condensation drops on the outer surface of a cylinder is considered. The equations of the surface of the drop are obtained by minimizing (for a given volume) the total energy of the drop, consisting of surface and gravitational energy, using the techniques of variational calculus.

On the solid surface, the surface tension acts to hold the drops, while drop removal forces may be surface forces resulting from viscous shear and pressure, or body forces, whether electrical, magnetic or gravity.

At the second part of this study, the main aim is to find the local heat flux including the effect of sweeping which obtained by summing the energy transferred to the condenser surface in the three phases. Total heat transferred to the condenser surface in the first phase can be calculated by direct condensation, just before the coalescences start. This phase is neglected due to the small effect to the local heat flux. Total heat transferred to the surface in the second phase is obtained by integrating heat flux over the time interval τ_{co} . Total heat transferred to the surface in the third phase is obtained by multiplying the mean heat flux at departure rate with time elapsed subtracting of sweeping period from τ_{co} .

3.1 Calculating the Departure Size of Drops

The size at which drops are removed from the surface is called the departure size. The departure size is an important parameter due to the relating with the dropsize distribution and the sweeping rate in dropwise condensation.

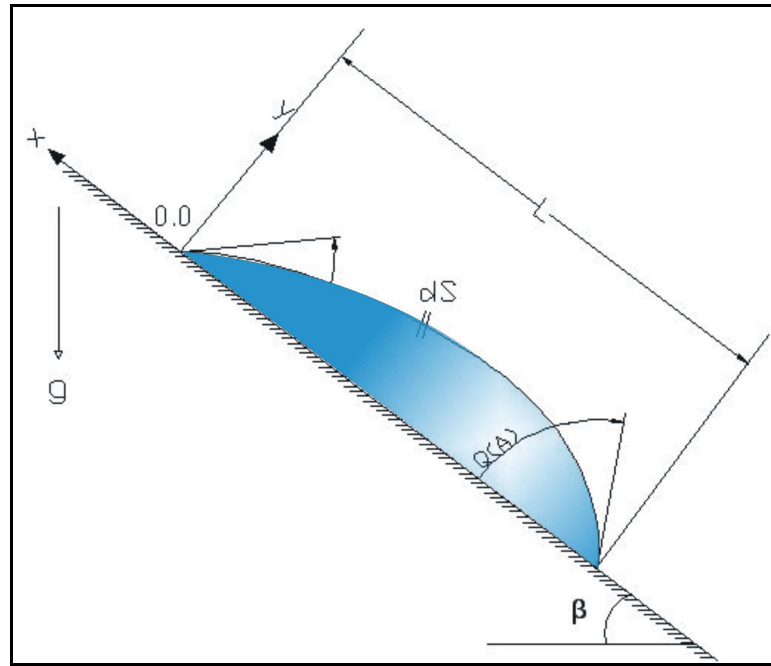


Fig. 3.1 Coordinate system for drop on a flat surface

In determining the effect that the drop departure size has upon the heat transfer rate, and dealing only with flat surfaces at this time, consideration must be given to the orientation between the condensation surface and gravity. A number of different cases can be distinguished over the orientation range $0 \leq \beta \leq \pi$, as indicated in Fig. 3.1:

- i) $\beta = 0$. If the surface is large, the drop grows continuously, and the process is continuously transient. For small surfaces with no constraints at the edges, surface tension in conjunction with gravity will remove the drop when it reaches the edge of the surface. The drop situation for $\beta = 0$ can be seen from below Fig. 3.2.

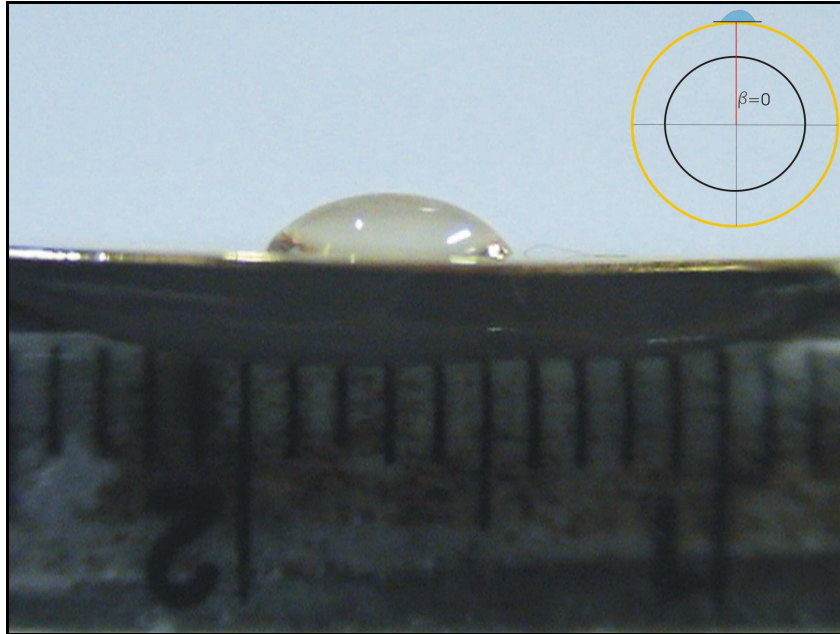


Fig. 3.2 Surface inclination is zero.

- ii) $0 \leq \beta \leq \pi/2$. In this range, the drop will slide along the surface, but until dropping down, the drop always remains in contact with the surface and sweeping a path clear by coalescence. The drop situation for $0 \leq \beta \leq \pi/2$ can be seen from below Fig. 3.3:

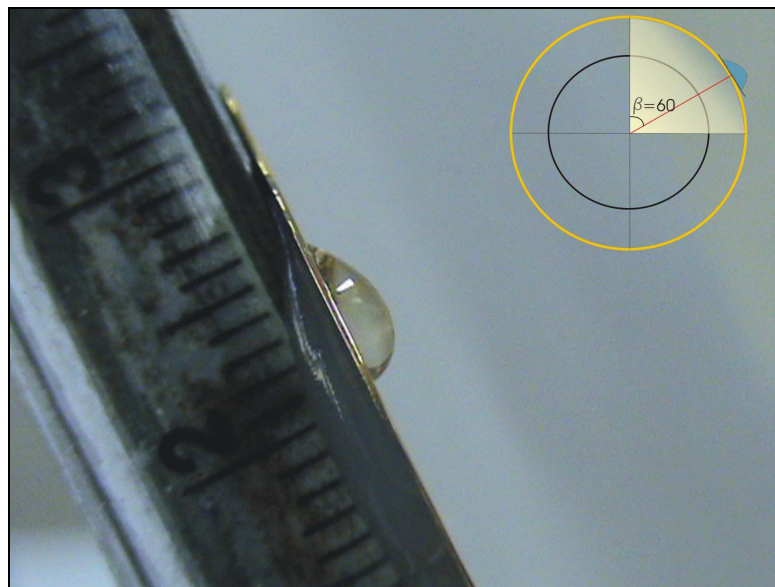


Fig. 3.3 Surface inclination is between 0 and $\pi/2$.

- iii) $\pi/2 \leq \beta \leq \pi$. Drop within this range may begin to roll, until reaching some critical size. The size of drop increases due to the coalescence, and depart from the surface when some other critical condition. Some accompanying effects of the sweeping action may be expected. The drop situation for $\pi/2 \leq \beta \leq \pi$ can be seen from below Fig.3.4:

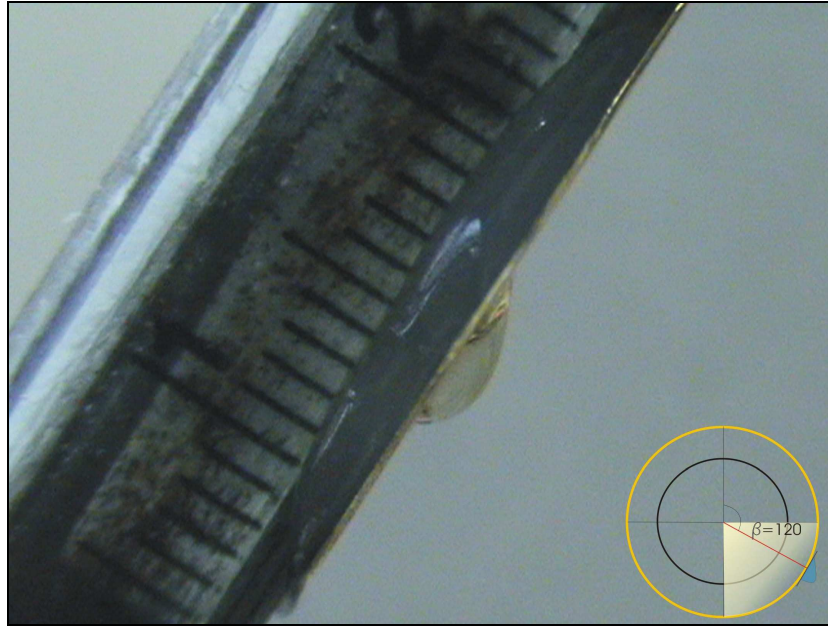


Fig. 3.4 Surface inclination is between $\pi/2$ and π .

- iv) $\beta = \pi$. The drops would depart vertical to the condensing surface, and would be expected to exert no influence outside their immediate surroundings. The drop situation for $\beta \leq \pi$ can be seen from below Fig. 3.5:

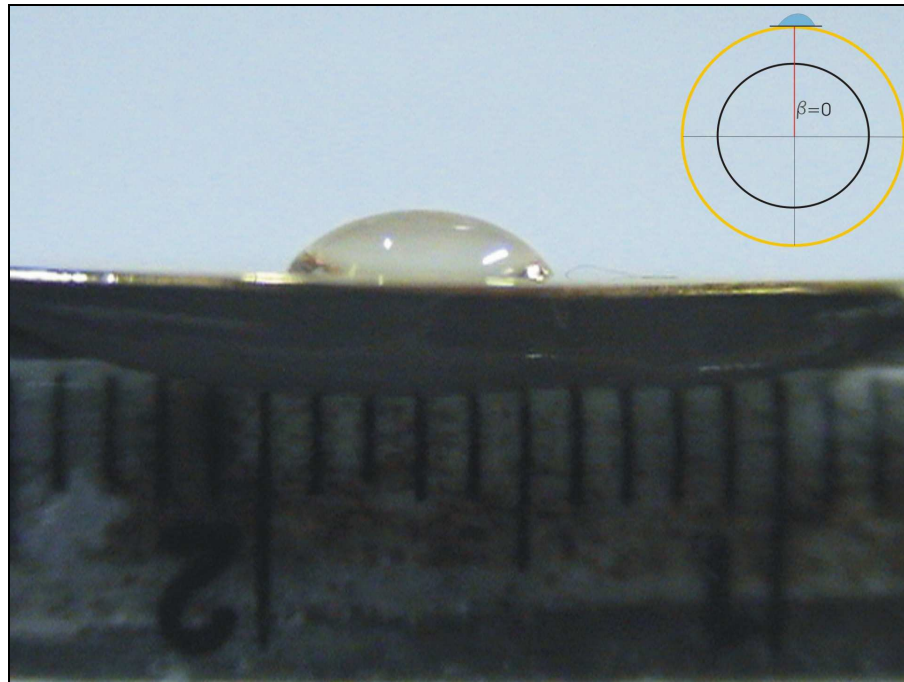


Fig. 3.5 Surface inclination is π .

The previous works are explained in literature review part of this study.

For the non – ax symmetric cases, energy methods are more convenient for mathematical treatment and will be used here. The equation of the surface of the drop is obtained by minimizing the total energy of the drop. The total energy consist of,

- The work of adhesion between the liquid drop and surrounding vapor
- The work of adhesion between the drop and the solid surface
- Gravitational potential energy

3.1.1 Work of Adhesion Between The Liquid Drop And The Surrounding Vapor

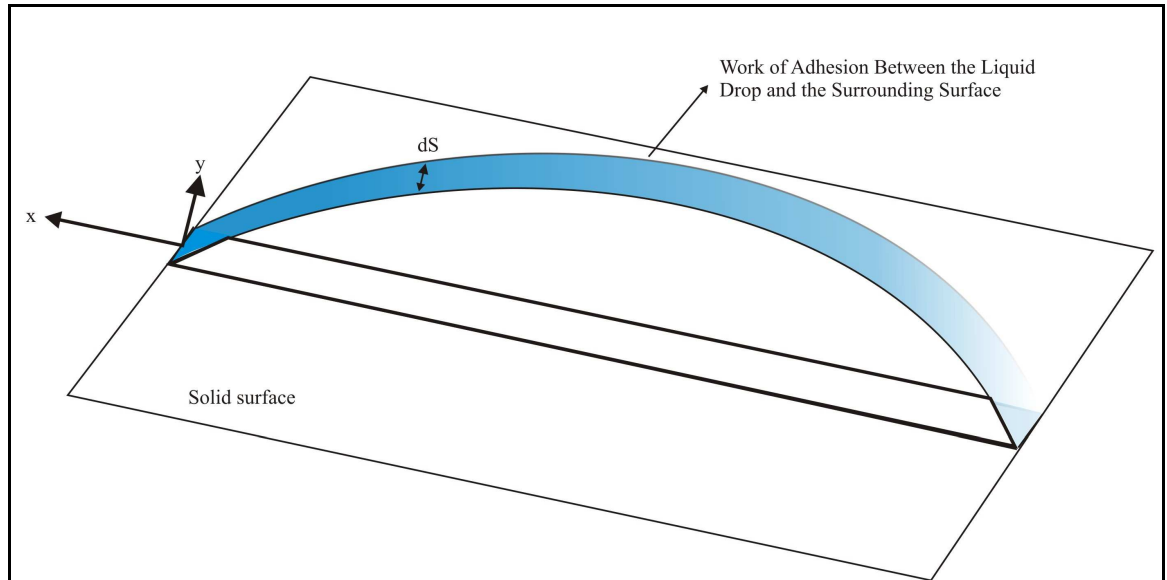


Fig. 3.6 The surface of work of adhesion

The below equation is the energy equation of the drop.

$$U_{lv} = \int_{-L}^0 \sigma_{lv} dS \quad (3.1)$$

Where:

U_{lv} : The work of adhesion between the liquid drop and the surrounding surface

σ_{lv} : Surface tension between liquid drop and vapor

L : Length of the drop

We defined the drop surface as semicircle. The centroid of the semicircle as shown in Figure 3.7 was defined as Eq. 3.2 by Adams (59). This equation will be used for all dS .

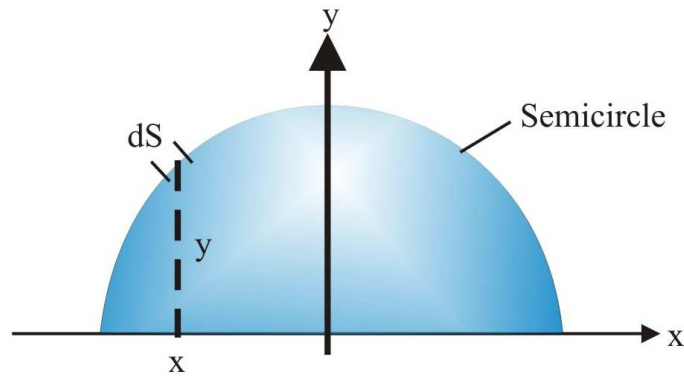


Fig. 3.7 The centroid of the semicircle

The centroid of the semicircle is;

$$dS = \left[1 + \left(\frac{dy}{dx} \right)^2 \right]^{\frac{1}{2}} dx \quad (3.2)$$

When we add the Eq. 3.2 into Eq. 3.1, the result is,

$$U_{lv} = \int_{-L}^0 \sigma_{lv} \left[1 + \left(\frac{dy}{dx} \right)^2 \right]^{\frac{1}{2}} dx \quad (3.3)$$

3.1.2 Work of Adhesion between the Drop and the Solid Surface

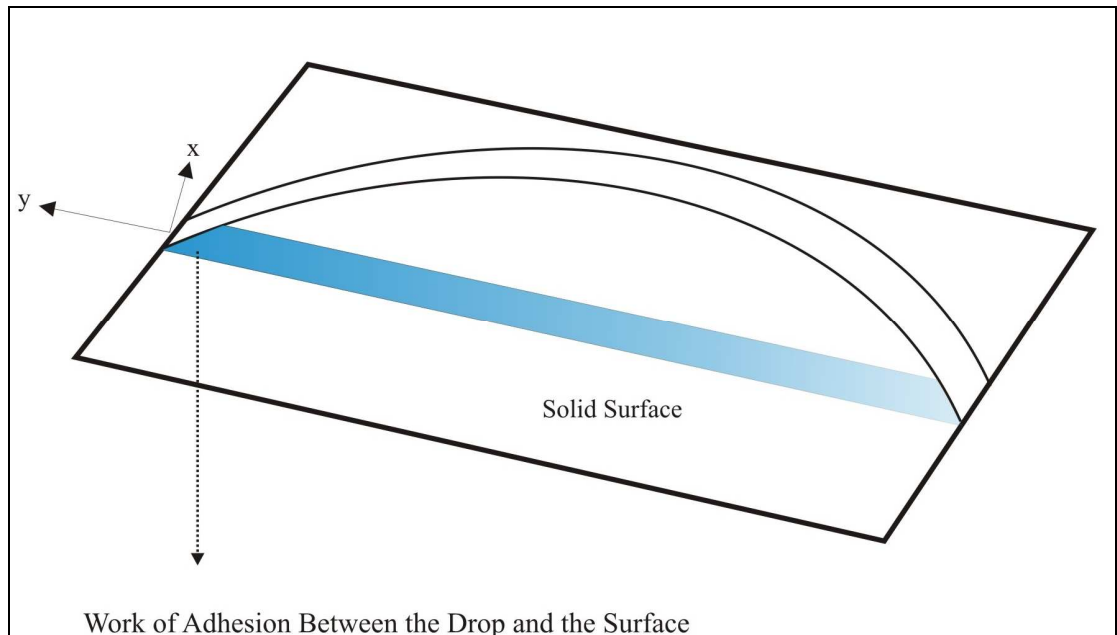


Fig. 3.8 The surface of work of adhesion

$$U_{ls} = \int_{-L}^0 (\sigma_{sv} - \sigma_{ls}) dx \quad (3.4)$$

Where:

U_{ls} : The work of adhesion between the liquid drop and the solid surface

σ_{sv} : Surface tension between the solid surface and the vapor

σ_{ls} : Surface tension between the liquid drop and the solid surface

3.1.3 Gravitational Potential Energy

Gravitational potential energy is the energy which is stored in an object as the result of its vertical position. The energy is stored as the result of the gravitational attraction of the Earth for the object. The gravitational potential energy depends on the mass and the height of the object. There is a direct relation between gravitational potential energy and the mass of an object; it means that more massive objects have greater gravitational potential energy. There is also a direct relation between gravitational potential energy and the height of an object; the higher that an object is elevated, the greater the gravitational potential energy. These relationships are expressed by the following equation:

$$U_g = mgh \quad (3.5)$$

Where:

- m : Mass of the drop
- g : Acceleration due to the gravity
- h : Height of the drop

For the drop on cylindrical surface, the conditions are the same. The drop mass is equal to density of water * volume of water. Also the height of drop is found by using Fig. 3.9.

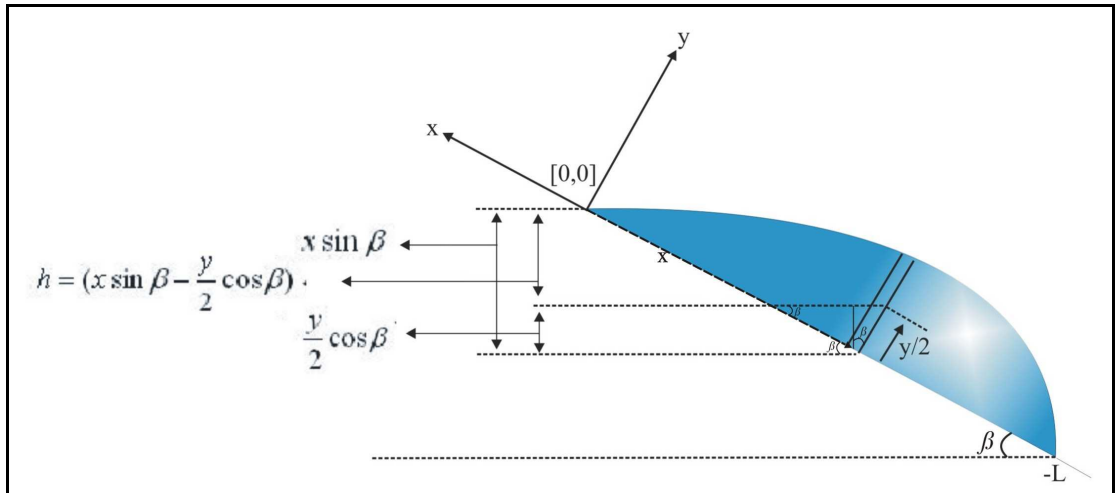


Fig. 3.9 The height equation of drop

By using Fig. the height is found as:

$$h = (x \sin \beta - \frac{y}{2} \cos \beta) \quad (3.6)$$

The mass:

$$m = \rho dV \quad (3.7)$$

The gravitational potential energy of drop is:

$$U_g = \int_{-L}^0 \rho g y (x \sin \beta - \frac{y}{2} \cos \beta) dx \quad (3.8)$$

The reference states implied for these energies are: no liquid-vapor interfacial area, no liquid-solid interfacial area, and the origin, respectively. All quantities are on a per unit width basis.

The volume of the drop is:

$$V = \int_{-L}^0 y dx \quad (3.9)$$

3.1.4 Making the Variable Dimensionless

For convenience and generality the variables will be made dimensionless using σ_{lv} for surface energies and $(\sigma_{lv}/\rho g)^{1/2}$ for length, as;

$$\begin{aligned}
 x^* &= \frac{x}{(\sigma_{lv}/\rho g)^{1/2}} & y^* &= \frac{y}{(\sigma_{lv}/\rho g)^{1/2}} & L^* &= \frac{L}{(\sigma_{lv}/\rho g)^{1/2}} \\
 U^* &= \frac{U}{(\sigma_{lv}^3/\rho g)^{1/2}} & V^* &= \frac{V}{(\sigma_{lv}/\rho g)^{1/2}} \\
 \sigma_v^* &= \frac{\sigma_{sv}}{\sigma_{lv}} & \sigma_l^* &= \frac{\sigma_{ls}}{\sigma_{lv}} & & (3.10)
 \end{aligned}$$

After dimensionless, the total energy and the volume per unit width of the drop are given by:

The total energy:

$$U^* = \int_{-L^*}^0 \left\{ \left[1 + \left(\frac{dy^*}{dx^*} \right)^2 \right]^{\frac{1}{2}} + (\sigma_v^* - \sigma_l^*) + y^* \left(x^* \sin \beta - \frac{y^*}{2} \cos \beta \right) \right\} dx^* \quad (3.11)$$

The volume per unit width:

$$V^* = \int_{-L^*}^0 y^* dx^* \quad (3.12)$$

3.1.5 Finding the Equation for the Interface Profile of Droplet by Using Calculus of Variations

The total energy of Eq. (3.11) can be expressed in the following form with the functional f for the purposes of applying the calculus of variations (variational method);

$$U^* = \int_{-L^*}^0 f \left(x^*, y^*, \frac{dy^*}{dx^*} \right) dx^* \quad (3.13)$$

The calculus of variations is defined as one of the oldest subjects in mathematics by the mathematicians. Calculus of variations is a field of mathematics that deals with functions of functions, as opposed to ordinary calculus which deals with functions of numbers. For example, such functional can be formed as integrals involving an unknown function and its derivatives. Besides its mathematical importance, it is also used in branches of mathematics, such as geometry or differential equations, and in physics, engineering, economics and biology.

Hereafter the asterisks (*) will be omitted and all quantities will be understood to be dimensionless. When departures from this become necessary, the context should make it clear as to which are being used.

For equilibrium the total energy of the drop must be at a minimum. The problem becomes one of finding the shape of the interface, which may be expressed by,

$$y^* = G(x) \quad (3.14)$$

The total energy of the system, given by Eq. (3.13) is a minimum with the constraint that the drop volume is constant:

$$V^* = \int_{-L^*}^0 G(x) dx^* = \text{CONSTANT} \quad (3.15)$$

This is a problem in calculus of variations. The upper edge of the drop is arbitrarily fixed at the origin, but the lower limit $x = -L^*$ of the function $G(x)$ which minimizes Eq. (3.13) can be considered as moving on a general curve given by:

$$\Gamma(x, y) = 0 \quad (3.16)$$

The problem can be seen from Fig. 3.10 that there are two solutions as y_1 and y_2 which minimize the total energy, where the lower limit lies on the general curve given by Eq. (3.16). Only one of these solutions should be satisfied when Eq. (3.16) is given as the line $y = 0$, so that $y = 0$ at $x = -L^*$.

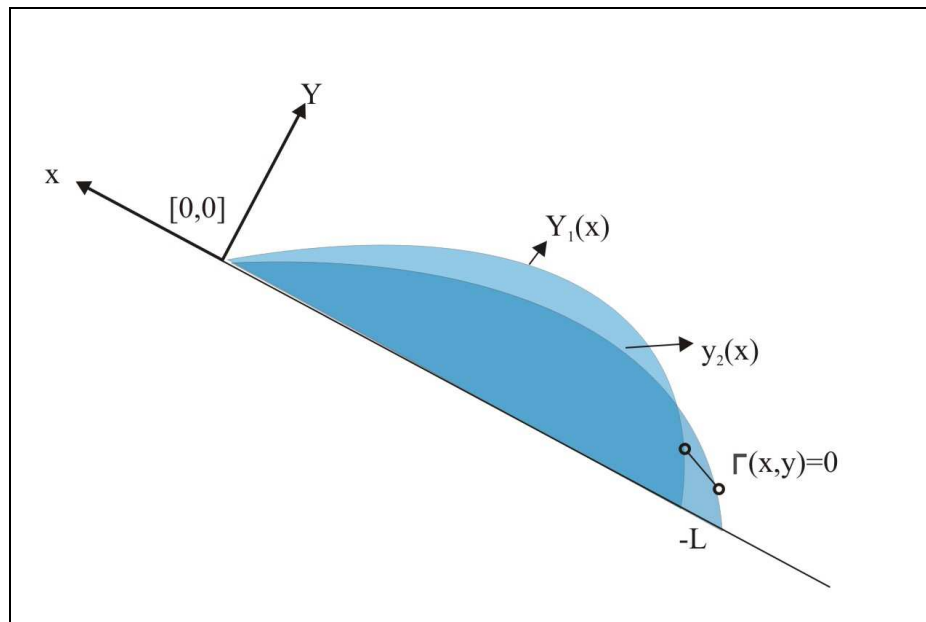


Fig. 3.10 Schematic of solution procedure

To minimize the total energy in Eq. (3.11), its first variation must vanish:

$$\delta U = 0 \quad (3.17)$$

The necessary condition is that the functional $f(x, y, y')$ in Eq. (3.13) must satisfy the Euler equation. Problems in the calculus of variations often can be solved by solution of the appropriate Euler-Lagrange equation.

$$\frac{\partial f^*}{\partial y^*} - \frac{d}{dx^*} \left(\frac{\partial f^*}{\partial y'^*} \right) = 0 \quad (3.18)$$

To satisfy the constraint of Eq. (3.15), the undetermined Lagrangian multiplier λ is introduced to produce a new functional:

$$f^*(x, y, y^l) = f(x, y, y^l) + \lambda G(x) \quad (3.19)$$

Substituting from Eq. (3.11) this becomes:

$$f^*(x, y, y^l) = \left[1 + \left(\frac{dy^*}{dx^*} \right)^2 \right]^{\frac{1}{2}} + (\sigma_v^* - \sigma_l^*) + y^*(x^* \sin \beta - \frac{y^*}{2} \cos \beta) + \lambda y^* \quad (3.20)$$

The problem is transformed to finding the extreme of:

$$U + \lambda V = \int_{-L^*}^0 f^*(x, y, y^l) dx \quad (3.21)$$

Or

$$\delta(U + \lambda V) = 0 \quad (3.22)$$

The Euler equation to be satisfied now is:

$$\frac{\partial f^*}{\partial y^*} - \frac{d}{dx^*} \left(\frac{\partial f^*}{\partial y'^*} \right) = 0 \quad (3.23)$$

Substituting Eq. (3.20) into the Euler Eq. (3.23),

$$\begin{aligned} & \frac{d}{dy^*} \left[\sqrt{1+(y'^*)^2} + x^* y^* \sin(\beta) - \frac{y^{*2}}{2} \cos(\beta) + \lambda y^* + (\sigma_V^* - \sigma_I^*) \right] - \\ & \frac{d}{dx^*} \frac{d}{dy'^*} \left[\left[\sqrt{1+(y'^*)^2} + x^* y^* \sin(\beta) - \frac{y^{*2}}{2} \cos(\beta) + \lambda y^* + (\sigma_V^* - \sigma_I^*) \right] \right] \quad (3.24) \\ & = 0 \end{aligned}$$

$$x^* \sin(\beta) - y^* \cos(\beta) + \lambda - \frac{d}{dx^*} \left[\frac{1}{(1+(y'^*)^2)^{1/2}} y'^* \right] = 0 \quad (3.25)$$

And the governing equation for the interface profile is obtained:

$$(x^* \sin(\beta) - y^* \cos(\beta) + \lambda) - \frac{d}{dx^*} \left[\frac{dy^*/dx^*}{(1+(\frac{dy^*}{dx^*})^2)^{1/2}} \right] = 0 \quad (3.26)$$

The departure sizes are measured experimentally and attempt is made to calculate them analytically. The MatCAD program prepared to calculate the departure size by solving the Eq. 3.26 is given in Appendix A. Since the resulting finite difference system of equation doesn't converge a solution, no numerical result will be presented here.

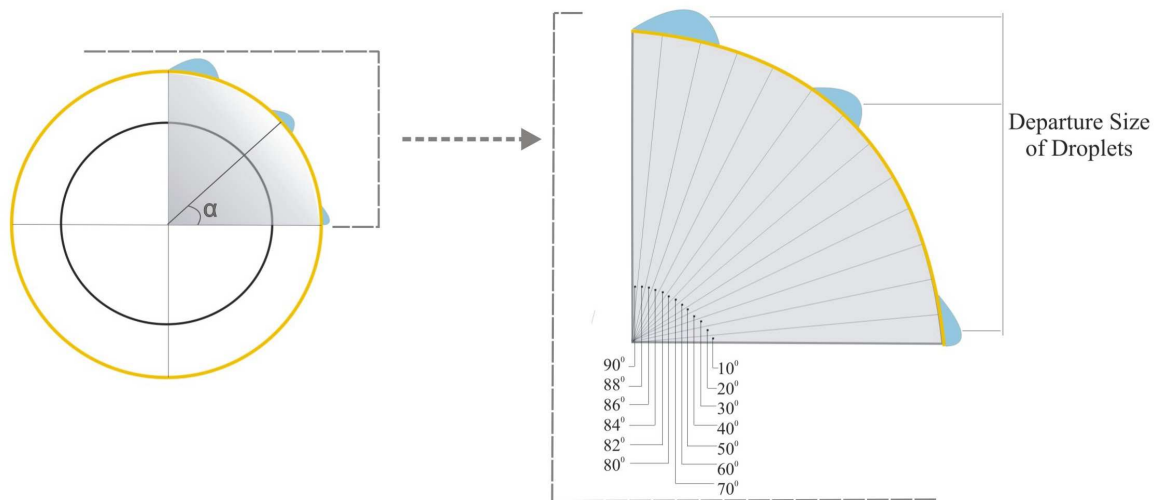


Fig. 3.11 Variation of departure size on the condenser surface

3.1.7 Finding Departure Size Experimentally

Simple experimental apparatus is constituted to find departure sizes for the different surface angles. The main aim of the experimental apparatus is facilitating to find the departure size of the surface of the cylinder for different angle of inclinations.

Experimental apparatus can be seen from Fig.3.12. In this apparatus, there is an adjustable iron rod scaled with a ruler. Back of that iron rod there is another ruler to define an angle of the surface, and on the iron rod, there is a gold surface which the drop is putting by using Ensulin Syringe. Ensulin Syringe is selected, because, the edge hole is very small and easy to put a little droplet onto growing drop.

The gold surface is polished carefully to remove the lines which can hinder to find the real values of departure size.

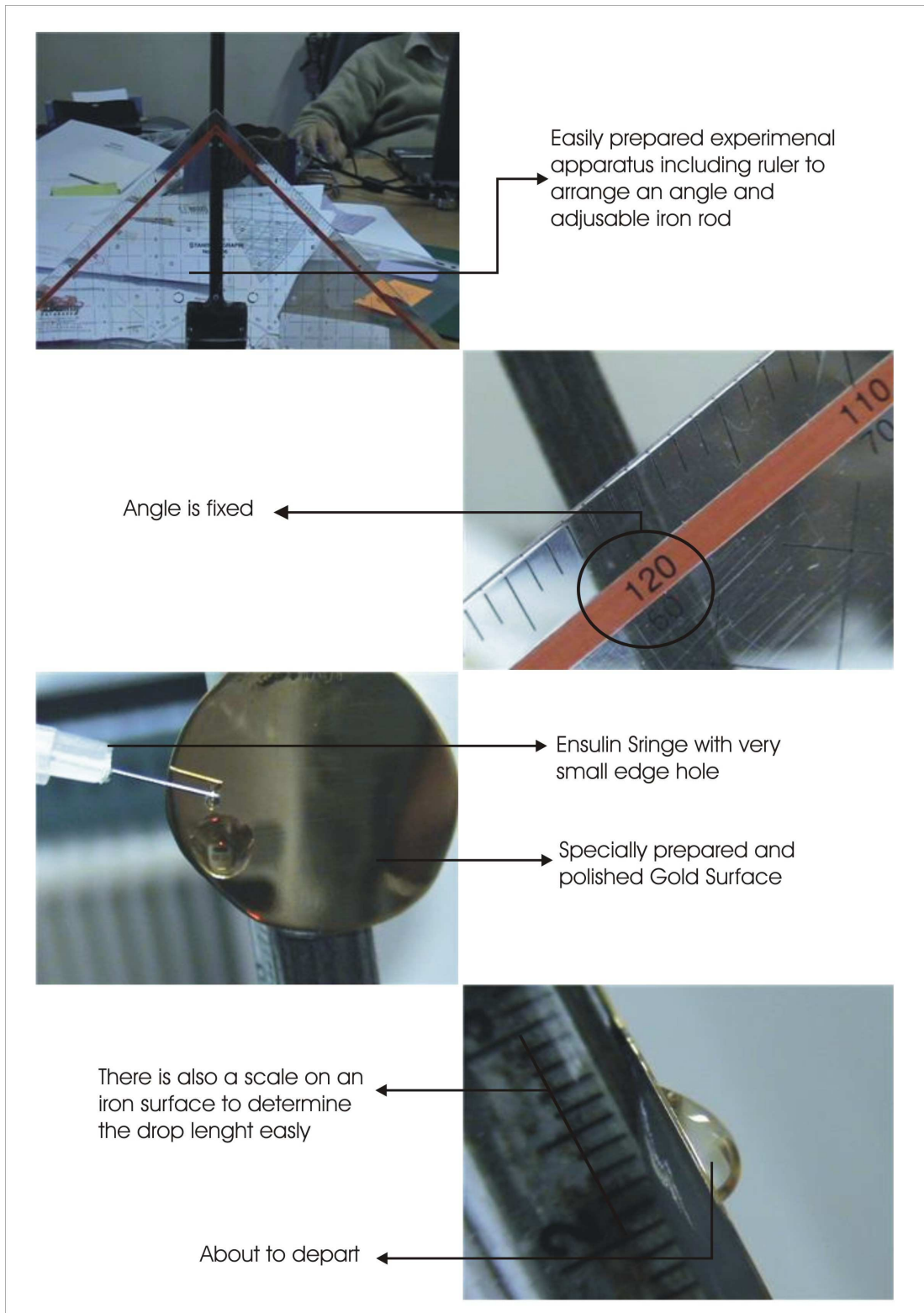


Fig. 3.12 Experimental Procedure

The camera is used to observe and to capture the departure size of drops. As seen from the Fig. 3.12 that the angle is adjusted to the 60° degree. And starting to put a

drop onto gold surface slowly, and also at the same time the camera is taken a picture serially, when the drop is started to depart from solid surface, the camera is stopped. The picture which the drop is about to depart is used to calculate the departure size, volume and mass of the droplet.

3.2 Calculating the Local Heat Transfer Including Sweeping Effect on the Cylindrical Surface

3.2.1 Conduction Through A Single Droplet

It is essential to formulate the heat transfer through a single droplet to calculate the heat transfer in dropwise condensation. Krischer and Grigull [59], taking advantages of the relatively large heat transfer at the edge of the droplet, obtained a simple relation for drop heat flux. On the other hand, Umur and Griffith [11] solved the conduction equation for a hemispherical droplet and obtained an exact solution for the drop heat flux. Both of the solutions mentioned above assumed a uniform interfacial heat transfer coefficient over the liquid vapor interface, and a uniform base temperature is taken. The assumption of a uniform interfacial heat transfer coefficient results in significant errors in the heat flux calculations, especially at drop sizes close to the critical size where the majority of the heat transfer takes place.

Yamali and Merte [60] approximated the heat flow lines near the edge of the droplet by arcs of circles, and taking an interfacial heat transfer coefficient that varies with interface temperature and a constant base temperature, obtained the following relation for the drop heat flux:

The total heat transfer rate for a drop of radius r as:

$$q_d(r) = \frac{2\pi K_1}{T_{sat}} (Ar - BK_2 \sin \theta) \left[-\cos \theta + \frac{r + B \cos \theta}{r} \ln \frac{r + B}{B} \right] \quad (3.27)$$

The mean heat flux at the base of the droplet becomes:

$$q_d''(r) = \frac{q_d(r)}{\pi r^2}$$

$$= \frac{2K_1 B}{r^2 T_{sat}} (r \Delta T_t - K_2 \sin \theta) \left[-\cos \theta + \frac{r + B \cos \theta}{r} \ln \frac{r + B}{B} \right] \quad (3.28)$$

Where heat transfer coefficient is expressed by,

$$h_e = \frac{K_1}{T_i} \left(1 - \frac{K_2}{R \Delta T} \right) \quad (3.29)$$

And

$$K_1 = \left(\frac{2\gamma}{2-\gamma} \right) \left(\frac{1}{2\pi} \right)^{1/2} \frac{h_{fg}^2 P_v^*}{G^{3/2} T_{sat}^{3/2}} \quad (3.30)$$

$$K_2 = \frac{2T_{sat} \sigma}{h_{fg} \rho_1} \quad (3.31)$$

$$\Delta T_t = T_{sat} - T_s \quad (3.32)$$

$$A = \frac{\Delta T_t k T_{sat}}{\theta K_1} \quad (3.33)$$

$$B = \frac{k T_{sat}}{\theta K_1} \quad (3.34)$$

Where

γ : Condensation coefficient (fraction of molecules that strike a surface and condense)

h_{fg} : Latent heat of vaporization

P_v^* : Saturation pressure corresponding to vapor temperature

G : Gas constant

- T_{sat} : Vapor saturation temperature
 T_i : Temperature of liquid-vapor interface
 T_s : Condenser surface temperature
 σ : Surface tension
 ρ_l : Liquid density
 ΔT_t : Difference between the vapor and the interface temperatures ($T_{\text{sat}} - T_s$)
 h_e : Equivalent heat transfer coefficient for the liquid-vapor interface at the point of interest.
 R : The radius of curvature of the interface at the point of interest

The geometry and nomenclature used for the drop conduction model is shown in Fig. 3.13.

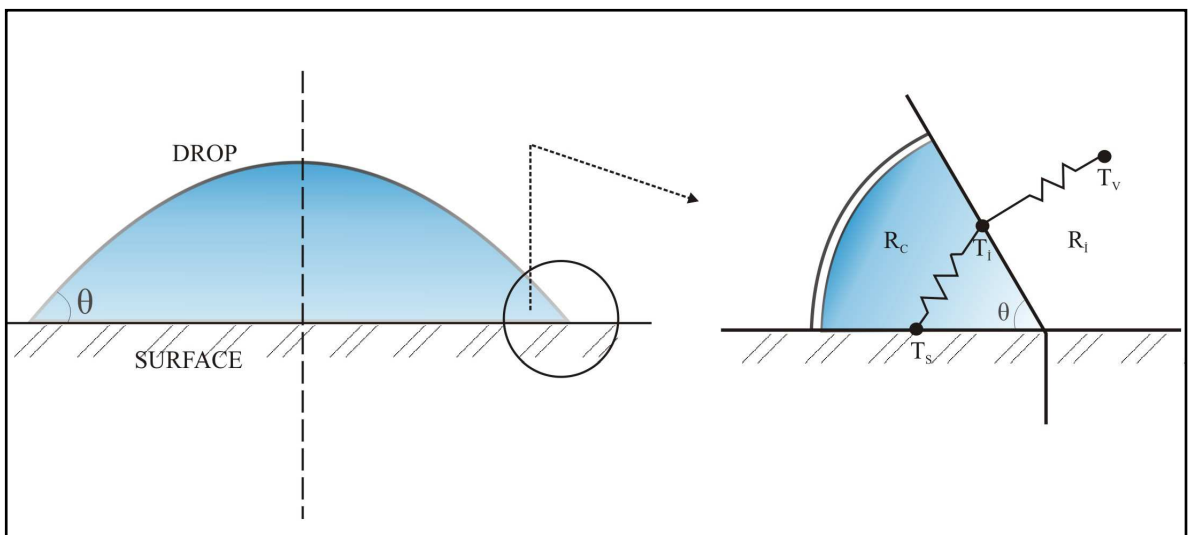


Fig. 3.13 Model for heat conduction through a droplet

3.2.2 Heat Flux in Direct Condensation Range

In the direct condensation, by the direct effect of vapor on the interface, drops grow only by the direct condensation, since no coalescences take place. When the drops

reach the continuous coalescences taking place with droplets of larger size, these continuous coalescences provide cleared surfaces on which fresh nucleation takes place. Also the vapor on interface continues, hence new droplets form continuously on these available sites.

The total heat flux is consisting of summed of both the heat flux in direct condensation range and heat flux in coalescences range. But the heat flux in direct condensation range is much smaller than the heat flux in coalescences range, because of that situation, heat flux in direct condensation range is neglected in this study.

3.2.3 Heat Flux in Coalescences Range

Heat flux in coalescence range is the most important part of total heat flux, because direct condensation effect is neglected. The droplet size distribution of coalescing droplets can be expressed by a function of the form given by Eq. (2.1), and conforms well to experimental measurements for values of n close to 1/3 found by Glicksman and Rose [19]. f_{co} in Eq. (2.1) is the fraction of area occupied by droplets in the size range from a radius r to the maximum radius r_{max} in the distribution. Variations in the experimental values of n given in the literature are speculated to be due to the sweeping of the surface by falling droplets. The magnitude of the sweeping effect varies with the heat flux, and this is reflected in variations of the droplet size distribution.

The size distribution given in Eq. (2.1) is considered valid only for the coalescence region because it is based on measurements made in this region only. As mentioned above that droplet growing by direct condensation are too small to be counted by the naked eye or even under a microscope. Consequently, Eq. (2.1) applies for droplets from the maximum size (departure size) down to the radius order of magnitude of the half distance between nucleation sites.

The fraction of area occupied by droplets in the coalescence region, within the dimensionless differential size range dr^* becomes, from Eq. 2.1 given by Yamali and Merte [61]:

$$df_{co} = nr^{*(n-1)} dr^* \quad (3.35)$$

The mean heat flux over the entire condensing surface due to the contributions

$$q''_{co} = \int_{r^*_{co}} \frac{1}{r^*} q''_d(r^*) nr^{*(n-1)} dr^* \quad (3.36)$$

Where

$$q''_d(r^*) \equiv q''_d(r) \quad (3.37)$$

Substituting Eq. (3.37) and Eq. (3.28) for $q''_d(r^*)$ into Eq. (3.36):

$$q''_{co} = \int_{r^*_{co}} \frac{1}{r^*} \frac{2K_1 B}{r_{dep}^2 r^{*2} T_{sat}} (r_{dep} r^* \Delta T_t - K_2 \sin \theta) x \left[-\cos \theta + \left(1 + \frac{B \cos \theta}{r_{dep} r^*} \right) \ln(1 + \delta r^*) \right] nr^{*(n-1)} dr^* \quad (3.38)$$

Where

- r^* : Nondimensional drop base radius ($= r / r_{dep}$)
- r_{dep} : Departure size of droplets

r_{co} : Mean radius at which droplets start coalescing
 r_{co}^* : Nondimensional average half distance between nucleation sites ($=r_{co} / r_{dep}$). It is also the size of the droplet at which coalescences begin.

And

$$r_{co}^* = \frac{r_{co}}{r_{dep}} \quad (3.39)$$

$$\delta \equiv \frac{r_{dep}}{B} \quad (3.40)$$

The total heat flux for dropwise condensation excluding the sweeping effect (e.g. dropwise condensation on a facedown surface) is the sum of the sequential contributions due to the coalescing drops and the drops growing by direct condensation:

$$q_T'' = q_{co}'' + q_{dc}'' \quad (3.41)$$

But the heat flux in direct condensation range is much smaller than the heat flux in coalescences range, hence the total heat flux for dropwise condensation excluding the sweeping effect is equal to heat flux due to the coalescing drops:

$$q_T'' = q_{co}'' \quad (3.42)$$

3.2.4 Heat Flux in Dropwise Condensation Including the Sweeping Effect

The heat flux can be provided by Eq. (3.42) for dropwise condensation, but this formula does not include the effect of sweeping of the surface by the departing droplets. This study's main part is "adding the effect of sweeping to the total heat flux in dropwise condensation". It was assumed in the derivation of Eq. (3.42) that

droplets reaching the departure size were removed without having any direct influence on neighboring areas. An example can be given for that situation where dropwise condensation takes place on a horizontal surface facing downward. Also the heat flux on a swept track following a falling droplet can also be calculated by Eq. (3.42) except that, unlike the case of the downward facing surface, the maximum drop radius in the swept area is smaller than the departure size, and is now a function of time. The heat flux therefore changes in decreasing manner as time passes [61].

In the models of Graham, Griffith [16] and Le Fevre, Rose [23], the sweeping effect was not given due to the formulation of the process. Comparisons of predictions based on these models with measurements obtained at earth gravity were satisfactory since the sweeping rates under such conditions are relatively low.

Yamali [1] explained that three parameters affect the sweeping rate:

I. The vapor to surface temperature difference

If the temperature difference is increased, the heat flux increases and the number of departing droplets per unit time increase; consequently the surface is swept frequently.

II. Body forces acting on the droplets

Increasing the body forces causes the droplets to depart at smaller sizes, and the sweeping rate thereby also increases.

III. The physical size of the condensing surface

Increasing the dimension of the condensing surface in the direction of the sweeping frequency because of the increased the heat transfer rate.

The height of the condenser surface is an important parameter where the surface is vertical to the ground; this can be provided by the vertical surface which

perpendicular to the ground and also different angles on cylindrical surface. The importance of the height of the condenser surface is coming from the effects of the sweeping of the surface. The example figure can be observed in Fig. 3.14, it is clear that at the top of the surface, no sweeping takes place, while the sweeping rate can be expected to increase at the lower parts of the surface, since more and more departing droplets join the falling droplets. The frequency of the sweeping at any height can be calculated by summing the number of departing droplets produced at any point on the surface over the height of the condenser surface to that point. In the Fig. 3.14, there are three differential horizontal strips on the condenser surface, and possible locations of drops departing in a unit time interval. This problem can be circumvented in one of two ways [1]:

a) If the departing droplet's center located precisely to a strip, this departing droplet is assumed to belong to that strip. The number of departing droplets can be found by counting the total number of drop centers within the strip.

b) In the second method, the average number of departing droplets within this strip is obtained by dividing the total area of departing droplets remaining in the differential strip by the base area of a single droplet.

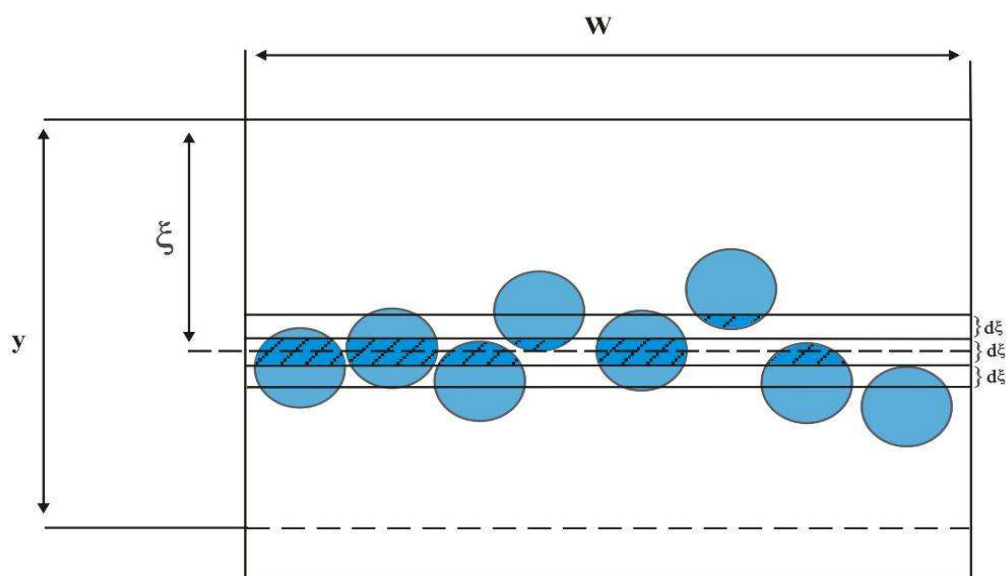


Fig. 3.14 Model for Determining the Local Number of Departing Drops on a Vertical Surface

Yamali [1] introduced a new parameter $f_d(y)$ described as the number of drops attaining the departure size, per unit time, per unit area, at a height y . By the way, he described some formulas to introduce the effect of sweeping on heat flux in dropwise condensation. All of the formulas below are described by Yamali [1], and these formulas will be used to introduce the effect of sweeping on the cylindrical surface by using the departure sizes which was measured depending on cylindrical surface in Chapter 3.1.

From the Fig. 3.14, the total number of departing droplets that cross a horizontal line at an altitude of y per unit time can be obtained by integrating this local number over the condenser area above this line, as:

$$f_s(y) = w \int_0^y f_d(\xi) d(\xi) \quad (3.43)$$

Where,

$f_s(y)$: Number of departing drops crossing elevation y , per unit time, for a condenser surface of width w .

$f_d(\xi)$: No. of drops attaining the departure size, per unit time, per unit area being considered, at a height ξ .

The above equation was solved by using trapezoid rule. To show how to apply the trapezoid rule to that equation, the trapezoid rule will be explained a little. To solve definite integral shown in Eq. 3.44,

$$I = \int_a^b f(x) d(x) \quad (3.44)$$

It is assumed that $f(x)$ is continuous on $[a, b]$ and subdivide $[a, b]$ into n subintervals of equal length h ,

$$x_0 = a, \quad x_1 = a+h, \quad x_2 = a+2h, \quad \dots, \quad x_n = a+nh = b. \quad (3.45)$$

It is assumed that $f(x)$ at each of these points is known:

$$y_0 = f(x_0), \quad y_1 = f(x_1), \quad y_2 = f(x_2) \quad \dots, \quad y_n = f(x_n). \quad (3.46)$$

The trapezoid rule approximates $\int_a^b f(x)d(x)$ by using straight line segments between the points (x_{j-1}, y_{j-1}) and (x_j, y_j) , ($1 \leq j \leq n$).

For example, for the first subinterval $[x_0, x_1]$, the integral of f is approximated as:

$$\int_{x_0}^{x_1} f(x)d(x) \approx h \frac{y_0 + y_1}{2} \quad (3.47)$$

As a result the n -subinterval Trapezoid Rule approximation to $\int_a^b f(x)d(x)$, denoted

T_n , is given by [58];

$$\begin{aligned} T_n &= h \left(\frac{1}{2} y_0 + y_1 + y_2 + y_3 + \dots + y_{n-1} + \frac{1}{2} y_n \right) \\ &= \frac{h}{2} \left(y_0 + 2 \sum_{j=1}^{n-1} y_j + y_n \right) \end{aligned} \quad (3.48)$$

This formulation principle is used to calculate the Eq. 3.43.

To analyze of the effect of sweeping, the most important concept is the sweeping period, defined as the time interval between two successive sweepings at a particular point on the condenser surface. The Fig. 3.15 which represents the condenser surface will be used to derive the sweeping period. Firstly, the condenser surface is divided into vertical strips of departure diameter of a drop (D_{dep}), such the point of interest,

A, lies at the center of one of the strips. As shown, above line y , departing droplets are randomly distributed over the strip such that on the average each strip has the same number of departing droplets, because of the random nature of dropwise condensation. Here again, it is necessary to describe carefully a strip having a departing droplet since, as is shown in Fig. 3.15 departing droplets most likely will be only partly contained within the strip under condensation: as a convention, a drop will be assumed to belong to a strip if its center is in that strip. The rate at which the number of departing droplets is produced within a strip above line y is then:

$$N_{dep}(y) = \frac{f_s(y)}{2w/r_{dep}} \quad (3.49)$$

Where $f_s(y)$ is;

$$f_s(y) = w \int_0^y f_d(\xi) d(\xi) \quad (3.50)$$

And also;

$$N_{dep} = \frac{r_{dep}}{2} \int_0^y f_d(\xi) d\xi \quad (3.51)$$

Where;

$f_s(y)$: Number of departing drops crossing elevation y , per unit time, for a condenser surface of width w .

$f_d(\xi)$: No. of drops attaining the departure size, per unit time, per unit area being considered, at a height ξ .

D_{dep} : Departure diameter of drop

w : Width

ξ : Height

Since any droplet remaining in the strip above sweeps the middle point (Point A in Fig. 3.15),

The average sweeping period is;

$$p(y) = \frac{2}{r_{dep} \int_0^y f_d(\xi) d\xi} \quad (3.52)$$

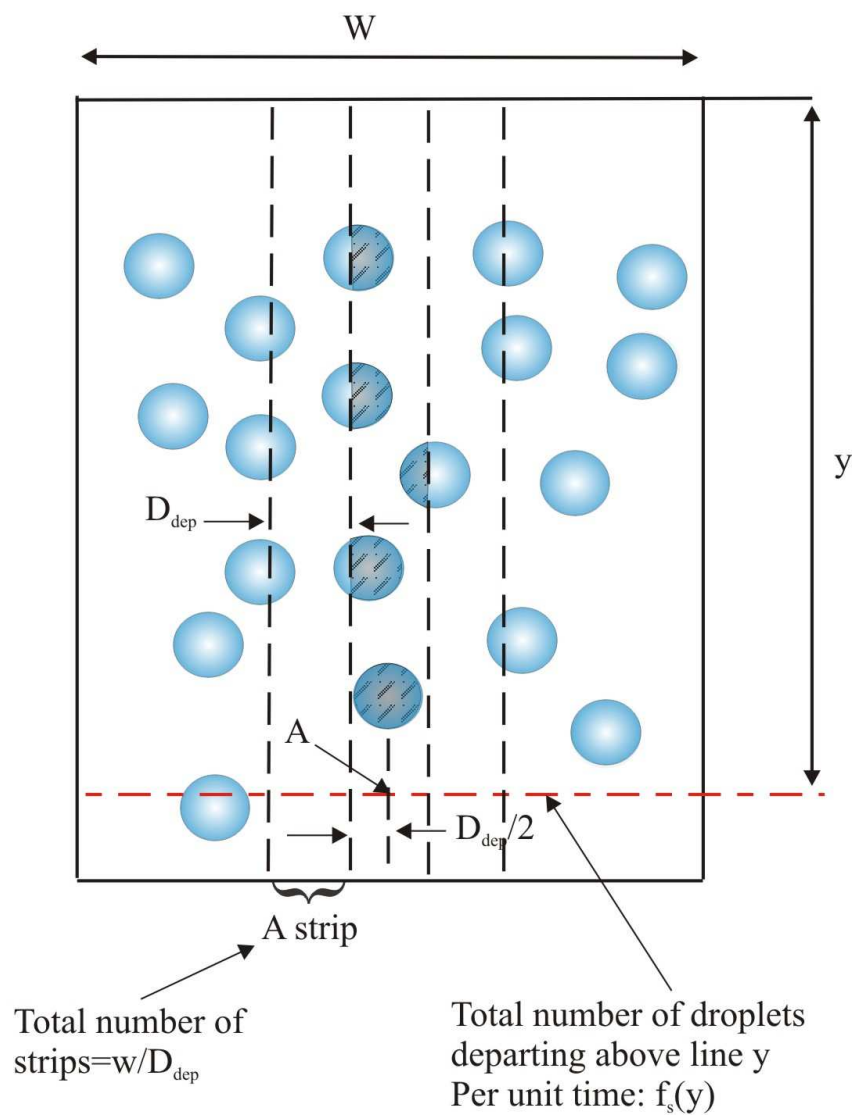


Fig. 3.15 Model for Sweeping Frequency [1]

In below figures, from Fig. 3.16 to Fig. 3.20, between two successive sweepings at a particular point are illustrated. These five figures are summarized the structure of direct condensation, coalescence range and sweeping effect. At the beginning of the condensation in Fig.3.16, the surface is completely bare, at the end of Fig. 3.20; the surface has a droplet which is about the drop. Various differential swept areas of height $d\xi$ at a given elevation y and at a given time τ following a sweep are placed side by side in below figures.

At $\tau=0$ the surface is completely bare (Fig.3.16).

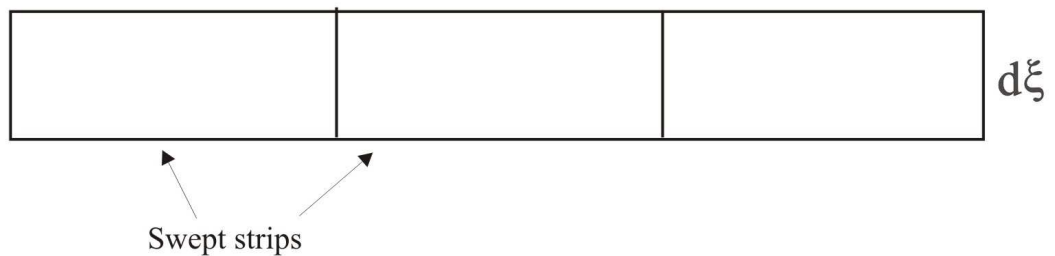


Fig.3.16 Bare Surface

After a time interval drops nucleate and begin growing by direct condensation until they reach size r_{co} (Fig.3.17). The time elapsed between the sweeping and this size will be called τ_{dc}

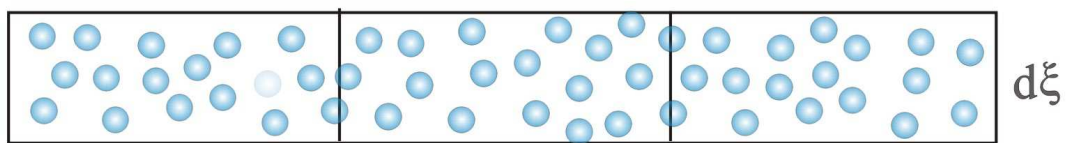


Fig.3.17 The Drops Which is affected only by direct condensation.

In Fig.3.18, the coalescences between adjacent drops started by growing of each droplet. At that time the growing is still continuing by effect of direct condensation and coalescences.

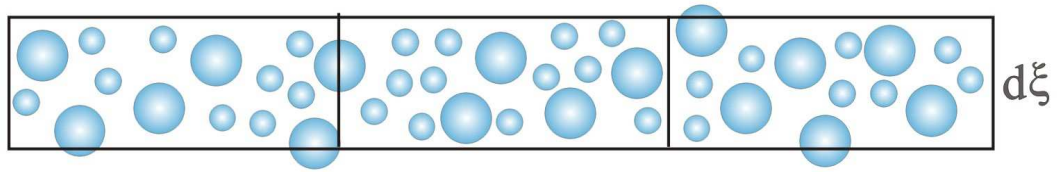


Fig.3.18 Coalescences Range

Until the departure size is reached (Fig. 3.19 and Fig. 3.20). The time elapsed between the onset of coalescence and the appearance of the first departing droplet will be called τ_{co} .

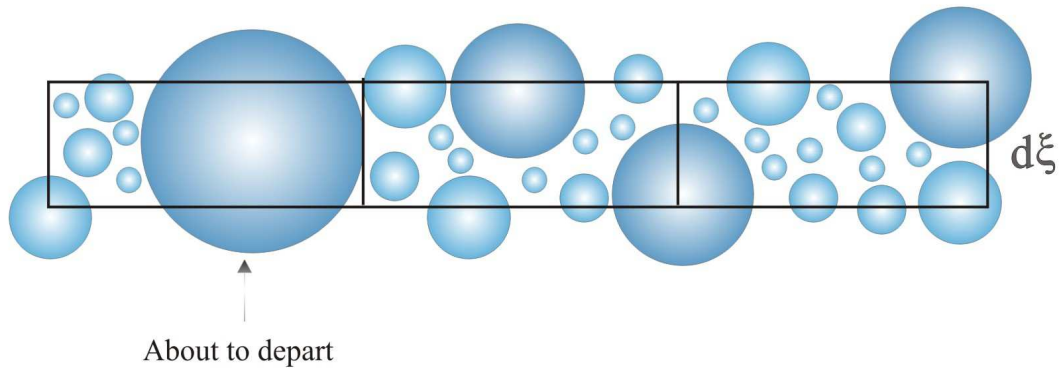


Fig. 3.19 Drops Distribution Where some of them are about to depart.

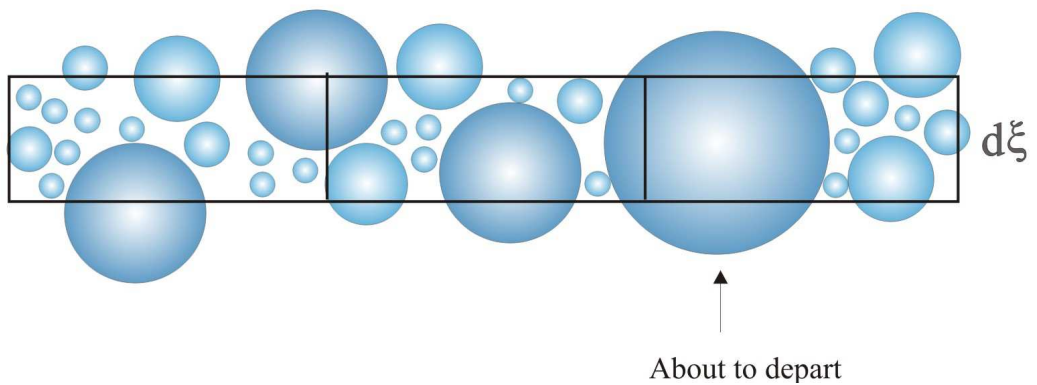


Fig. 3.20 Another Drops Distribution Where some of them are about to depart

Therefore, the time elapses between the sweeping and the first appearance of a departing droplet will be:

$$\tau = \tau_{co} + \tau_{dc} \quad (3.53)$$

Also, here the τ_{dc} is neglected due to the small effect. Hence the time will be

$$\tau = \tau_{co} \quad (3.54)$$

This will be defined as the total growth period.

It is shown in above Figures illustrated from Fig. 3.16 to Fig. 3.19 that the drop size distribution is changed until drops begin departing. However, after Fig. 3.19 and Fig. 3.20 distribution will not change further and one drop has departed, and new drops nucleate within the area cleared. At the same time other drops continue to grow by coalescences and direct condensation, and another drop at another location reaches to the departure size. In other words, Fig. 3.19 and Fig. 3.20 have the same drop size distribution. Only that portion of droplets present within the strip of thickness $d\xi$ are assumed to belong to the strip, as explained previously. This description of the phenomena taking place between to successive sweepings demonstrates in a swept area to attain the same size distribution as the droplets in the upswept areas. Only after this time interval can the swept region again participate in producing departing droplets.

Eq. 3.42 gives the total heat flux for dropwise condensation for the case where the drop size distribution within the coalescence region is given by Eq. 2.1 and where there is no sweeping. It is claimed now that this expression can be used to find the instantaneous heat flux at any altitude by substituting the instantaneous value of r_{max} , which varies between r_{co} and r_{dep} . After the onset of coalescence, r_{max} varies from r_{co} to r_{dep} in a time interval τ_{co} , and then remains at that value until the differential strip at elevation y is swept again.

One question that should be answered before going further whether τ can be greater than $p(y)$. In other words, can some regions on the surface be swept before that region reaches a size distribution that produces a departing droplet? It can be shown by reasoning that this is not possible; τ can be, at most, equal to p , but can never be larger than p . The reasoning is as follows:

At $y=0$ (at the top of the condenser surface) p is infinitely large (since there is no sweeping), hence $p > \tau$. As y increases p decreases, since the number of departing droplets per unit time interval above the elevation line y increases. For large values of y , p approaches τ . As $(p - \tau)$ approaches zero, p no longer decreases as y increases, because the number of departing droplets does not increase further with an increasing y , or, beyond a certain height y , no droplets reach the departure size. In other words, the asymptotic value of p for large values of y is equal to τ .

If no sweeping were to take place, $f_d(y)$ on a differential strip as in Fig. 3.16, 3.20 would be given by,

$$f_d(y) = \frac{q''(r_{dep})}{m_d h_{fg}} \quad (3.55)$$

Where, m_d is the mass of a departing droplet and calculated for each departure size of drops in different angles. This is also the maximum possible rate at which departure sized drops can be generated per unit area at any height. Because of the sweeping, however, no departure sized drops can be produced within the differential strip during the total growth period τ . Only within the time interval $(p - \tau)$ can departure sized droplets which are generated in the differential strip. Therefore, in order to obtain a time average of the function over a sweeping cycle Eq. 3.55 must be multiplied by the factor,

$$\frac{p(y) - \tau}{p(y)} \quad (3.56)$$

The sweeping process has an additional affect on $f_d(y)$ because of the area occupied by droplets on the differential strip as they are falling. Since departing droplets have a large thermal resistance, the fraction of the area covered by them while they are in motion can be considered to be insulated. If the average number of falling droplets per unit area given by $D_d(y)$, then the fraction of the areas not covered by these droplets becomes

$$(1 - D_d(y) \frac{\pi}{16} r_{dep}^2) \quad (3.57)$$

The expression for $f_d(y)$ as influenced by the sweeping process, now becomes:

$$f_d(y) = \frac{(1 - D_d(y) \frac{\pi}{16} r_{dep}^2) (\frac{p(y) - \tau}{p(y)} q''(r_{dep}))}{m_d h_{fg}} \quad (3.58)$$

The number of falling droplets in motion per unit condenser surface area at height y can be expressed as

$$D_d(y) = \frac{f_s(y)}{vw} \quad (3.59)$$

Where, v is the velocity of the falling droplets. The velocity is calculated for each drop to try to find the exact results. Most of the literature articles assumed uniform velocity for each drop on different angle. The values of velocity will be shown on results and discussion part. Viscous forces and gravity are acting in opposite directions and govern the velocity of the falling droplet. From the balance of these two forces, it can be shown that

$$v \approx \frac{r_{dep}^2 g q_1}{4\mu} \quad (3.60)$$

Where

- μ : Condensate viscosity
- g : Acceleration due to gravity

Departure size of drops is calculated by solving the equation of the surface of the drop is obtained by minimizing the total energy of the drop in first part of mathematical analysis and will be used to calculate all the functions.

Substituting Eqs. 3.43, 3.52, 3.58 and departure size of drops which calculated at first part of mathematical analysis, the time average sweeping frequency is obtained as integral equation:

$$f_d(y) = \frac{q''(r_{dep})}{m_d h_{fg}} \left[1 - \frac{\pi r_{dep}^2}{16\nu} \int_0^y f_d(\xi) d\xi \right] \left[1 - \frac{\tau r_{dep}}{2} \int_0^y f_d(\xi) d\xi \right] \quad (3.61)$$

The time elapsed between the sweeping and the first appearance of a departing droplet τ is given by Eq. 3.54 which τ is equal to τ_{co} .

To determine the Eq. 3.61, τ_{co} must be found by using Eq. 3.62.

$$\tau_{co} = \int_{r_{co}}^{r_{dep}} \frac{n\rho_1 Kvolh_{fg}}{\pi(n+1)} (1 + nr_{co}^{n+1} r_{max}^{-(n+1)}) dr_{max} \quad (3.62)$$

In this equation, the most important parameter is $qt(r_{max})$ which must be determined to calculate the Eq. 3.62. But, this can not be calculated as a number, because $qt(r_{max})$ is a function of the maximum drop size in the population, also r_{max} is a function of time. It is clear that r_{dep} is not a r_{max} for the droplets. r_{max} is a drop size between coalescence size and departure size of droplet. In Eq. 3.62, gives the time for the maximum drop size in the population to reach the r_{dep} from the coalescence drop size. In previous pages, the $qt(r_{dep})$ calculated by Eq. 3.28, but for determining the

$qt(r_{max})$ to calculate the time, different ranges are defined for all different surface angles. For all droplets, the coalescence size is assumed to be $2.6 \cdot 10^{-6}$ m, but on the other hand, for all surface angles, there are different departure sizes. By using this principle $\tau = \tau_{co}$ will be calculated on the next chapter for each drop on different angles. Once τ is known $f_d(y)$ can be obtained from Eq. 3.61. Substituting $f_d(y)$ into Eq. 3.52 gives the sweeping period at any elevation y .

To determine the local heat flux on the surface, the events taking place between two successive sweepings at the location of interest must be considered. Immediately following a sweeping action drops nucleate and grow with no coalescences up to the size r_{co} , within the time period τ_{dc} . The drops then begin to coalesce and grow until the size distribution is indistinguishable from upswept area. During this second phase of growth the heat flux is changing due to the change in the drop size distribution. In the third phase the maximum drop size is equal to departure size, and no further changes in size distribution take place, and the heat flux thereafter remains constant until the next sweeping. These three phases take place during a time interval of p and are shown in Fig. 3.21.

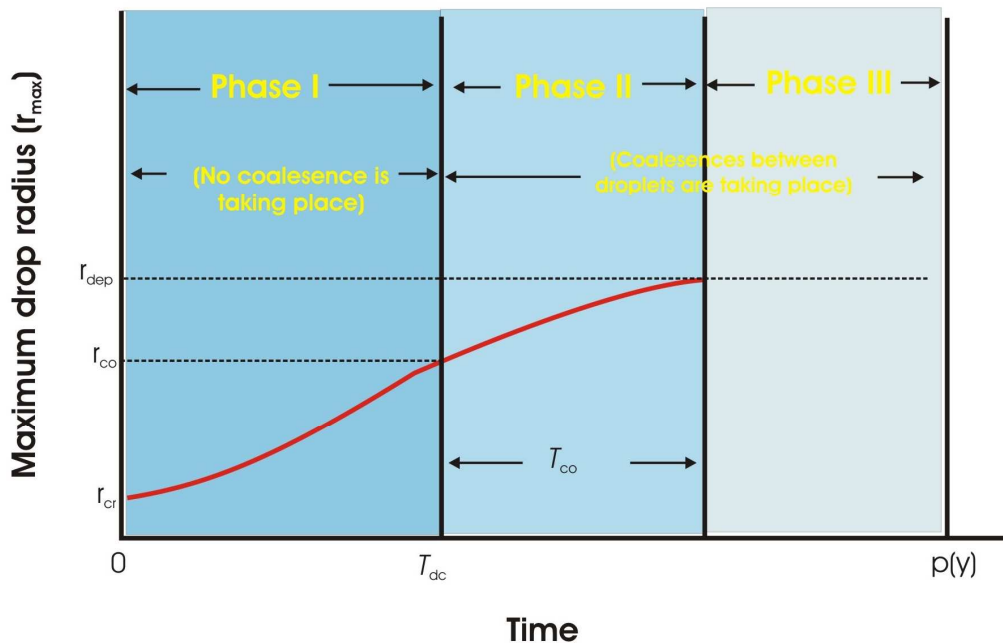


Fig. 3.21 Variation of Maximum Drop Radius Between Two Sweepings

Total heat transferred to the condenser surface in the first phase Q_{pI} can be calculated by direct condensation, just before the coalescences start. This phase is neglected due to the small effect to the local heat flux. Hence, Q_{pI} is assumed to be zero.

$$Q_{pI} = 0 \quad (3.63)$$

Total heat transferred to the surface in the second phase is obtained by integrating heat flux over the time interval τ_{co} .

$$Q_{pII} = \int_0^{\tau_{co}} q''_T(r_{max}) dt \quad (3.64)$$

Total heat transferred to the surface in the third phase is obtained by multiplying the mean heat flux at departure rate with time elapsed subtracting of sweeping period from τ_{co} .

$$Q_{pIII} = (p - \tau) q''_T(r_{dep}) \quad (3.65)$$

The time averaged local heat flux can be found by summing the energy transferred to the condenser surface in the three phases, and then dividing to sum by the total period of time elapsed (p). The final result should be multiplied by Eq. (3.57), because of the fact that the falling droplets cover an area of $(D_d(y) \frac{\pi}{16} r_{dep}^2)$ on a unit condenser surface area and their very large thermal resistances insulate the covered surface. Summing Eqs 3.63, 3.64, 3.65 and performing this operation gives the time averaged local heat flux:

$$q''_{loc}(y) = \frac{(1 - D_d(y) \frac{\pi}{16} r_{dep}^2)}{p(y)} (Q_{pI} + Q_{pII} + Q_{pIII}) \quad (3.66)$$

Since the lower regions of the condenser surface are swept more frequently than the upper regions, the local heat flux can be expected to increase with an increase in y . The average heat flux from the upper edge of the condenser surface to the height y can be expressed as:

$$q_{av}''(y) = \frac{1}{y} \int_0^y q_{loc}''(\xi) d\xi \quad (3.67)$$

On the next chapter, the calculation of all above equations will be done and the figures will be drawn. At the end of all calculation, results will be interpreted.

CHAPTER 4

RESULTS AND DISCUSSION

The mechanism of dropwise condensation on a cylindrical surface has been described before and the equations have been derived to calculate the departure size of droplets on cylindrical surface, heat flux through a single droplet, heat flux through a droplet population with and without sweeping effect.

An attempt was made to solve the resulting differential equations with the necessary boundary conditions by using the finite difference technique. System of nonlinear equations were tried to be solved by using the Newton Raphson Method. It was observed that the resulting nonlinear system of equations didn't converge to a solution. It is not known if the nonconvergence is the result of the characteristic of the system of equation or simply the result of a programming error. Therefore, experimental measurements were made to determine the departure size of the droplet at various angles on the cylindrical surface. These measured departure sizes are used in the dropwise condensation heat transfer calculations.

Secondly, Analytical model proposed in the study is used to predict the variation of the dropwise condensation heat flux as a function of the departure size will be solved. The effect of sweeping by departing drops is incorporated into the model and is calculated for cylinders of different diameters. In these calculations were performed for various vapor to condenser surface temperature differences (ΔT_f) to ascertain its effect on dropwise condensation heat transfer.

4.1 Calculation of Departure Size

The departure sizes are measured experimentally and attempt is made to calculate them analytically. The MatCAD program prepared to calculate the departure size by solving the Eq. 3.26 is given in Appendix A. Since the resulting finite difference system of equation doesn't converge a solution, no numerical result will be presented here. Instead the measured departure sizes are presented in tables and figures.

Experimental measurements of departure size were made by using the simple experimental apparatus which was explained in Chapter 3. How the departure sizes of droplet were determined is shown in Fig. 4.1 at a slope angle of $\beta=60^\circ$. As it can be seen in the figure, for $\beta=60^\circ$, the departure size of the drop is measured as 5.3 mm. The result of the measurements is shown in Table 4.1.

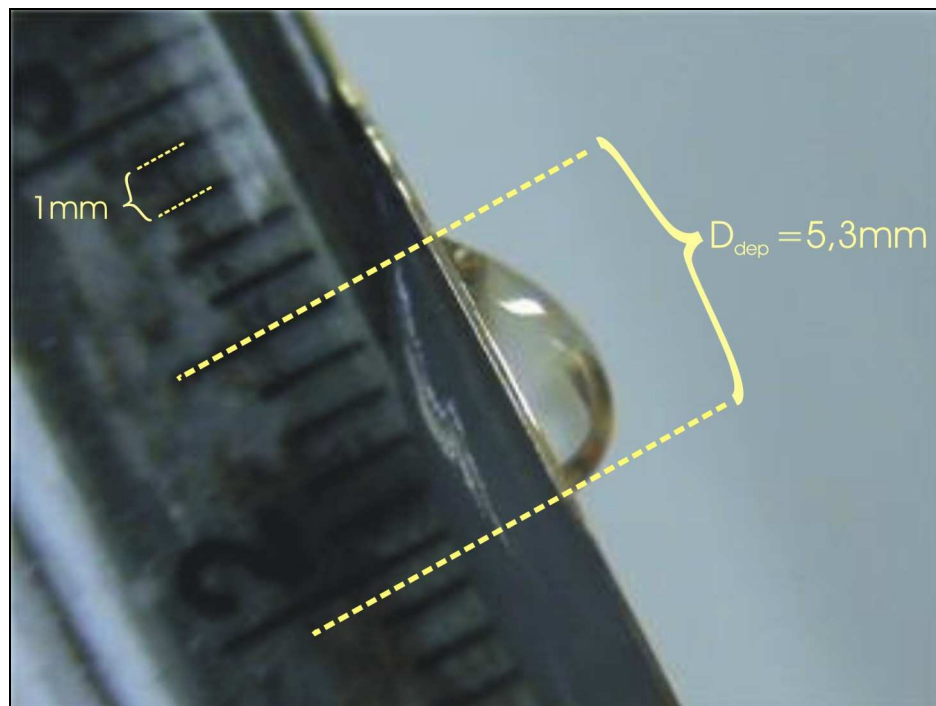


Fig. 4.1 An example of experimental calculation of departure size

Table 4.1 Experimental results of departure size for cylindrical condenser surface at β (angle) between 0 and π

Angle (β) ($^{\circ}$)	Departure Size (D_{dep}) (m)	r_{dep} (m)
1	0,011450	0,005725
10	0,009700	0,004850
20	0,008350	0,004175
30	0,007610	0,003805
40	0,006605	0,003303
50	0,005725	0,002863
60	0,005050	0,002525
70	0,004457	0,002229
80	0,004008	0,002004
90	0,003595	0,001798
100	0,0041	0,00205
110	0,00465	0,00233
120	0,0048	0,0024
130	0,0049	0,00245
140	0,0051	0,00255
150	0,00531	0,00266
160	0,00564	0,00282
170	0,0061	0,00305
180	0,0065	0,00325

In Fig 4.2 and 4.3, the profiles of the droplets at varies angles of inclination are shown for comparison purposes.

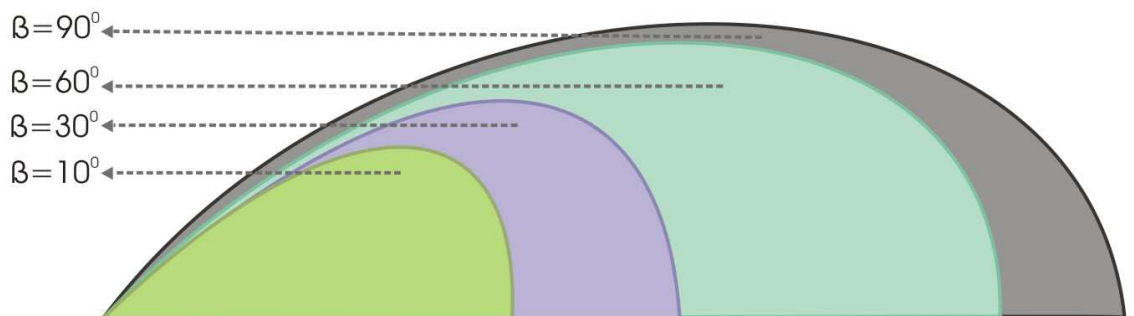


Fig. 4.2 The profiles of droplets between 0° and 90° .

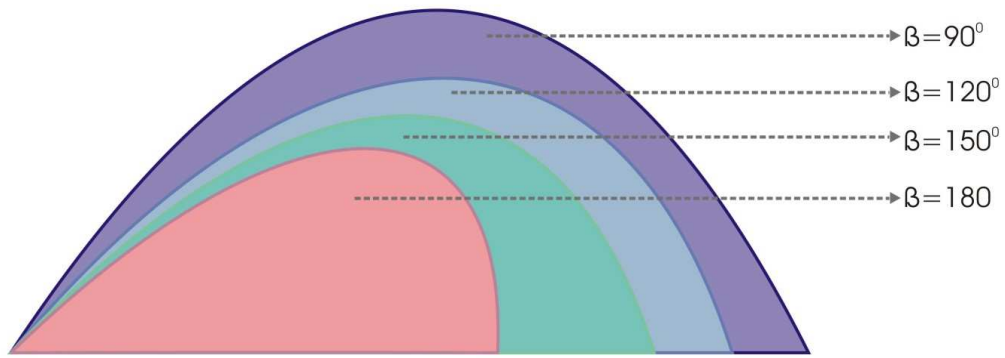


Fig. 4.3 The profiles of droplets between 90° and 180° .

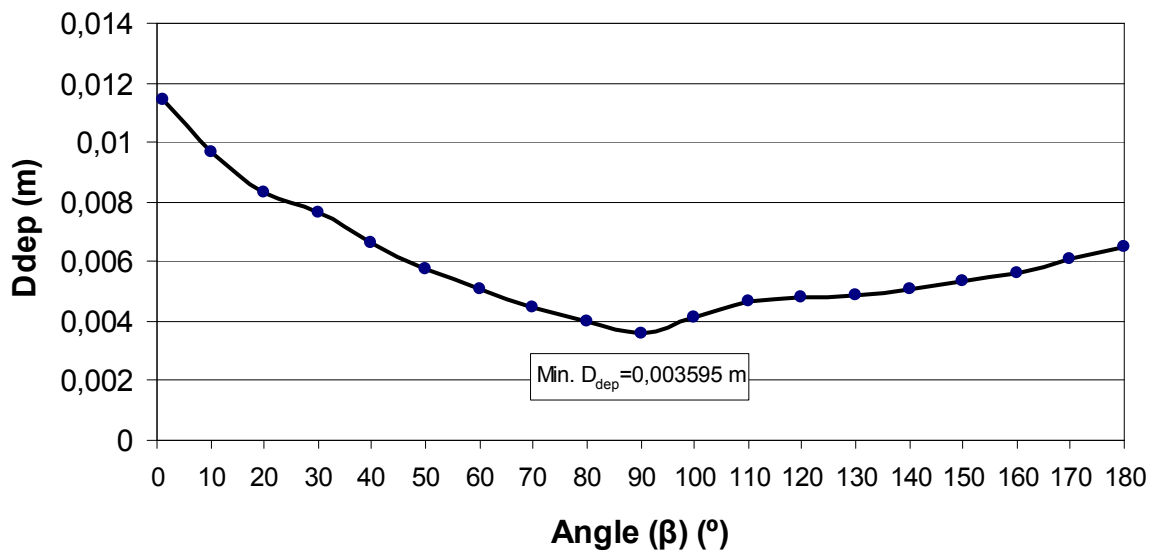


Fig. 4.4 Variation of departure size with angle β

Variation of departure size for cylindrical condenser surface with angle of inclination is shown in Fig. 4.4 to gain a better insight. It can be seen from Fig. 4.4 that the departure size of drop on cylindrical surface decreases with an increase of a surface angle until it becomes 90° (vertical position). The experimental measurements show that the maximum departure size occurs at the top of the surface (zero slope angle), whereas the minimum departure size occurs at 90° (vertical position).

4.2 Mean Heat Flux through a Single Droplet

Mean heat flux at the base of the droplet can be calculated by using Eq. 3.28. Figs 4.5 to 4.7 show the variation of the mean drop base heat flux with drop size at different vapor to base temperature differences. The computations are done by using saturated water properties at atmospheric pressure and the condensation coefficient is taken as unity. All the parameters can be seen in Table 4.2.

Table 4.2 The parameters of Eq. 3.28

Symbol	Parameter	Value and Unit
γ	Condensation coefficient	1
h_{fg}	Latent heat of vaporization of water	2257872 (J/kg)
θ	The contact angle	$65^\circ = 1.134$ rad
G	The gas constant	461.5 (J/kgK)
P_v^*	Saturation pressure corresponding to vapor temperature	0.954×10^5 (N/m ²)
σ	Surface tension of water	0.0589 (N/m)
ρ_l	Liquid density of water	958 (kg/m ³)
k	Thermal conductivity of water	0.679 (W/mK)
T_{sat}	Saturation Temperature	100 °C = 373 K

The analysis was made for three different “vapors to condenser surface temperature differences (ΔT_t)” which are 1K, 10K, 100K. The results can be seen from the Figures 4.5 to 4.7 below. These figures give the mean base heat flux for a single droplet as a function of drop radius. The minimum drop radius in these figures is taken as the critical radius which is given by equation 3.28. The critical radius depends on the surface subcooling. The critical radius for surface subcooling of 1K, 10K and 100 K are calculated as 8.10^{-7} m, 8.10^{-8} m and 8.10^{-9} m, respectively.

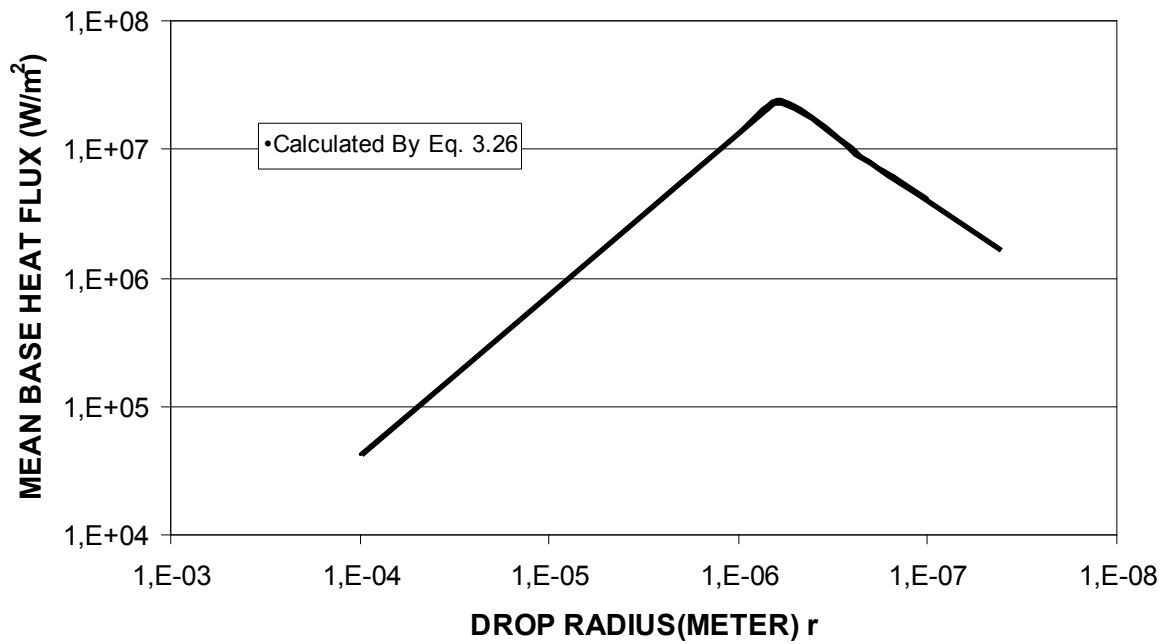


Fig.4.5 Heat Flux versus Droplet Size at $\Delta T_t = 1$ °C.

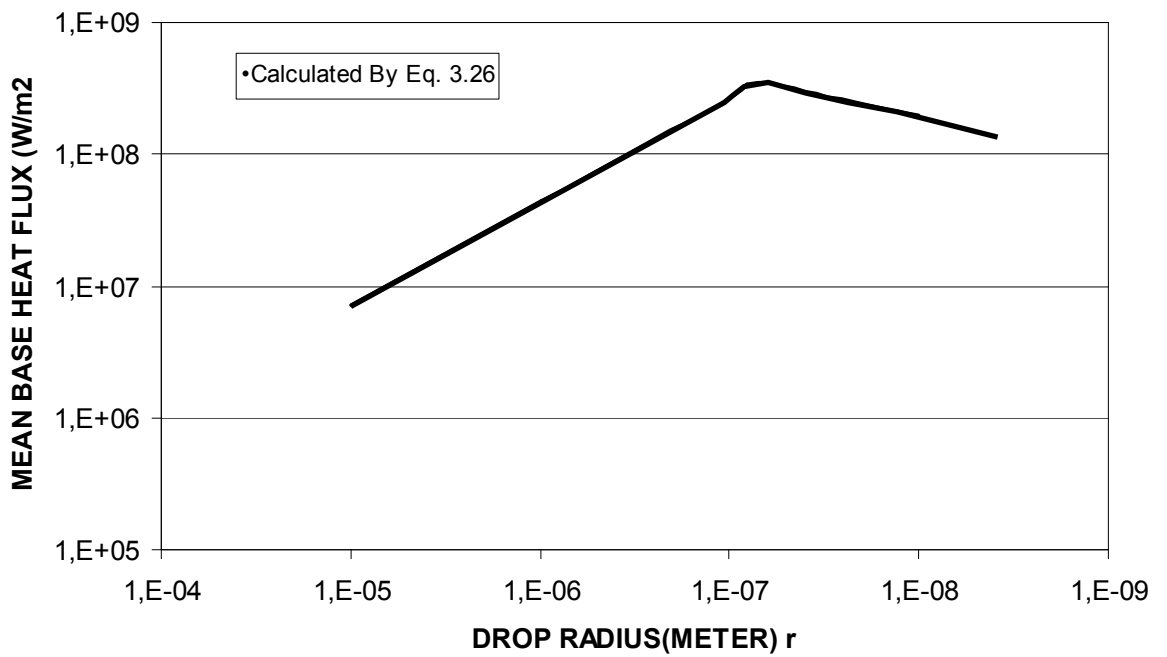


Fig.4.6 Heat Flux versus Drop Radius at $\Delta T_t = 10$ °C

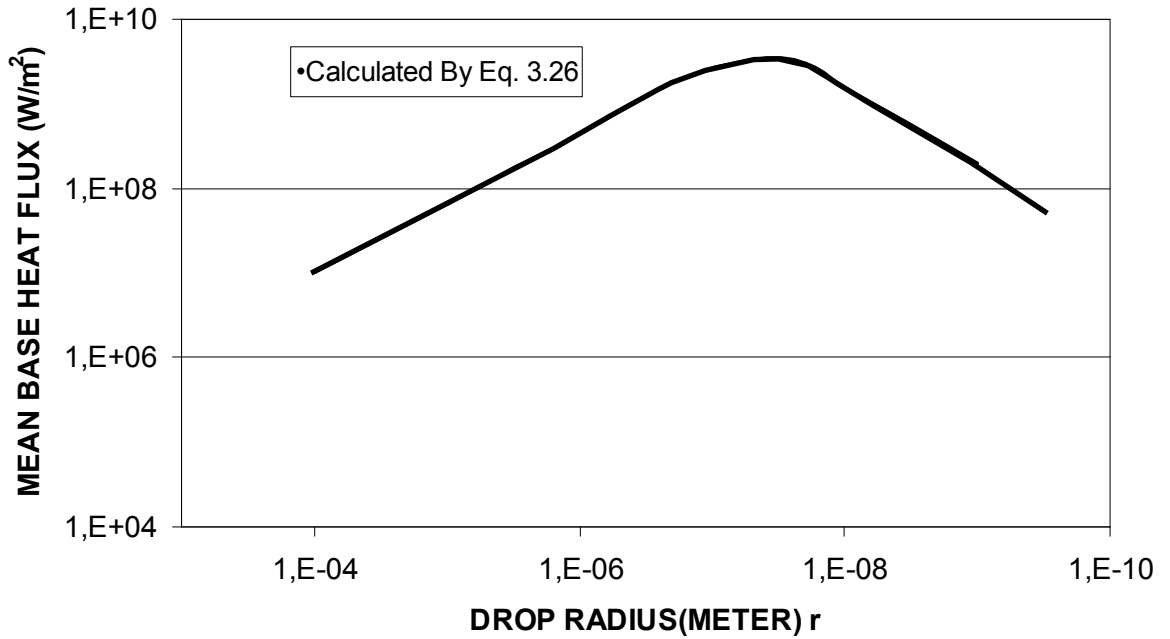


Fig.4.7 Heat Flux versus Droplet Size at $\Delta T_t = 100^\circ\text{C}$

It can be understood clearly from the figures that the mean heat flux decreases by increasing of the drop radius. From these results, it is clearly seen that large droplets have low heat flux at the base therefore they can be considered as an insulator on the condenser surface.

Since the overall thermal resistance of the drops change considerably with radius, large differences between the base temperatures of droplets of different sizes can be expected. Which results in large temperature differences in very short distances are over the condenser surface area. This effect might be quite important for condenser surface of low or moderate thermal conductivity.

4.3 Drop Departure Rate

The results of numerical calculations using the analytical model developed in second part of the Chapter III are presented in Figures 4.8 to 4.30, for the condensation of

saturated steam at atmospheric pressure. It is necessary to determine the mean spacing between the nucleation sites ($2r_{co}$). A single value was used in all computations performed here as $r_{co} = 2.6 \times 10^{-6}$ m [1]. The contact angle is taken as 65° . The condensation coefficient and the exponent n in the drop size distribution function for the coalescence region (in Eq. 2-1) are taken as 1 and $1/3$, respectively. The surface subcooling is taken 10K and 50K.

The mass of the droplet is calculated by using the drop profiles one of which is shown in Fig. 4.1. The Departure size and the height of droplet can be measured by using the profiles obtained experimentally. In Fig. 4.8, the method used to calculate the mass of the droplet is described. In this figure the droplet is contained in a rectangle, such that the height of the rectangle is equal to the height of the droplet and the length of the rectangle is equal to the base diameter of the droplet. In average, for droplets of varies shape, it is found graphically that the volume of the droplet is 0.65 of the volume of the rectangular prism that contains departing droplet.



Fig. 4.8 Method used to calculate the mass of the droplet

In general the mass of the departing droplet at any angular position is given by;

$$m_d = V d \quad (4.1)$$

In this equation, V is the volume the droplet and d is the density of the condensing liquid which will be taken as 958 kg/m^3 for saturated water at 100 C° . The volume of the rectangular prism that contains the departing droplet is equal to the product of the height, the length and the width of the droplet. The height and length of the droplet are obtained from the pictures of the drop profiles. In general, the width of the droplet is increases with an increase in the length of the droplet and its value is very close to the length. Therefore in drop volume calculations the width of the

rectangular prism that contains the droplet is taken to be equal to the length of the rectangular prism. The error caused by this approximation minimized by adjusting the average value of the ratio of the drop volume to the volume of rectangular prism which is obtained as 0.65. The results of the departing drop mass calculations are presented in table 4.3.

Table 4.3 The mass of the droplets.

Angle (β) (°)	Departure Size $D_{dep}(m)$	Height(m)	Volume (m^3)	Density (kg/m^3)	m_d (kg)
1	0,01145	0,0021	1,56293E-08	958	1,497E-05
10	0,0097	0,0021	1,32405E-08	958	1,268E-05
20	0,00835	0,0021	1,13978E-08	958	1,092E-05
30	0,00761	0,002	9,893E-09	958	9,477E-06
40	0,006605	0,002	8,5865E-09	958	8,226E-06
50	0,005725	0,002	7,4425E-09	958	7,130E-06
60	0,00505	0,0019	6,23675E-09	958	5,975E-06
70	0,004457	0,0019	5,5044E-09	958	5,273E-06
80	0,004008	0,0018	4,68936E-09	958	4,492E-06
90	0,003595	0,0018	4,20615E-09	958	4,029E-06
100	0,0041	0,002	5,33E-09	958	5,106E-06
110	0,00465	0,002	6,045E-09	958	5,791E-06
120	0,0048	0,0024	7,488E-09	958	7,174E-06
130	0,0049	0,0028	8,918E-09	958	8,543E-06
140	0,0051	0,0029	9,6135E-09	958	9,210E-06
150	0,00531	0,0031	1,06997E-08	958	1,025E-05
160	0,00564	0,0034	1,24644E-08	958	1,194E-05
170	0,0061	0,0037	1,46705E-08	958	1,405E-05
180	0,0065	0,004	1,69E-08	958	1,619E-05

The velocity of the falling droplets depends on the angle of inclination. Therefore an experiment to determine the relation between the drop velocity and the slope of the surface is devised. For this purpose, the velocity of a departing droplet is measured experimentally by using a glass surface at varies angle of inclination. During the experiments, a length on a glass surface is marked and the surface angle of the glass is set. The velocity of the departing droplet is measured by measuring the time period

that is needed for the droplet to pass this given length. The results of the velocity measurements are shown in table 4.6.

Table 4.4 The velocity of the droplets

Angle(β)	Ddep	v (m/s)
0	0,01145	0,461
10	0,0097	0,475
20	0,00835	0,483
30	0,00761	0,502
40	0,006605	0,514
50	0,005725	0,525
60	0,00505	0,535
70	0,004457	0,554
80	0,004008	0,572
90	0,003595	0,60
100	0,0041	0,58
110	0,00465	0,55
120	0,0048	0,52
130	0,0049	0,502
140	0,0051	0,485
150	0,00531	0,47
160	0,00564	0,46
170	0,0061	0,42
180	0,0065	0,39

Heat flux as a function of the departure size at various angular positions without the effect of sweeping was calculated by using Eq. 3.28. The MatCAD program prepared to calculate the departure size heat flux without sweeping effect by solving the Eq. 3.26 is given in Appendix B. The results are presented on Table 4.5 and Figure 4.9. These results were used in Eq. 3.61 to obtain drop departure rates.

Table 4.5 Departure Size Heat Flux of the Drops

	$\Delta T=10K$	$\Delta T=50K$
Angle(β)	$q_T''(r_{dep})$	$q_T''(r_{dep})$
0	1,09E+06	5,45E+06
10	1,14E+06	5,70E+06
20	1,20E+06	5,98E+06
30	1,23E+06	6,17E+06
40	1,29E+06	6,45E+06
50	1,35E+06	6,76E+06
60	1,41E+06	7,04E+06
70	1,46E+06	7,32E+06
80	1,52E+06	7,58E+06
90	1,57E+06	7,84E+06
100	1,50E+06	7,52E+06
110	1,44E+06	7,22E+06
120	1,42E+06	7,15E+06
130	1,42E+06	7,10E+06
140	1,40E+06	7,01E+06
150	1,38E+06	6,92E+06
160	1,36E+06	6,79E+06
170	1,32E+06	6,62E+06
180	1,30E+06	6,49E+06

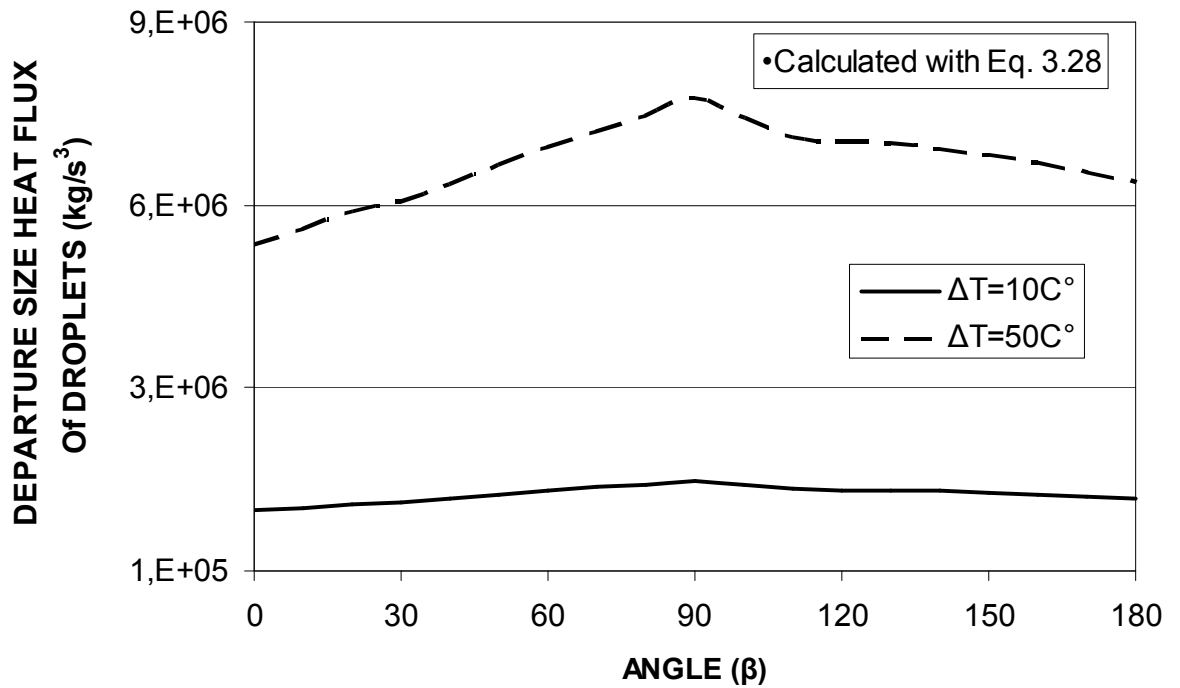


Fig. 4.9 Departure Size Heat Flux of Droplets

The time elapsed between the sweeping and the first appearance of a departing droplet τ is given by Eq. 3.54 which τ is equal to τ_{co} and can be calculated by using Eq.3.62. The MatCAD program prepared to calculate the time elapsed between the sweeping and the first appearance of a departing droplet τ given in Appendix C.

First, the heat flux for a given drop population with a given maximum drop size is calculated by using Eq. 3.38 and presented in Figures 4.10 and 4.11. Maximum drop size in these calculations ranges from r_{co} to r_{dep} . A second degree polynomial was fitted to these calculation results and the second degree polynomial obtain was shown on the Figures.

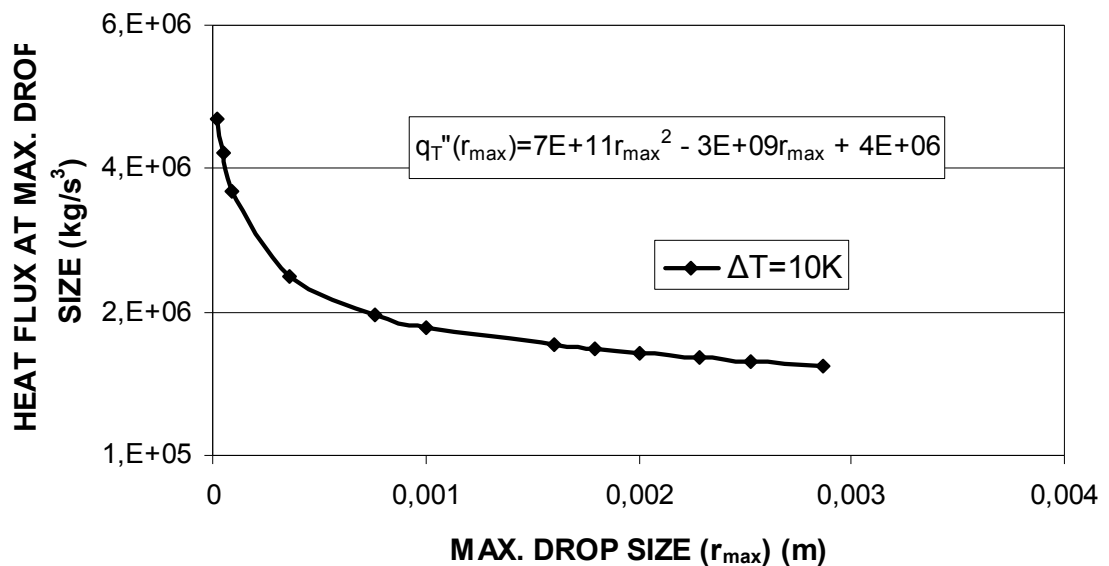


Fig 4.10 The equation of maximum drop size at $\Delta T=10K$

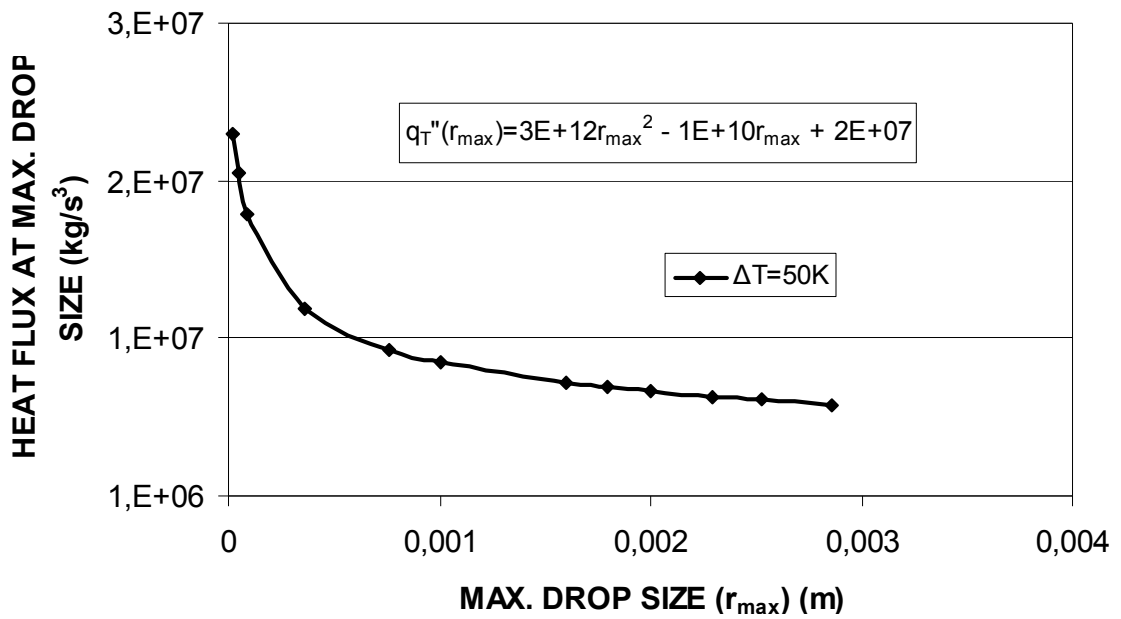


Fig 4.11 The equation of maximum drop size at $\Delta T=50K$

By using the second degree polynomial equation obtained in Figures 4.10 and 4.11. And also by using the equation the time elapsed between the sweepings as functions of angular position were calculated, and the results are presented in Table 4.6.

Table 4.6 The time elapsed between the sweepings (τ)

	$\Delta T=10K$	$\Delta T=50K$
Angle(β)	τ	τ
0	0,632	0,06
10	0,609	0,057
20	0,581	0,053
30	0,558	0,05
40	0,512	0,046
50	0,451	0,041
60	0,384	0,037
70	0,315	0,032
80	0,259	0,029
90	0,21	0,025
100	0,339	0,03
110	0,356	0,034
120	0,368	0,035
130	0,39	0,036
140	0,413	0,037
150	0,443	0,039

160	0,48	0,041
170	0,506	0,043
180	0,109	0,046

The drop departure rate is calculated by solving the integral equation given by Eq. 3.61. In this equation the integral is expressed in terms of the local values of drop departure rates by using a trapezoid rule which is explained in Chapter III. An initial value at the top the cylindrical surface where $\beta = 0$ must be assumed for the local drop departure rate since the solution of the integral equation, Eq. 3.61, requires a boundary condition at $\beta = 0$. On the other hand at $\beta = 0$ the drop is infinitely large, therefore calculations are commenced at $\beta = 1$. This approximation causes a small error in the calculations which can be lessened by taking smaller angles if high accuracy is desired. Since at $\beta = 1$ surface is very close to the top no applicable number of droplets reaches to that point and therefore the drop departure rate here is equal to the heat flux given by Eq. 3.42, divided by the latent heat and the mass of a single departing droplet. This value is also taken as the initial value for the local drop departure rate to be iterated in Eq. 3.61.

The calculations are performed for the three different values of the diameters which are 2,3 cm, 5 cm and 10 cm. Values of the local drop departure rates calculated with Eq. 3.61 are shown in Figs. 4.12 to 4.14.

Table 4.7 Drop Departure Rate at $\Delta T=10$ K

	For $\Delta T=10$ K		
Angle(β)	D=2,3 cm	D=5 cm	D=10 cm
0	32183	32183	32183
10	27603	22579	15697
20	23292	16071	8566
30	19847	11809	5046
40	17025	8880	3104
50	14714	6794	1959
60	12791	5267	1257
70	11176	4125	815
80	9808	3256	532
90	8641	2586	349
100	7639	2065	229
110	6774	1655	151

120	6022	1331	100
130	5367	1073	66
140	4794	866	43
150	4290	701	29
160	3845	568	19
170	3451	460	13
180	3102	374	8

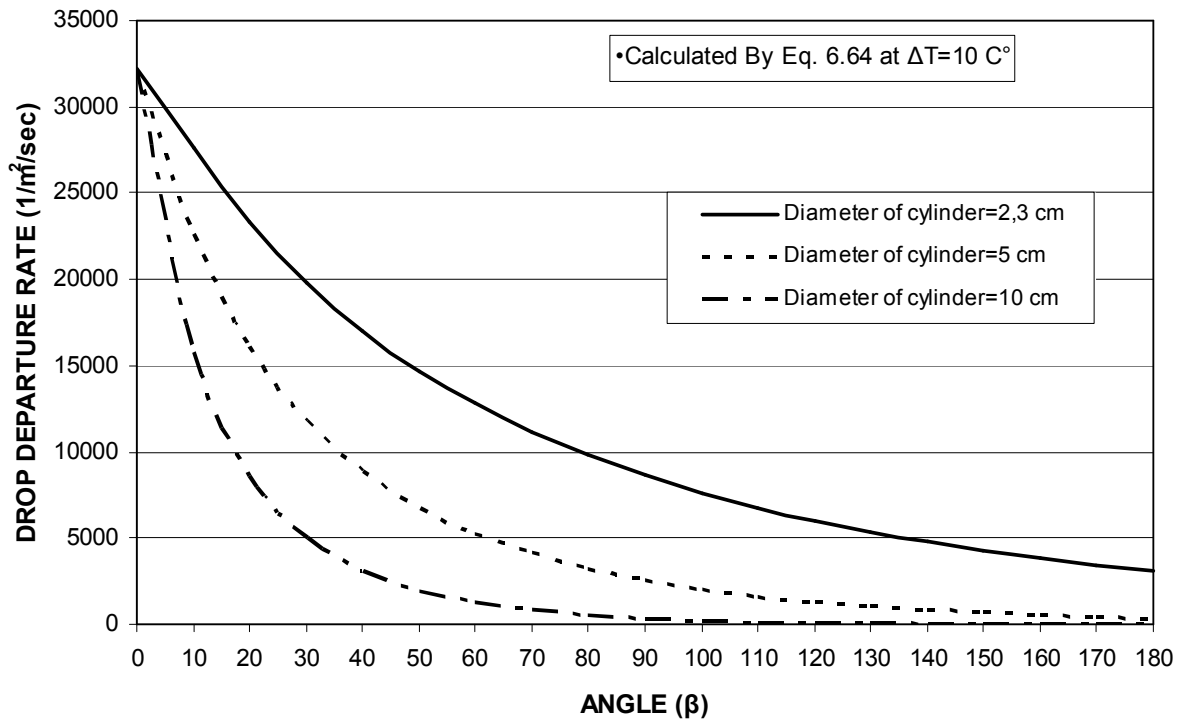


Fig 4.12 Drop Departure Rate at $\Delta T=10\text{ K}$

It is noted that the drop departure rate decreases sharply from its maximum value at the upper edge. This means that the sweeping rate becomes sufficiently large as one proceeds down the surface to reduce significantly the possibility that drops growing locally will attain the departure size.

As the cylinder diameter changes, initial value of the drop departure rate remains the same. Nevertheless, for larger cylinders the decrease of drop departure rate is faster.

For $D = 0.1\text{ m}$ at $\Delta T = 10\text{ K}$, at an angle around 100° , the drop departure rate becomes negligibly small. For $D = 0.05\text{ m}$ at $\Delta T = 10\text{ K}$ and $D = 0.023\text{ m}$ at $\Delta T = 10$ the angles around which the drop departure rate diminishes are 140° and 180° , respectively.

Table 4.8 Drop Departure Rate at $\Delta T=50$ K.

Angle(β)	For $\Delta T=50$ K		
	D=2,3 cm	D=5 cm	D=10 cm
0	160888	160888	160888
10	101491	83020	57717
20	73194	50501	26918
30	54066	32170	13745
40	42074	21944	7670
50	32939	15209	4386
60	28040	11546	2756
70	24508	9045	1788
80	20614	6844	1119
90	18442	5520	744
100	15395	4162	462
110	13280	3245	296
120	11774	2602	195
130	9583	1915	117
140	7827	1414	70
150	5800	948	39
160	5012	740	25
170	4119	549	15
180	3481	419	9

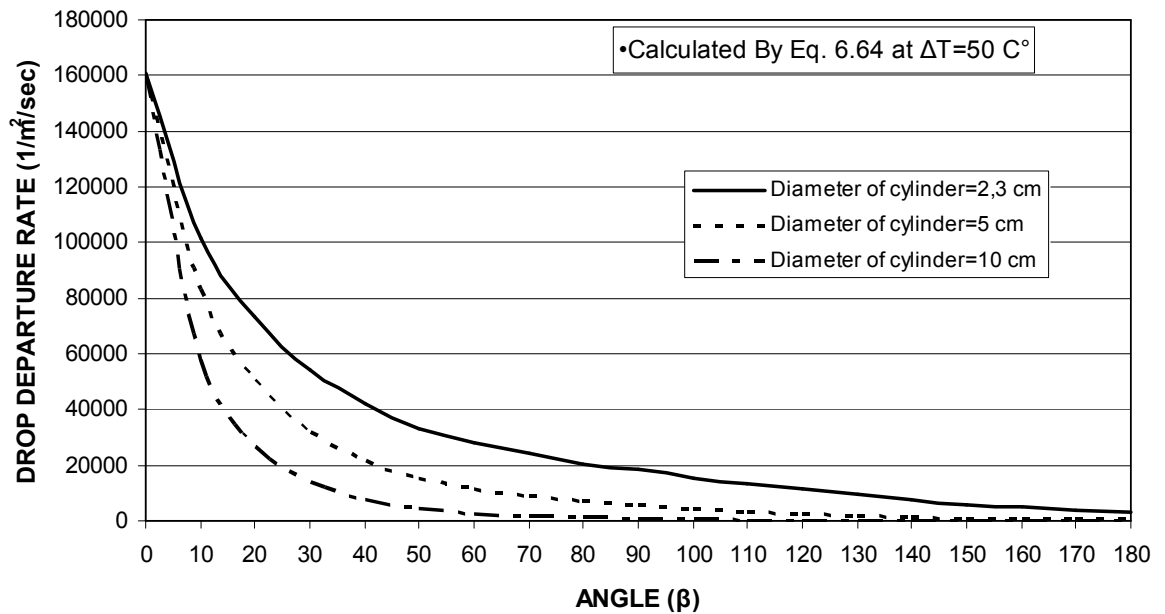


Fig 4.13 Drop Departure Rate at $\Delta T=50$ K

In Fig. 4.13 drop departure rate as function of angular position is shown at $\Delta T=50$ K. It can be seen from these figures that increasing the subcooling results in an increase

in the initial drop departure rate. This is the natural outcome of the increase in heat transfer that results from the increase of the subcooling.

When Fig. 4.12 and 4.13 are compared, it is observed that the angle at which the drop departure rate diminishes becomes smaller at larger surface subcooling. This is the natural outcome of the increase sweeping rates at higher heat transfer rates which results from higher surface subcooling.

For a better comparison drop departure rate is graphed as a function angular position at two different surface subcooling in Fig.4.14 which clearly shows the effect of the surface subcooling on drop departure rate.

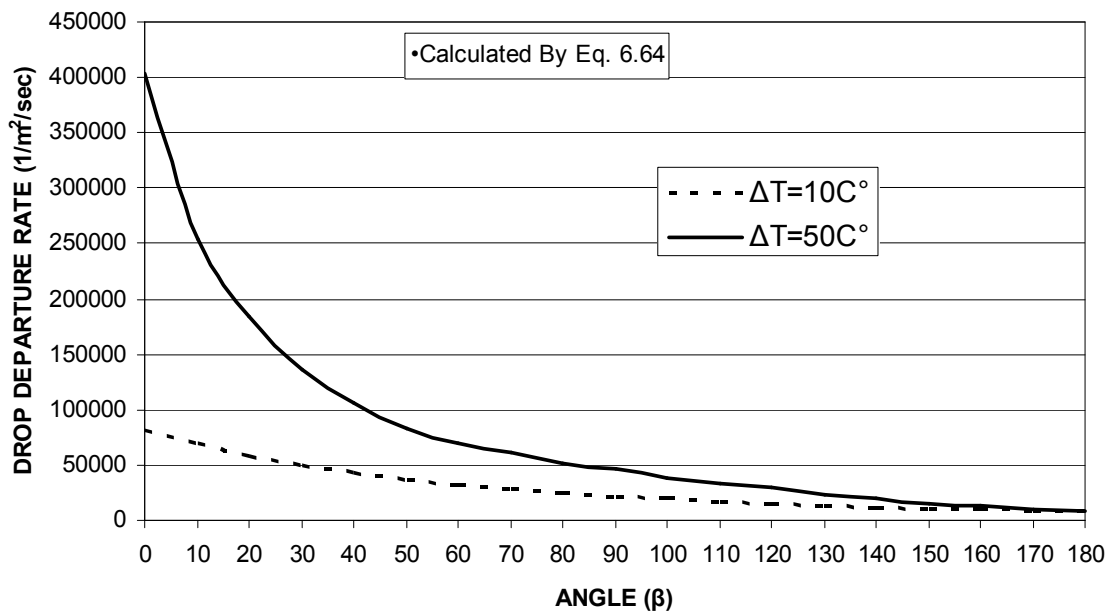


Fig 4.14 Variation of drop departure rate with angular position at D =2.3 cm

4.4 Drop Sweeping Frequency

Figures 4.15 to 4.17 show the variations of drop sweeping frequency with angular position computed with Eq. 3.43 and Eq. 3.61.

Table 4.9 Drop Sweeping Frequency

	$\Delta T=10K$	$\Delta T=50K$	$\Delta T=10K$	$\Delta T=50K$	$\Delta T=10K$	$\Delta T=50K$
Angle(β)	D=2,3 cm	D=2,3 cm	D=5 cm	D=5 cm	D=10 cm	D=10 cm
0	0	0	0	0	0	0
10	60	262	119	532	209	953
20	111	437	204	823	315	1322
30	154	564	264	1003	374	1499
40	191	660	310	1121	409	1593
50	222	735	344	1202	432	1645
60	250	796	370	1260	446	1676
70	274	849	390	1305	455	1696
80	295	894	407	1340	460	1709
90	313	933	419	1367	464	1717
100	330	967	429	1388	467	1722
110	344	996	438	1404	468	1726
120	357	1021	444	1417	470	1728
130	368	1042	449	1427	470	1729
140	378	1060	454	1434	471	1730
150	387	1073	457	1439	471	1730
160	396	1084	460	1443	471	1731
170	403	1093	462	1446	471	1731
180	409	1101	464	1448	471	1731

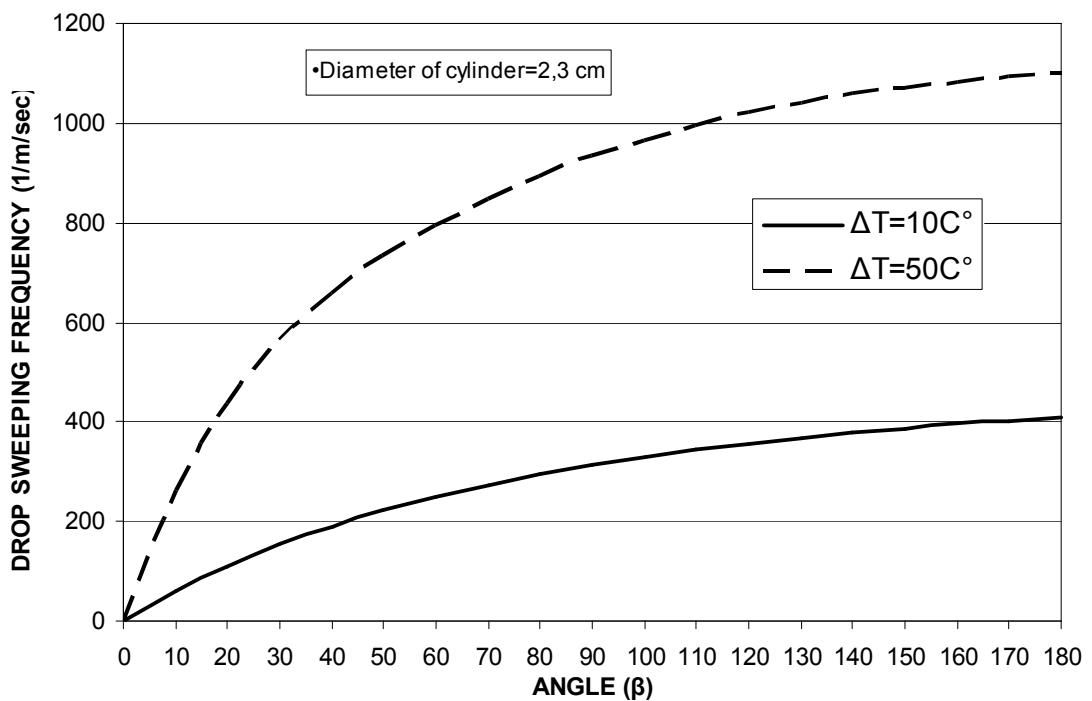


Fig. 4.15 Variation of the Sweeping Period of Falling Drops with Different Surface Angles where the cylinder diameter is 2.3 cm

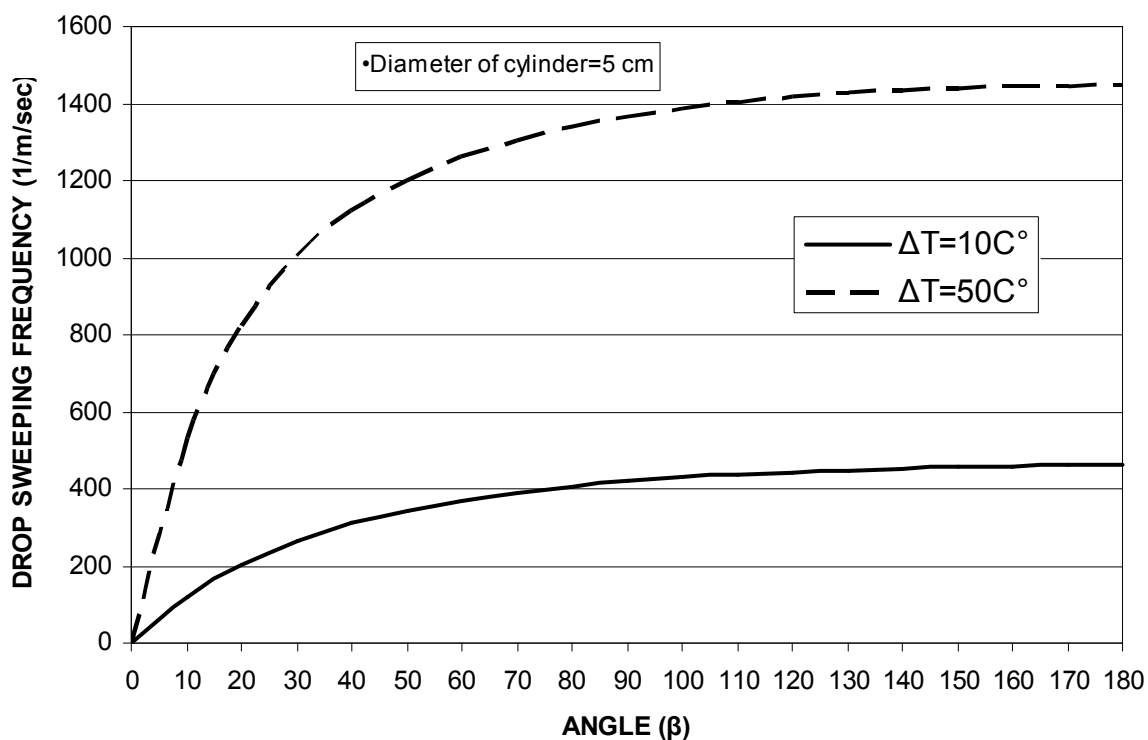


Fig. 4.16 Variation of the Sweeping Period of Falling Drops with Different Surface Angles where the cylinder diameter is 5 cm

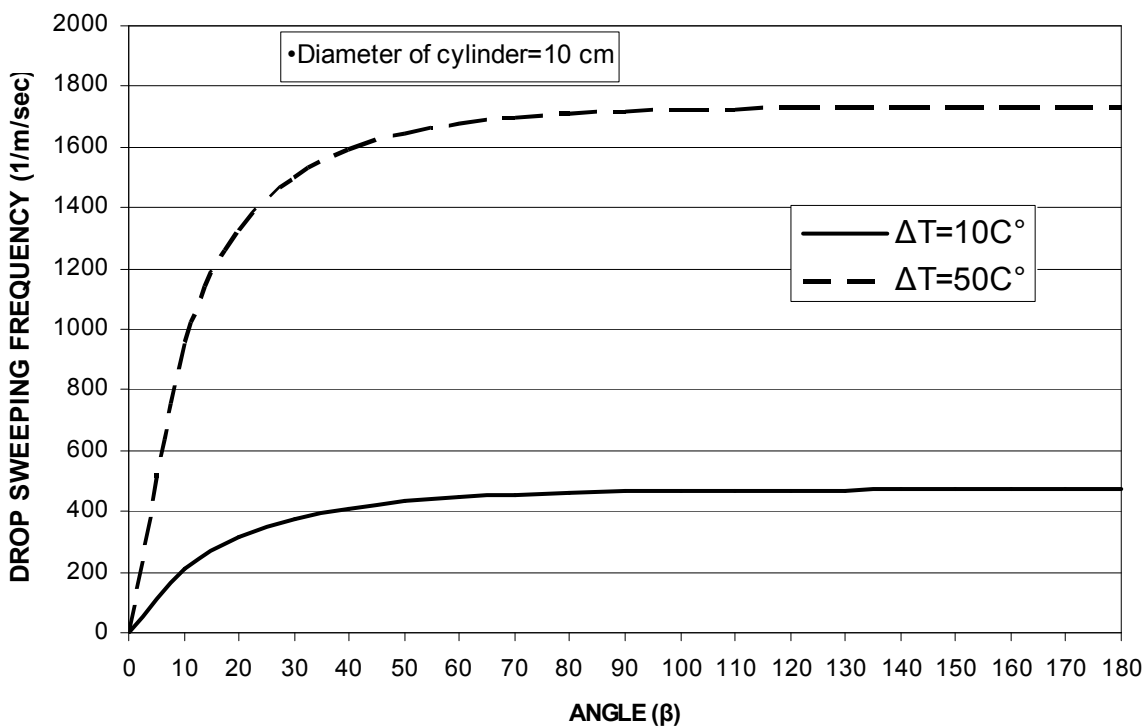


Fig. 4.17 Variation of the Sweeping Period of Falling Drops with Different Surface Angles where the cylinder diameter is 10 cm

These figures show that the sweeping frequency reach an asymptotic value. This is due to the fact that as angular position increases the surface of the cylinder swept faster as the number of departing droplets above that position increases. Faster sweeping of the surface prevents the formation of the departing droplets and eventually the surface is swept fast enough, so that no departing droplet can materialize.

It is seen from the same figures that the asymptotic value of the drop sweeping frequency is larger at larger diameters. Nevertheless, it is also observed that the effect of the diameter on sweeping frequency is not very strong.

4.5 Fraction of Condenser Area Covered By Falling Drops

The local fraction of the condenser area covered by falling droplets is given by $Dd(y) * \pi / 4 * D_{dep}^2$, where $D(y)$ is calculated from Eq. 3.59, and are plotted versus the angle of inclination, for the various subcoolings and cylindrical diameters in Figs. 4.18 to 4.20.

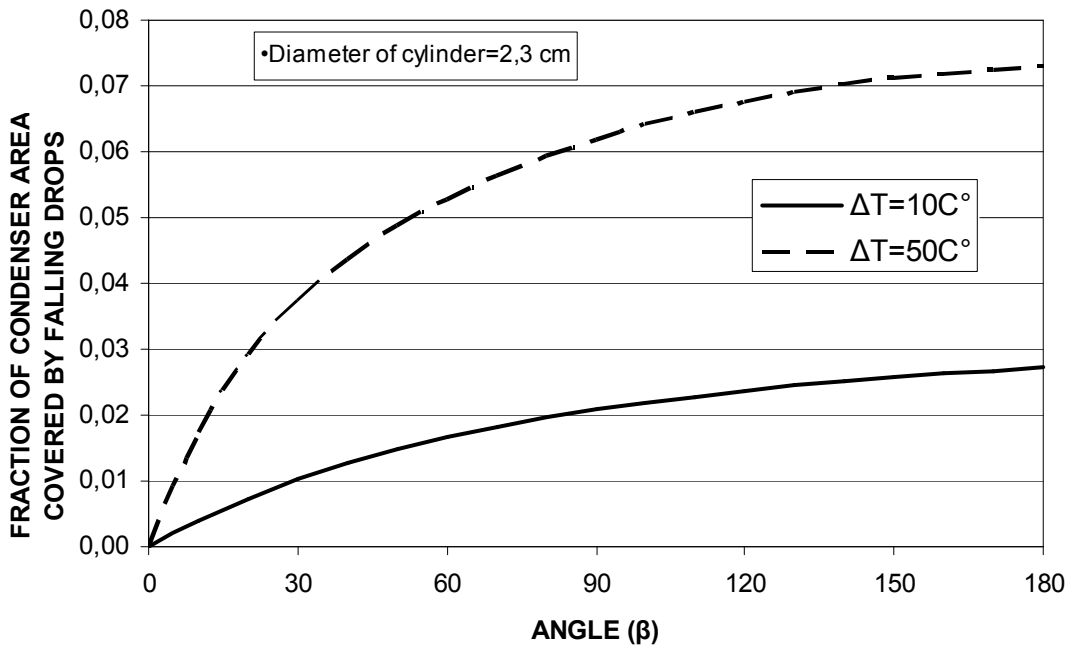


Fig. 4.18 Fraction of Condenser Area Covered by Falling Droplets Versus Angle where the cylinder diameter is 2,3 cm

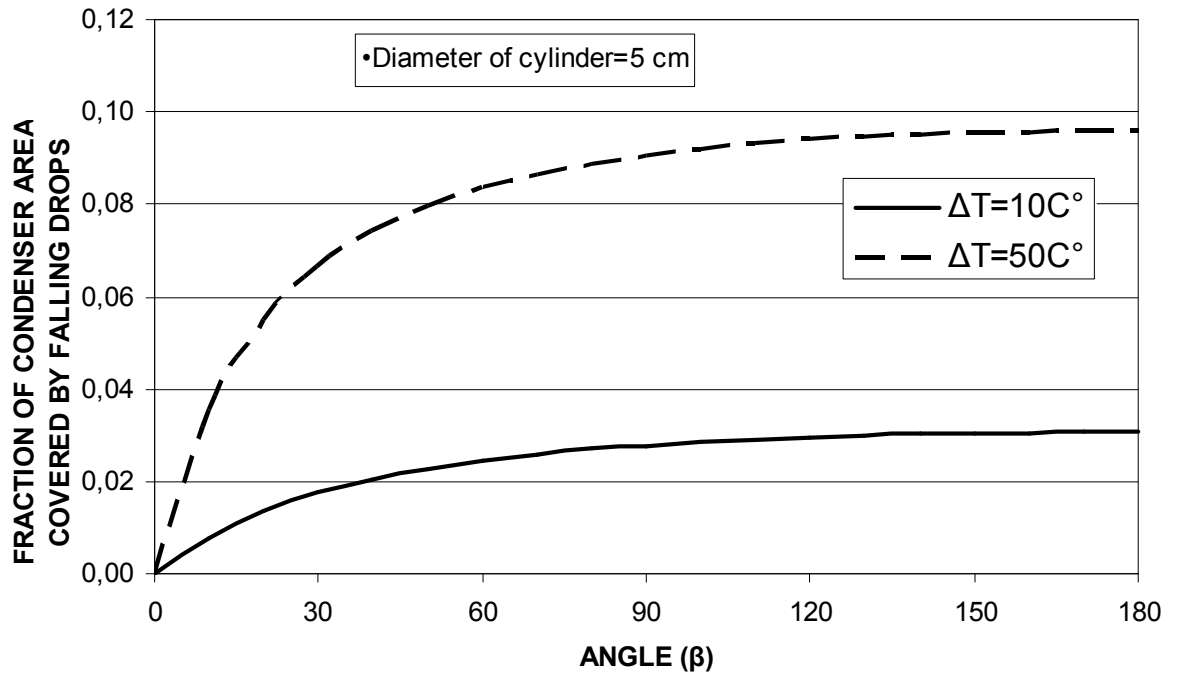


Fig. 4.19 Fraction of Condenser Area Covered by Falling Droplets Versus Angle where the cylinder diameter is 5 cm

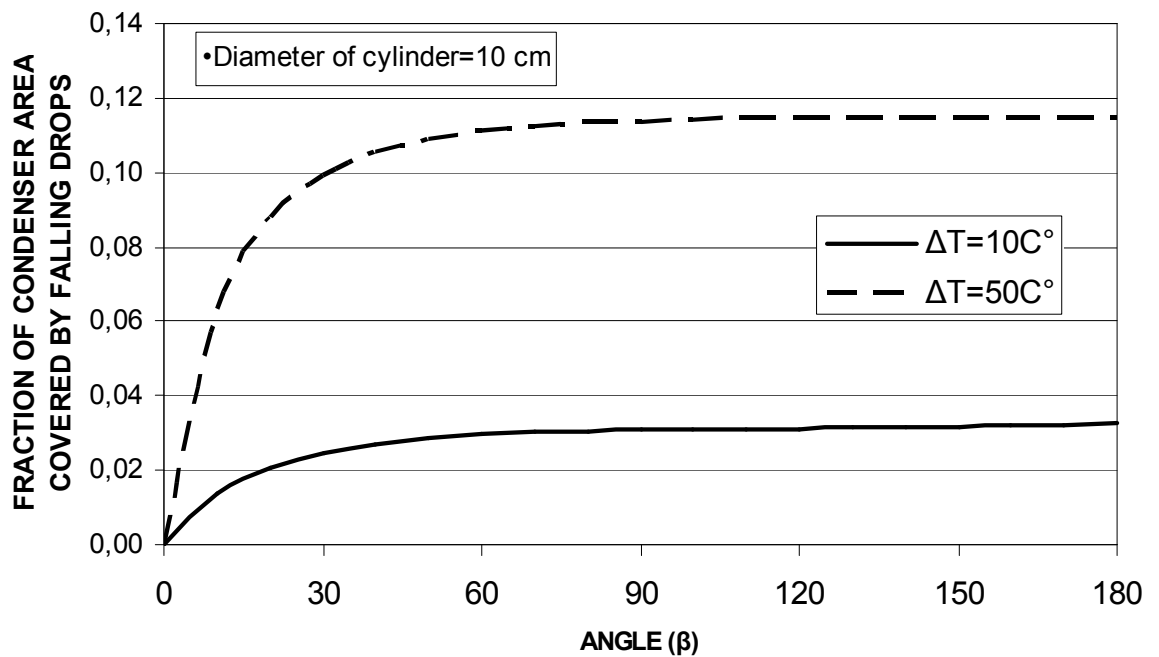


Fig. 4.20 Fraction of Condenser Area Covered by Falling Droplets Versus Angle where the cylinder diameter is 10 cm

The fraction of the condenser surface covered by the falling droplets becomes large at large angles and large subcoolings in general. Nevertheless its observed from this figures that even at large subcoolings and large cylinder diameters, the fraction of the condenser area covered by falling drops is small.

At larger diameters the surface area covered by departing droplets is larger. Nevertheless this effect seems to be feeble.

4.6 Sweeping Period of The Falling Drops

In Figures 4.21 to 4.23 the variation of sweeping period of the falling drops as a function of the angular position is presented. It is observed that the sweeping period approaches an asymptotic value at large angle.

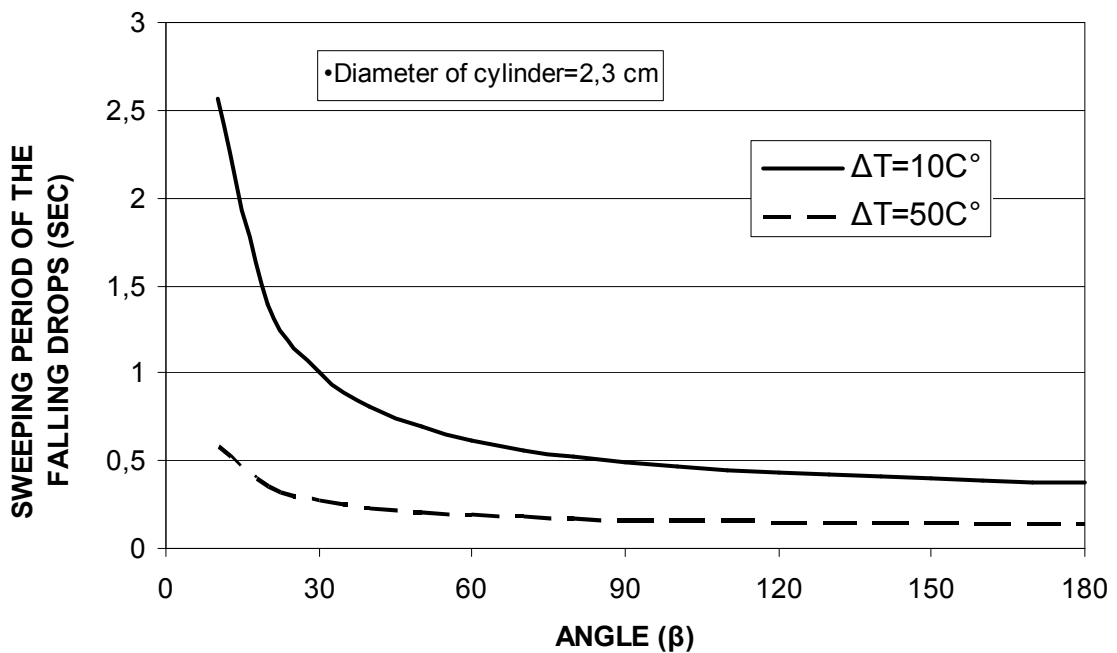


Fig. 4.21 Fraction of Condenser Area Covered by Falling Droplets Versus Angle where the cylinder diameter is 10 cm

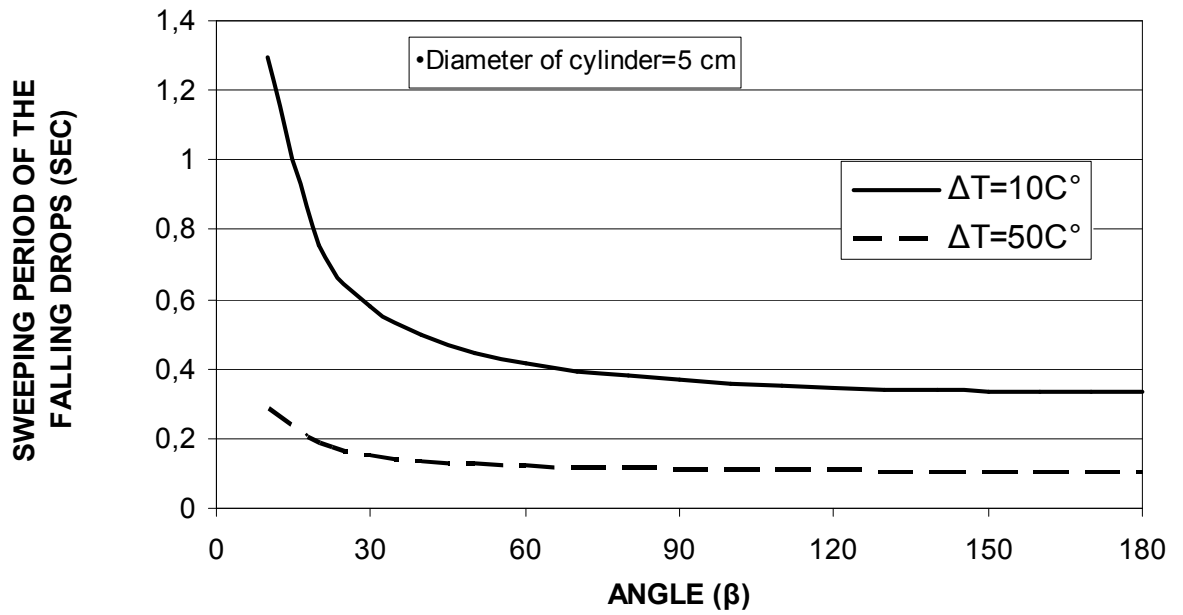


Fig. 4.22 Fraction of Condenser Area Covered by Falling Droplets Versus Angle where the cylinder diameter is 10 cm

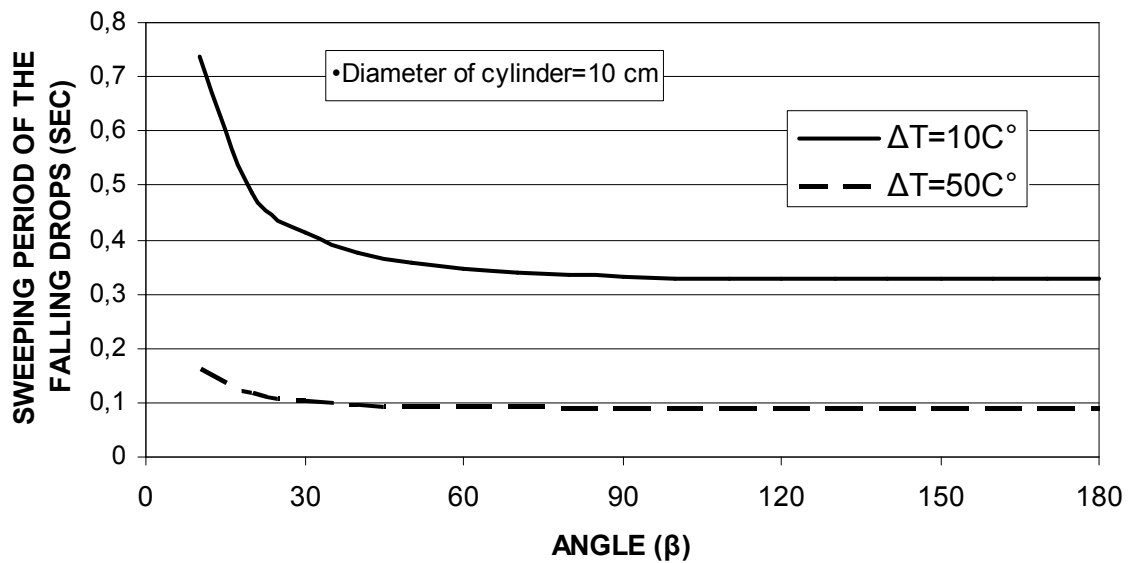


Fig. 4.23 Fraction of Condenser Area Covered by Falling Droplets Versus Angle where the cylinder diameter is 10 cm

Sweeping period decreases with an increase in a diameter of the cylinder and drops to the asymptotic value with in 30 degrees. At smaller diameters it is observed that surface subcooling as a smaller effect on sweeping period.

4.7 Local Heat Flux

The events taking place between two successive sweepings at the location of interest must be considered to determine the local heat flux on the surface. Immediately following a sweeping action drops nucleate and grow with no coalescences up to the size r_{co} , within the time period τ_{dc} . The drops then begin to coalesce and grow until the size distribution is indistinguishable from upswept area. During this second phase of growth the heat flux is changing due to the change in the drop size distribution. In the third phase the maximum drop size is equal to departure size, and no further changes in size distribution take place, and the heat flux thereafter remains constant until the next sweeping.

Total heat transferred to the condenser surface in the first phase Q_{pI} can be calculated by direct condensation, just before the coalescences start. This phase is neglected due to the small effect to the local heat flux. Hence, Q_{pI} is assumed to be zero.

Eq. 3.64 (Q_{pII}) and Eq. 3.65 (Q_{pIII}) were calculated and put into Eq. 3.66 to obtain the local heat flux. The values of the local heat flux were presented on Figures 4.24 to 4.27.

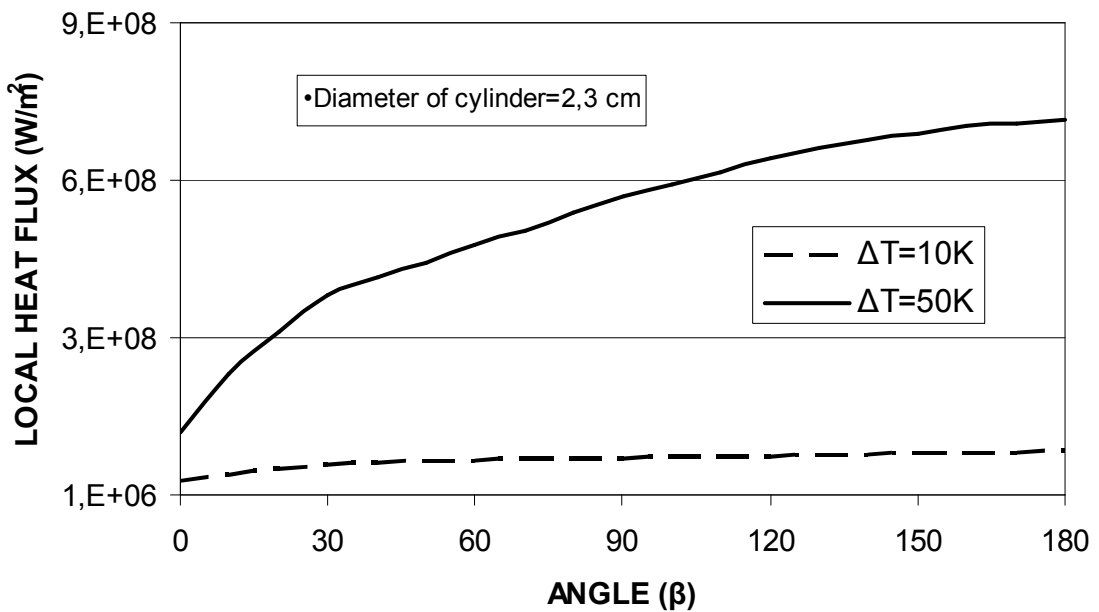


Fig 4.24 Local Heat Flux as a Function of Angle of Inclination for D=2,3 cm

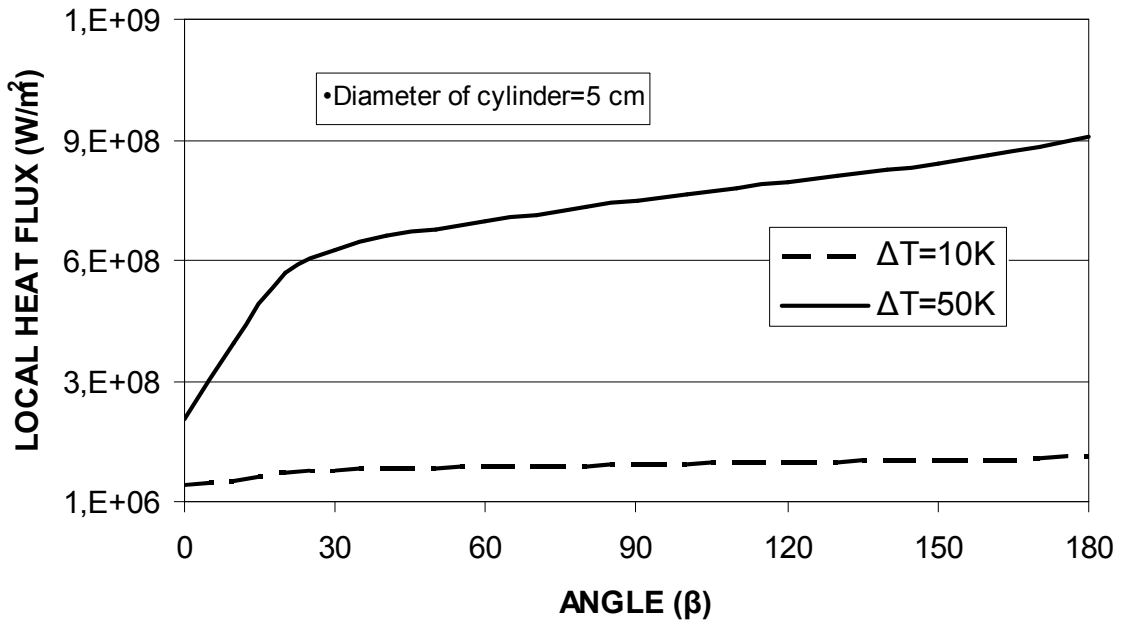


Fig 4.25 Local Heat Flux as a Function of Angle of Inclination for D=5 cm

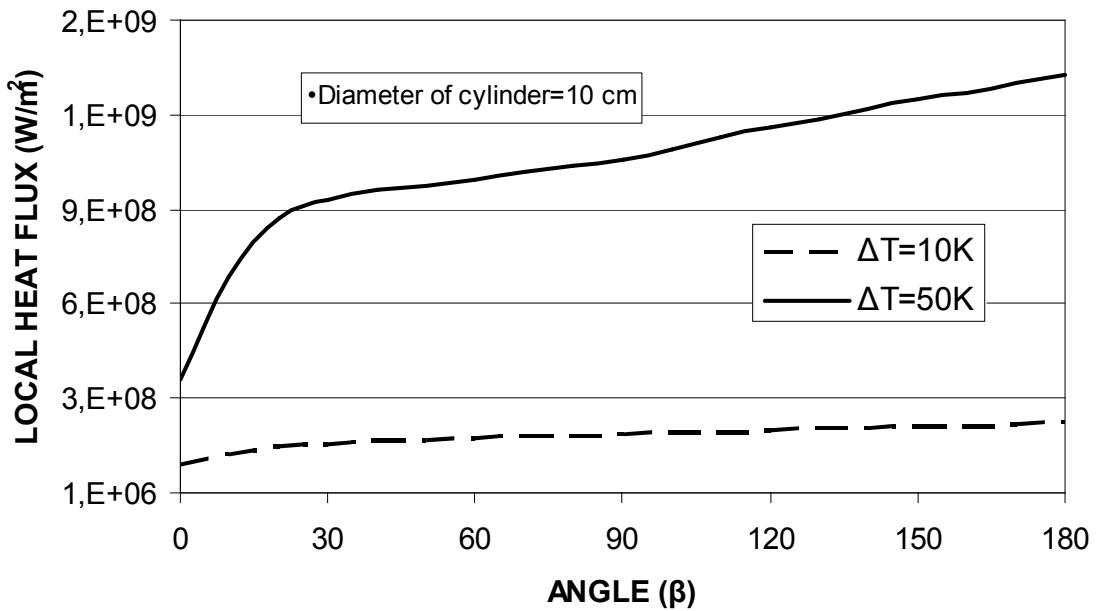


Fig 4.26 Local Heat Flux as a Function of Angle of Inclination for D=10 cm

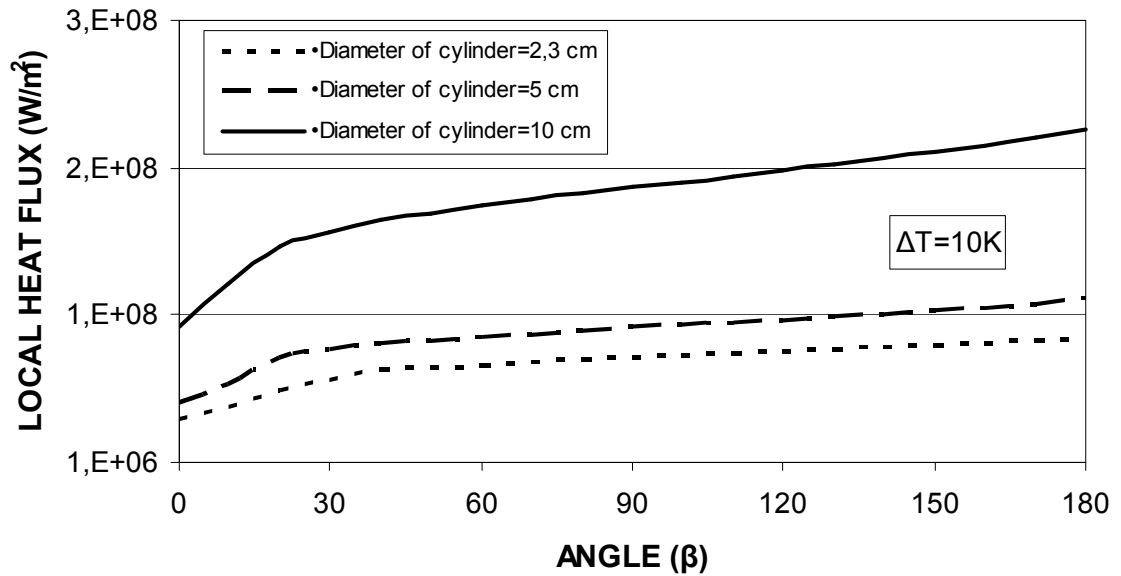


Fig 4.27 Local Heat Flux as a Function of Angle of Inclination for all diameters at $\Delta T=10K$

The variation of local heat flux as a function of angular position is shown it is clearly seen that with an increase in angular position Local heat flux increases with a decreasing rate. This is due to the sweeping effect of the departing droplet.

It is seen from the Fig. 4.27 that for the same angular position at larger diameters, the local heat flux becomes larger. That is due to the fact that at larger diameters the effect of sweeping droplets becomes larger.

4.8 Average Heat Flux

The average heat flux calculation results are presented in Figures 4.28 to 4.29.

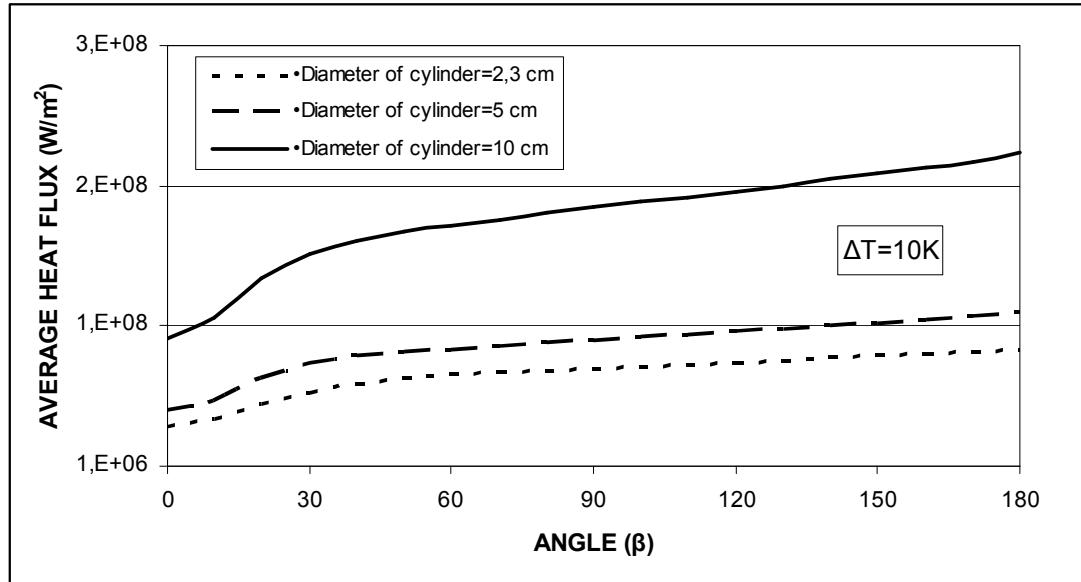


Fig 4.28 Average Heat Flux as a Function of Angle of Inclination for all diameters at $\Delta T=10K$

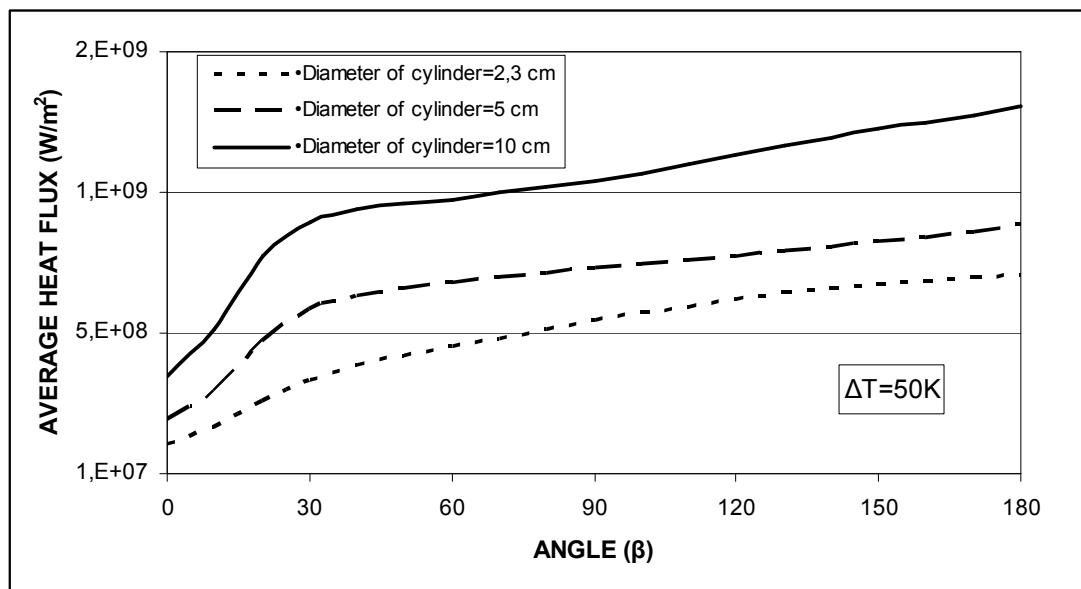


Fig 4.29 Average Heat Flux as a Function of Angle of Inclination for all diameters at $\Delta T=50K$

In these figures the average value obtained for the same location becomes larger than the local values since the local heat flux gets bigger as one gets down along the surface of the cylinder. Comparing the results of the average heat flux values at different diameters show that at larger diameters the average heat flux becomes larger. This is due to the increased sweeping effect at larger diameters.

CHAPTER 5

CONCLUSIONS

Analytical and experimental data were presented for dropwise condensation on the cylindrical surface. The calculations were performed for the three different values of the diameters which are 2,3 cm, 5 cm and 10 cm.

The departure size of drop on cylindrical surface decreases with an increase of a surface angle until it becomes 90° . The experimental measurements show that the maximum departure size occurs at the top of the surface (zero slope angle), whereas the minimum departure size occurs at 90° (vertical position)

The drop departure rate decreases sharply from its maximum value at the upper edge. This means that the sweeping rate becomes sufficiently large as one proceeds down the surface to reduce significantly the possibility that drops growing locally will attain the departure size.

The sweeping frequency reaches an asymptotic value. This is due to the fact that as angular position increases the surface of the cylinder swept faster as the number of departing droplets above that position increases. The asymptotic value of the drop sweeping frequency is larger at larger diameters. Nevertheless, it is also observed that the effect of the diameter on sweeping frequency is not very strong.

The fraction of the condenser surface covered by the falling droplets becomes large at large angles and large subcoolings in general.

Sweeping period decreases with an increase in a diameter of the cylinder and drops to the asymptotic value with in 30 degrees.

Local heat flux increases with a decreasing rate. This is due to the sweeping effect of the departing droplet. For the same angular position at larger diameters, the local heat flux becomes larger.

Larger diameters the average heat flux becomes larger. This is due to the increased sweeping effect at larger diameters.

6.1 Recommendations for Future Work

In further studies, the analytical results can be found by using MadCAD program which prepared by I and my supervisor. The results can be compared with the experimental results of this study.

It is possible to determine the results by increasing the subcoolings and cylindrical diameters to compare with the results of this study.

Various coated surface can be prepared to determine the various results which can be compared with gold surface used in this study.

One cylinder under another cylinder can be constituted. In that position, departing droplets will start sweeping from upper cylinders and continue sweeping by dropping on to bottom cylinders. Hence, the sweeping frequency of the bottom cylinder will show different attempt from the upper cylinder.

REFERENCES

1. Yamali, C., “Dropwise Condensaiton under High Gravity and at Large Subcooling”, Ph.D. Thesis, University of Michigan (1983).
2. Vemuri, S. “Experimental and Theoretical Studies on Non-Filmwise Condensation Techniques for Enhancing Heat Transfer in the Process of Steam Condensation”, Ph.D. Thesis, University of Nevada, Reno (2005).
3. E. Schmidt, W. Schurig, W. Sellschop, “Versuche uber die kondensation von wasserdampf in film — und tropenform, Tech. Mech. Thermodyn. (Forsch. Ing. Wes.), vol. 1, p. 53–63, 1930.
4. Jakob., M. , “Heat Transfer in Evaporation and Condensation – II”, Mechanical Engineering, vol. 58 , p. 729 –739, 1936.
5. E. Baer and J. M. McKelvey, “Heat Transfer in Dropwise Condensation”, Delaware Science Symposium, University of Delaware, 1958.
6. Emmons, H., “The Mechanism of Drop Condensation”, Trans. Am. Inst. Chemical Eng., vol. 35, p. 109, 1939.
7. Erb, R.A. and Thelen, E., “Dropwise Condensation”, First International Symposium on Water Desalination, Washington, D.C. (Oct. 3-9, 1965).
8. Eucken, A., “Energie- und Stoffaustausch an Grenzflächen”, Die Naturwissenschaften, vol. 14, p. 209-218, 1937.

9. Welch, J.F. and Westwater, J.W., "Microscopic Study of Dropwise Condensation", International Heat Transfer Conference, Colorado, U.S.A., p. 302, 1961.
10. McCormick, J.L. and Baer, E., "Dropwise Condensation on Horizontal Surfaces", Developments in Mechanics, Pergamon Press, N.Y., p. 749-775, 1965.
11. Umur, A. and Griffith, P., "Mechanism of Dropwise Condensation", Trans. ASME, Journal of Heat Transfer, 87C, p. 275-282, 1965.
12. McCormick, J.L. and Westwater, J.W., "Drop Dynamics and Heat Transfer during Dropwise Condensation of Water Vapor on a Horizontal Surface", Chemical Engineering Progress Symposium Series, vol. 62, no. 64, p. 120-134, 1966
13. Fatica N. and Katz, D.L, "Dropwise Condensation", Chem. Eng. Progress, vol. 45, no.11, p.661-674, 1949.
14. Sugawara, S. and Michiyoshi, I., "Dropwise Condensation", Mem. Fac. Engng, Kyoto Univ., vol. 18, No.2, 1956.
15. Wenzel, H., "Der Wärmeübergang bei der Tropfenkondensation", Linde-Ber. Tech. Wiss., vol. 18, p. 44, 1964.
16. Graham, C. and Griffith, P., "Dropsizes Distribution and Heat Transfer in Dropwise Condensation" Int. J. Heat Mass Transfer, vol. 16, p. 337-346, 1973.
17. Kodali, S., "A Study of Dropwise and Film Condensation under Variable Gravity Fields" Ph.D. thesis, University of Michigan, 1981.
18. Tanaka H., "A theoretical study of dropwise condensation", Trans. ASME Journal of Heat Transfer, vol. 97, p.72-78, 1975.

19. Glicksman, L. R. and Rose, J. W. "Dropwise Condensation-The Distribution of Drop Sizes", *Int. J. Heat and Mass Transfer*, vol.11, p. 411-425, 1973.
20. Gose, E. E., Mucciardi, A. N. and Baer, E., "Model for Dropwise Condensation on Randomly Distributed Sites", *Int. J. Heat Mass Transfer*, vol. 10, p. 15, 1967.
21. Tanasawa, I. and Tachibana, F., "A synthesis of the total process of dropwise condensation using the method of computer simulation", *Proc. Fourth Int. Heat Transfer Conference 6*, 1970.
22. Glicksman, L.R., Hunt, A.W., "Numerical Simulation of Dropwise Condensation", *Int. J. Heat Mass Transfer*, vol. 15, p. 2251-2269, 1972.
23. Le Fevre, E.J. and Rose, J.W., "A Theory of Heat Transfer by Dropwise Condensation", *Proc. of 3rd. Inter. Heat Transfer Conf.*, vol. 2, p. 362 – 375, 1966.
24. Tanaka, H., "Measurements of Dropsize Distributions during Transient Dropwise Condensation", *Trans. A.S.M.E., Journal of Heat Transfer*, vol. 97, p. 341-346, 1975.
25. Wu, H. W. and Maa, J. R., "On the heat transfer in dropwise condensation", *The Chemical Engineering Journal*, vol.12, p. 225-231, 1976.
26. Maa J. R., "Drop size distribution and heat flux of dropwise condensation", *Chemical Engineers J.*, vol.16, p. 171-176, 1978.
27. Yu-Ting Wu, Chen-Xin Yang and Xiu-Gan Yuan, "A Theoretical Study of the Effect of Surface Thermal Conductivity on Heat Transfer coefficient in Dropwise Condensation", *Numerical Heat Transfer*, part A, 40, p. 169-179, 2001.
28. Sadhal, S. S. and Plesset, M. S., "Effect of solid properties and contact angle in dropwise condensation theory", *Transactions of the ASME Journal of Heat Transfer*, vol. 101, p. 48-54, 1979.

29. Abu-Orabi, M., "Modeling of heat transfer in dropwise condensation", *Int. J. Heat Mass Transfer*, vol. 41, no. 1, p. 81-87, 1998.
30. Tower, R.E. and Westwater, J.W., "Effect of plate inclination on heat transfer during dropwise condensation of steam", *Chem. Engng Prog. Symp. Ser.*, 66 (102), p. 21-25, 1970.
31. Laplace, P.S., "Sur L'Action Capillaire", *Traite de Mecanique Celeste*, 4, Suppl. to Part X, 349-498, Paris : Courcier 1806.
32. Young, T., "An Essay on the Cohesion of Fluids", *Philos. Trans. R. Soc.*, London, vol. 95, p. 65-87, 1805.
33. Neumann, A. and Good, R.J., "The Thermodynamics of Contact Angles, 1 Heterogeneous Solid Surfaces", *J. Colloid Interface Sci.*, vol. 38, p. 341-358, 1972.
34. Bashfort, F. and Adams J.C., "An Attempt to Test the Theory of Capillary Action", Cambridge University Press, 1883.
35. Hartland, S. and Hartley, R.W., "Axisymmetric Fluid-Liquid Interfaces", Amsterdam, Elsevier Scientific Publ., 1976.
36. Chesters, A.K., "An analytical solution for the profile and volume of a small drop or bubble symmetrical about a vertical axis", *J. Fluid Mech.*, vol. 81, p. 609-624, 1977.
37. Pitts, E., "The stability of pendent liquid drops. Part 2 : Axial symmetry", *J. Fluid Mech.*, vol. 63, p. 487-508, 1974.
38. Larkin, B.K., "Numerical Solution of the Equation of Capillarity", *J. Colloid Interface Sci.*, vol. 23, p. 305-312, 1972

39. Neumann, A.W, "Contact Angles. In: Padday, J. F., (ed.): Wetting, Spreading and Adhesion", London, Academic Press, 1978.
40. Pitts, E., "The stability of pendent liquid drops. Part 1 : Drops formed in a narrow gap", J. Fluid Mech., vol. 59, p. 753-767, 1973.
41. Othmer, D.F., "The Condensation of Steam" Industrial and Engineering Chemistry, vol. 21, p. 576, 1929.
42. Sparrow, E.M. and Lin, S.H. "Condensation Heat Transfer in the Presence of a Non-Condensable Gas", J. Heat Transfer (C), vol. 86, p. 430-436, 1964.
43. Hampson, H. "The Condensation of Steam on a Tube with Filmwise or Dropwise Condensation and in the Presence of a Non-Condensable Gas", Int. Dev. In Heat Transfer, Proc. of 1961-1962. Int. Heat-Transfer Conf. Amer. Soc. Mech. Engrs., 310, 1963.
44. Potter, C.J, Tanner, D.W., Pope, D. and West, D. "Heat Transfer in Dropwise Condensation – Part II", Int. J. Heat Mass Transfer, vol. 8, p. 427-436, 1964
45. McCormick, J.L. and Westwater, J.W., "The Nucleation Sites for Dropwise Condensation", Chemical Engineering Science, vol. 20, p. 1021-1031, 1965.
46. Blackman, L. C. F., Dewar, M. J. S. and Hampson, H. "An Investigation of compounds promoting the dropwise condensation of steam," J. Applied Chem., vol. 7, p. 160-171, 1957.
47. Blackman, L. C. F. and Dewar, M. J. S. "Promoters for the dropwise condensation of steam: Parts I-IV", J. Chem. Soc., p. 162-176, 1957.
48. Das, A. K., Kilty, H. P., Marto, P. J., Andeen, B. G. and Kumar, A., "The use of an organic self-assembled monolayer coating to promote dropwise condensation

- of steam on horizontal tubes,” ASME, J. Heat Transfer, vol. 122, p. 278-286, 2000.
49. Erb, R.A. and Thelen, E., “Dropwise condensation characteristics of permanent hydrophobic systems”, U.S. Off. Saline Water Res. Dev. Rep., no. 184, 1966.
 50. Wilkins, D. G., Bromley, L. A. and Read, S. M., “Dropwise and filmwise condensation of water vapor on gold,” AIChE Journal, vol. 19, p. 119-127, 1973.
 51. Haraguchi T., Shimada S. and Kumagia S., “The effect of polyvinyl den chloride coating thickness on promotion of dropwise steam condensation”, Int J Heat Mass Transfer, vol. 34, p. 3047–3054, 1991.
 52. Holden, K.M., Wanniarachchi, A.S., Marto, P.J. and Rose, J. W., “The use of organic coating for the promotion of dropwise condensation of steam”, J. Heat Transfer, vol. 109, p. 768–774, 1987.
 53. Marto P.J., Looney D.J. and Rose J.W., “Evaluation of organic coating for the promotion of dropwise condensation of steam”, Int. J. Heat Mass Transfer, vol. 29, p. 1109–1117, 1986.
 54. O’Neill, G.A. and Westwater, J.W., “Steam condensation on electroplated silver surfaces”, Int. J. Heat Mass Transfer, vol.27, p. 1539–1549, 1984.
 55. Guo, X.F., Bai, L., Cai, Z.Y. and Lin, J.F., “Dropwise condensation on a horizontal tube”, J. Eng. Thermophys., vol. 11, p. 72–75, 1991.
 56. Yang, J.H. and Cheng, L.X., “Study on dropwise condensation heat transfer on composite electroplating surface”, Chem. Eng., vol. 24, p. 38–41, 1996.
 57. Shea F.L. and Krase, N.W., “Drop-Wise and Film Condensation of Steam”, Trans. Am. Inst. Chem. Eng., vol. 36, p. 463-470, 1940.
 58. Adams, R.A., “Calculus: Third Edition”, Addison Wesley, 1995.

59. Krischer S. and Grigull U., "Microscopic study of dropwise condensation", *Warme- und Stoffübertragung*, vol. 4, p. 48-59, 1971.

60. Yamali C. and Merte H., "Conduction heat transfer through condensation drops with variable interphase coefficients, Symposium on Fundamentals of Two-Phase Flow, Boiling and Condensation.", ASME W/A Meeting, New Orleans LA, 9-14 December, 1982.

61. Yamali, C. and Merte H., "A theory of dropwise condensation at large subcooling including the effect of the sweeping", *Heat and Mass Transfer*, Vol. 38, p. 191-202, 2002.

APPENDIX A

MATCAD SOURCE PROGRAM I DEPARTURE SIZE

$$x_s \cdot \sin(\beta) - y_s \cdot \cos(\beta) + \lambda - \frac{d}{dxs} \left[\frac{1}{\left(1 + y_{sp}(xs)\right)^2} \cdot y_{sp}(xs) \right]$$

$$y_1 \cdot \sin(\beta) - u_1 \cdot \cos(\beta) + \lambda - \left[\frac{1}{\sqrt{1 + \left(\frac{u_{i+1} - u_i}{\Delta y}\right)^2}} \cdot \left(\frac{u_{i+1} - u_i}{\Delta y}\right) - \frac{1}{\sqrt{1 + \left(\frac{u_i - u_{i-1}}{\Delta y}\right)^2}} \cdot \left(\frac{u_i - u_{i-1}}{\Delta y}\right) \right] \cdot \frac{1}{\Delta y}$$

```

res :=
neq ← 9
δ ← 1.5415
θ ← 65 · π / 180
β ← 45 · π / 180
u0 ← 0.0001
ny ← neq + 1
Δy ← δ / ny
for i ∈ 1 .. ny - 2
    y1 ← δ · (i) / ny
    u1 ← δ · (y1) - (y1)2
uinc ← δ / 100
bb ← u
i ← 0

```

$$C_0 \leftarrow -y_i \cdot \sin(\beta) + u_{i+1} \cdot \cos(\beta) + u_0 - \left[\frac{1}{\sqrt{1 + \left(\frac{u_{i+2} - u_{i+1}}{\Delta y}\right)^2}} \cdot \left(\frac{u_{i+2} - u_{i+1}}{\Delta y}\right) - \frac{1}{\sqrt{1 + \left(\frac{u_{i+1} - 0}{\Delta y}\right)^2}} \cdot \left(\frac{u_{i+1} - 0}{\Delta y}\right) \right] \cdot \frac{1}{\Delta y}$$

$i \leftarrow ny - 3$

$$C_i \leftarrow -y_i \cdot \sin(\beta) + u_{i+1} \cdot \cos(\beta) + u_0 - \left[\frac{1}{\sqrt{1 + \left(\frac{\Delta y \cdot \tan(\theta) - u_{i+1}}{\Delta y}\right)^2}} \cdot \left(\frac{\Delta y \cdot \tan(\theta) - u_{i+1}}{\Delta y}\right) - \frac{1}{\sqrt{1 + \left(\frac{u_{i+1} - u_i}{\Delta y}\right)^2}} \cdot \left(\frac{u_{i+1} - u_i}{\Delta y}\right) \right] \cdot \frac{1}{\Delta y}$$

$i \leftarrow ny - 2$

$$C_i \leftarrow -y_i \cdot \sin(\beta) + (\Delta y \cdot \tan(\theta)) \cdot \cos(\beta) + u_0 - \left[\frac{1}{\sqrt{1 + \left(\frac{0 - \Delta y \cdot \tan(\theta)}{\Delta y}\right)^2}} \cdot \left(\frac{0 - \Delta y \cdot \tan(\theta)}{\Delta y}\right) - \frac{1}{\sqrt{1 + \left(\frac{\Delta y \cdot \tan(\theta) - u_i}{\Delta y}\right)^2}} \cdot \left(\frac{\Delta y \cdot \tan(\theta) - u_i}{\Delta y}\right) \right] \cdot \frac{1}{\Delta y}$$

for iter \in 1..10

for $i \in$ 1..ny - 4

$$C_i \leftarrow -y_i \cdot \sin(\beta) + u_{i+1} \cdot \cos(\beta) + u_0 - \left[\frac{1}{\sqrt{1 + \left(\frac{u_{i+2} - u_{i+1}}{\Delta y}\right)^2}} \cdot \left(\frac{u_{i+2} - u_{i+1}}{\Delta y}\right) - \frac{1}{\sqrt{1 + \left(\frac{u_{i+1} - u_i}{\Delta y}\right)^2}} \cdot \left(\frac{u_{i+1} - u_i}{\Delta y}\right) \right] \cdot \frac{1}{\Delta y}$$

for $ie \in 0..neq - 1$
for $iv \in 0..neq - 1$
 $\psi_{ie,iv} \leftarrow 0$
for $i \in 1..nv - 4$

$$\psi_{i,i+1} \leftarrow \psi_{i,i} \leftarrow \frac{1}{uinc} \left[\left[-y_i \sin(\beta) + (u_{i+1} + uinc) \cdot \cos(\beta) + u_0 - \frac{1}{\sqrt{1 + \left[\frac{u_{i+2} - (u_{i+1} + uinc)}{\Delta y} \right]^2}} \left[\frac{u_{i+2} - (u_{i+1} + uinc)}{\Delta y} \right] - \frac{1}{\sqrt{1 + \left[\frac{(u_{i+1} + uinc) - u_1}{\Delta y} \right]^2}} \right] \right]$$

$$\psi_{i,i+2} \leftarrow \frac{1}{uinc} \left[\left[-y_i \sin(\beta) + u_{i+1} \cdot \cos(\beta) + u_0 - \frac{1}{\sqrt{1 + \left[\frac{(u_{i+2} + uinc) - (u_{i+1})}{\Delta y} \right]^2}} \left[\frac{(u_{i+2} + uinc) - (u_{i+1})}{\Delta y} \right] - \frac{1}{\sqrt{1 + \left[\frac{(u_{i+1}) - u_1}{\Delta y} \right]^2}} \left[\frac{(u_{i+1}) - u_1}{\Delta y} \right] \right] \right]$$

$$\psi_{i,i} \leftarrow \frac{1}{uinc} \left[\left[-y_i \sin(\beta) + u_{i+1} \cdot \cos(\beta) + u_0 - \frac{1}{\sqrt{1 + \left[\frac{(u_{i+2}) - (u_{i+1})}{\Delta y} \right]^2}} \left[\frac{(u_{i+2}) - (u_{i+1})}{\Delta y} \right] - \frac{1}{\sqrt{1 + \left[\frac{(u_{i+1}) - (u_1 + uinc)}{\Delta y} \right]^2}} \left[\frac{(u_{i+1}) - (u_1 + uinc)}{\Delta y} \right] \right] \right]$$

$$\psi_{i,nv-10} \leftarrow \frac{1}{uinc} \left[\left[-y_i \sin(\beta) + u_{i+1} \cdot \cos(\beta) + (u_0 + uinc) - \frac{1}{\sqrt{1 + \left[\frac{(u_{i+2}) - (u_{i+1})}{\Delta y} \right]^2}} \left[\frac{(u_{i+2}) - (u_{i+1})}{\Delta y} \right] - \frac{1}{\sqrt{1 + \left[\frac{(u_{i+1}) - (u_1)}{\Delta y} \right]^2}} \left[\frac{(u_{i+1}) - (u_1)}{\Delta y} \right] \right] \right]$$

$$\left[\left[\frac{(u_{i+1} + uinc) - u_1}{\Delta y} \right] \right] \frac{1}{\Delta y} \left[-y_i \sin(\beta) + u_{i+1} \cdot \cos(\beta) + u_0 - \frac{1}{\sqrt{1 + \left(\frac{u_{i+2} - u_{i+1}}{\Delta y} \right)^2}} \left(\frac{u_{i+2} - u_{i+1}}{\Delta y} \right) - \frac{1}{\sqrt{1 + \left(\frac{u_{i+1} - u_1}{\Delta y} \right)^2}} \left(\frac{u_{i+1} - u_1}{\Delta y} \right) \right] \right] \frac{1}{\Delta y}$$

$$- \left[-y_i \sin(\beta) + u_{i+1} \cdot \cos(\beta) + u_0 - \frac{1}{\sqrt{1 + \left(\frac{u_{i+2} - u_{i+1}}{\Delta y} \right)^2}} \left(\frac{u_{i+2} - u_{i+1}}{\Delta y} \right) - \frac{1}{\sqrt{1 + \left(\frac{u_{i+1} - u_1}{\Delta y} \right)^2}} \left(\frac{u_{i+1} - u_1}{\Delta y} \right) \right] \right] \frac{1}{\Delta y}$$

$$- \left[-y_i \sin(\beta) + u_{i+1} \cdot \cos(\beta) + u_0 - \frac{1}{\sqrt{1 + \left(\frac{u_{i+2} - u_{i+1}}{\Delta y} \right)^2}} \left(\frac{u_{i+2} - u_{i+1}}{\Delta y} \right) - \frac{1}{\sqrt{1 + \left(\frac{u_{i+1} - u_1}{\Delta y} \right)^2}} \left(\frac{u_{i+1} - u_1}{\Delta y} \right) \right] \right] \frac{1}{\Delta y}$$

$$- \left[-y_i \sin(\beta) + u_{i+1} \cdot \cos(\beta) + u_0 - \frac{1}{\sqrt{1 + \left(\frac{u_{i+2} - u_{i+1}}{\Delta y} \right)^2}} \left(\frac{u_{i+2} - u_{i+1}}{\Delta y} \right) - \frac{1}{\sqrt{1 + \left(\frac{u_{i+1} - u_1}{\Delta y} \right)^2}} \left(\frac{u_{i+1} - u_1}{\Delta y} \right) \right] \right] \frac{1}{\Delta y}$$

$$\begin{aligned}
& i \leftarrow ny - 3 \\
\psi_{i,i+1} \leftarrow \psi_{i,i} & \leftarrow \frac{1}{u_{inc}} \left[-y_i \sin(\beta) + (u_{i+1} + u_{inc}) \cos(\beta) + u_0 - \frac{1}{\sqrt{1 + \left(\frac{\Delta y \tan(\theta) - (u_{i+1} + u_{inc})}{\Delta y} \right)^2}} \left[\frac{\Delta y \tan(\theta) - (u_{i+1} + u_{inc})}{\Delta y} \right] - \frac{1}{\sqrt{1 + \left(\frac{(u_{i+1} + u_{inc}) - (u_i)}{\Delta y} \right)^2}} \right] \\
\psi_{i,i} \leftarrow \frac{1}{u_{inc}} & \left[-y_i \sin(\beta) + u_{i+1} \cos(\beta) + u_0 - \frac{1}{\sqrt{1 + \left(\frac{\Delta y \tan(\theta) - (u_{i+1})}{\Delta y} \right)^2}} \left[\frac{\Delta y \tan(\theta) - (u_{i+1})}{\Delta y} \right] - \frac{1}{\sqrt{1 + \left(\frac{(u_{i+1}) - (u_i + u_{inc})}{\Delta y} \right)^2}} \left[\frac{(u_{i+1}) - (u_i + u_{inc})}{\Delta y} \right] \right] \\
\psi_{i,ny-10} \leftarrow \frac{1}{u_{inc}} & \left[-y_i \sin(\beta) + u_{i+1} \cos(\beta) + (u_0 + u_{inc}) - \frac{1}{\sqrt{1 + \left(\frac{\Delta y \tan(\theta) - (u_{i+1})}{\Delta y} \right)^2}} \left[\frac{\Delta y \tan(\theta) - (u_{i+1})}{\Delta y} \right] - \frac{1}{\sqrt{1 + \left(\frac{(u_{i+1}) - (u_i)}{\Delta y} \right)^2}} \left[\frac{(u_{i+1}) - (u_i)}{\Delta y} \right] \right] \\
& i \leftarrow ny - 10 \\
\psi_{i,i+1} \leftarrow \psi_{i,i} & \leftarrow \frac{1}{u_{inc}} \left[-y_i \sin(\beta) + (u_{i+1} + u_{inc}) \cos(\beta) + u_0 - \frac{1}{\sqrt{1 + \left(\frac{u_{i+2} - (u_{i+1} + u_{inc})}{\Delta y} \right)^2}} \left[\frac{u_{i+2} - (u_{i+1} + u_{inc})}{\Delta y} \right] - \frac{1}{\sqrt{1 + \left(\frac{(u_{i+1} + u_{inc}) - 0}{\Delta y} \right)^2}} \left[\frac{(u_{i+1} + u_{inc}) - 0}{\Delta y} \right] \right] \\
\psi_{i,i+2} \leftarrow \frac{1}{u_{inc}} & \left[-y_i \sin(\beta) + u_{i+1} \cos(\beta) + u_0 - \frac{1}{\sqrt{1 + \left(\frac{(u_{i+2} + u_{inc}) - (u_{i+1})}{\Delta y} \right)^2}} \left[\frac{(u_{i+2} + u_{inc}) - (u_{i+1})}{\Delta y} \right] - \frac{1}{\sqrt{1 + \left(\frac{(u_{i+1}) - 0}{\Delta y} \right)^2}} \left[\frac{(u_{i+1}) - 0}{\Delta y} \right] \cdot \frac{1}{\Delta y} \right] - \left[-y_i \right]
\end{aligned}$$

$$\begin{aligned}
& \left[\frac{1}{u_i} \left[\frac{(u_{i+1} + u_{inc}) - u_i}{\Delta y} \right] \cdot \frac{1}{\Delta y} \right] - \left[-y_i \sin(\beta) + u_{i+1} \cos(\beta) + u_0 - \frac{1}{\sqrt{1 + \left(\frac{\Delta y \tan(\theta) - u_{i+1}}{\Delta y} \right)^2}} \left(\frac{\Delta y \tan(\theta) - u_{i+1}}{\Delta y} \right) - \frac{1}{\sqrt{1 + \left(\frac{u_{i+1} - u_i}{\Delta y} \right)^2}} \left(\frac{u_{i+1} - u_i}{\Delta y} \right) \right] \cdot \frac{1}{\Delta y} \\
& \left[\frac{1}{\Delta y} \right] - \left[-y_i \sin(\beta) + u_{i+1} \cos(\beta) + u_0 - \frac{1}{\sqrt{1 + \left(\frac{\Delta y \tan(\theta) - u_{i+1}}{\Delta y} \right)^2}} \left(\frac{\Delta y \tan(\theta) - u_{i+1}}{\Delta y} \right) - \frac{1}{\sqrt{1 + \left(\frac{u_{i+1} - u_i}{\Delta y} \right)^2}} \left(\frac{u_{i+1} - u_i}{\Delta y} \right) \right] \cdot \frac{1}{\Delta y} \\
& \left[\frac{1}{\Delta y} \right] - \left[-y_i \sin(\beta) + u_{i+1} \cos(\beta) + u_0 - \frac{1}{\sqrt{1 + \left(\frac{\Delta y \tan(\theta) - u_{i+1}}{\Delta y} \right)^2}} \left(\frac{\Delta y \tan(\theta) - u_{i+1}}{\Delta y} \right) - \frac{1}{\sqrt{1 + \left(\frac{u_{i+1} - u_i}{\Delta y} \right)^2}} \left(\frac{u_{i+1} - u_i}{\Delta y} \right) \right] \cdot \frac{1}{\Delta y} \\
& \left[\frac{(u_{i+1} + u_{inc}) - 0}{\Delta y} \right] \cdot \frac{1}{\Delta y} - \left[-y_i \sin(\beta) + u_{i+1} \cos(\beta) + u_0 - \frac{1}{\sqrt{1 + \left(\frac{u_{i+2} - u_{i+1}}{\Delta y} \right)^2}} \left(\frac{u_{i+2} - u_{i+1}}{\Delta y} \right) - \frac{1}{\sqrt{1 + \left(\frac{u_{i+1} - 0}{\Delta y} \right)^2}} \left(\frac{u_{i+1} - 0}{\Delta y} \right) \right] \cdot \frac{1}{\Delta y} \\
& \sin(\beta) + u_{i+1} \cos(\beta) + u_0 - \frac{1}{\sqrt{1 + \left(\frac{u_{i+2} - u_{i+1}}{\Delta y} \right)^2}} \left(\frac{u_{i+2} - u_{i+1}}{\Delta y} \right) - \frac{1}{\sqrt{1 + \left(\frac{u_{i+1} - 0}{\Delta y} \right)^2}} \left(\frac{u_{i+1} - 0}{\Delta y} \right) \cdot \frac{1}{\Delta y}
\end{aligned}$$

$$\begin{aligned}
\psi_{i,i+2} &\leftarrow \frac{1}{\text{uinc}} \left[-y_i \sin(\beta) + u_{i+1} \cos(\beta) + u_0 - \left[\frac{1}{\sqrt{1 + \left(\frac{u_{i+2} + \text{uinc} - u_{i+1}}{\Delta y} \right)^2}} \left[\frac{u_{i+2} - u_{i+1}}{\Delta y} \right] - \frac{1}{\sqrt{1 + \left(\frac{u_{i+1} - 0}{\Delta y} \right)^2}} \left[\frac{u_{i+1} - 0}{\Delta y} \right] \right] \cdot \frac{1}{\Delta y} \right] \\
\psi_{i,ny-10} &\leftarrow \frac{1}{\text{uinc}} \left[-y_i \sin(\beta) + u_{i+1} \cos(\beta) + (u_0 + \text{uinc}) - \left[\frac{1}{\sqrt{1 + \left(\frac{u_{i+2} - u_{i+1}}{\Delta y} \right)^2}} \left[\frac{u_{i+2} - u_{i+1}}{\Delta y} \right] - \frac{1}{\sqrt{1 + \left(\frac{u_{i+1} - 0}{\Delta y} \right)^2}} \left[\frac{u_{i+1} - 0}{\Delta y} \right] \right] \cdot \frac{1}{\Delta y} \right] - y_i \\
i &\leftarrow ny - 2 \\
\psi_{i,i} &\leftarrow \frac{1}{\text{uinc}} \left[-y_i \sin(\beta) + (\Delta y \tan(\theta)) \cos(\beta) + u_0 - \left[\frac{1}{\sqrt{1 + \left(\frac{0 - (\Delta y \tan(\theta))}{\Delta y} \right)^2}} \left[\frac{0 - (\Delta y \tan(\theta))}{\Delta y} \right] - \frac{1}{\sqrt{1 + \left(\frac{(\Delta y \tan(\theta)) - u_1}{\Delta y} \right)^2}} \left[\frac{(\Delta y \tan(\theta))}{\Delta y} \right] \right] \right] \\
\psi_{i,ny-10} &\leftarrow \frac{1}{\text{uinc}} \left[-y_i \sin(\beta) + (\Delta y \tan(\theta)) \cos(\beta) + (u_0 + \text{uinc}) - \left[\frac{1}{\sqrt{1 + \left(\frac{0 - (\Delta y \tan(\theta))}{\Delta y} \right)^2}} \left[\frac{0 - (\Delta y \tan(\theta))}{\Delta y} \right] - \frac{1}{\sqrt{1 + \left(\frac{(\Delta y \tan(\theta)) - u_1}{\Delta y} \right)^2}} \left[\frac{(\Delta y \tan(\theta))}{\Delta y} \right] \right] \right] \\
\text{del} &\leftarrow -(\psi^{-1}) \cdot C \\
u &\leftarrow u + \text{del} \\
\text{bb} &\leftarrow \text{augment}(\text{bb}, \text{del})
\end{aligned}$$

$$\begin{aligned}
&\left[\begin{array}{l} y_i \sin(\beta) + u_{i+1} \cos(\beta) + u_0 - \left[\frac{1}{\sqrt{1 + \left(\frac{u_{i+2} - u_{i+1}}{\Delta y} \right)^2}} \left(\frac{u_{i+2} - u_{i+1}}{\Delta y} \right) - \frac{1}{\sqrt{1 + \left(\frac{u_{i+1} - 0}{\Delta y} \right)^2}} \left(\frac{u_{i+1} - 0}{\Delta y} \right) \right] \cdot \frac{1}{\Delta y} \\ \sin(\beta) + u_{i+1} \cos(\beta) + u_0 - \left[\frac{1}{\sqrt{1 + \left(\frac{u_{i+2} - u_{i+1}}{\Delta y} \right)^2}} \left(\frac{u_{i+2} - u_{i+1}}{\Delta y} \right) - \frac{1}{\sqrt{1 + \left(\frac{u_{i+1} - 0}{\Delta y} \right)^2}} \left(\frac{u_{i+1} - 0}{\Delta y} \right) \right] \cdot \frac{1}{\Delta y} \end{array} \right] \\
&\left[\begin{array}{l} - \left(\frac{u_1 + \text{uinc}}{\Delta y} \right) \cdot \frac{1}{\Delta y} \left[-y_i \sin(\beta) + (\Delta y \tan(\theta)) \cos(\beta) + u_0 - \left[\frac{1}{\sqrt{1 + \left(\frac{0 - \Delta y \tan(\theta)}{\Delta y} \right)^2}} \left(\frac{0 - \Delta y \tan(\theta)}{\Delta y} \right) - \frac{1}{\sqrt{1 + \left(\frac{\Delta y \tan(\theta) - u_1}{\Delta y} \right)^2}} \left(\frac{\Delta y \tan(\theta) - u_1}{\Delta y} \right) \right] \cdot \frac{1}{\Delta y} \right] \\ \frac{\tan(\theta) - u_1}{\Delta y} \cdot \frac{1}{\Delta y} \left[-y_i \sin(\beta) + (\Delta y \tan(\theta)) \cos(\beta) + u_0 - \left[\frac{1}{\sqrt{1 + \left(\frac{0 - \Delta y \tan(\theta)}{\Delta y} \right)^2}} \left(\frac{0 - \Delta y \tan(\theta)}{\Delta y} \right) - \frac{1}{\sqrt{1 + \left(\frac{\Delta y \tan(\theta) - u_1}{\Delta y} \right)^2}} \left(\frac{\Delta y \tan(\theta) - u_1}{\Delta y} \right) \right] \cdot \frac{1}{\Delta y} \right] \end{array} \right]
\end{aligned}$$

APPENDIX B

MATCAD SOURCE PROGRAM II TOTAL HEAT FLUX WITHOUT SWEEPING EFFECT

$$\begin{array}{llll}
 \gamma := 1 & P_v := 0.954 \cdot 10^5 \left(\frac{\text{N}}{\text{m}^2} \right) & n := \frac{1}{3} & \theta := 65 \\
 \\
 h_{fg} := 2257872 \left(\frac{\text{J}}{\text{kg}} \right) & \theta_{\text{rad}} := 1.134 & T_{\text{sat}} := 371\text{K} & r_{\text{co}} := 2.6 \cdot 10^{-6} \text{m} \\
 \\
 G_{\text{gas}} := 461.5 \left(\frac{\text{J}}{\text{kg} \cdot \text{K}} \right) & \sigma := 0.0589 \left(\frac{\text{N}}{\text{m}} \right) & T_s := 364\text{K} & \rho_l := 958 \left(\frac{\text{kg}}{\text{m}^3} \right) \\
 \\
 k := 679 \cdot 10^{-3} \left(\frac{\text{W}}{\text{m} \cdot \text{K}} \right) & & & \\
 \\
 k_1 := \left(2 \cdot \frac{\gamma}{2 - \gamma} \right) \cdot \left[\frac{1}{[2 \cdot (3.14)]^{\frac{1}{2}}} \right] \cdot \left(\frac{h_{fg}^2 \cdot P_v}{G_{\text{gas}}^{\frac{2}{3}} \cdot T_{\text{sat}}^{\frac{2}{3}}} \right) & & k_2 := \left(\frac{2 \cdot T_{\text{sat}} \cdot \sigma}{h_{fg} \cdot \rho_l} \right) & \\
 \\
 k_1 = 5.479 \times 10^9 \frac{\text{kg}}{\text{s}^3} & & k_2 = 2.02 \times 10^{-8} \text{m} \cdot \text{K} & +
 \end{array}$$

$$\Delta T_t := 50 \quad r_{dep} := 3.25 \cdot 10^{-3}$$

+

$$r_{col} := \frac{2.6 \cdot 10^{-6}}{3.25 \cdot 10^{-3}}$$

$$r_{col} \rightarrow .800000000000000000000000e-3$$

$$\beta := \frac{3.25 \cdot 10^{-3}}{4.098 \cdot 10^{-8}}$$

$$\beta \rightarrow 79306.979014153245486$$

$$q_{trdep} := \int_{r_{col}}^1 \left(2 \cdot k_1 \cdot \frac{B}{r_{dep}^2 \cdot r^2 \cdot T_{sat}} \right) \cdot (r_{dep} \cdot r \cdot \Delta T_t - k_2 \cdot \sin(\theta)) \cdot \left[-\cos(\theta) + \left(1 + \frac{B \cdot \cos(\theta)}{r_{dep} \cdot r} \right) \cdot \ln(1 + \beta \cdot r) \right] \cdot n \cdot (r^{n-1}) \, dr$$

$$q_{trdep} = 6.488 \times 10^6$$

APPENDIX C

MATCAD SOURCE PROGRAM III THE TIME ELAPSED BETWEEN THE SWEEPINGS

$$\rho_1 := 958 \qquad \theta_{\text{rad}} := 1.134 \qquad \theta := 65$$

$$\text{hfg} := 2257872 \qquad n := \frac{1}{3} \qquad \text{Kvol} := 1.135513581$$

$$\text{rco} := 2.6 \cdot 10^{-6} \qquad \text{rdep} := 0.00325$$

$$\Delta T_t := 50 \qquad \text{qt}(\text{rmax}) := 3 \cdot 10^{12} \cdot \text{rmax}^2 - 1 \cdot 10^{10} \cdot \text{rmax} + 2 \cdot 10^7$$

$$\tau_{\text{co}} := \int_{\text{rco}}^{\text{rdep}} \frac{\left[\frac{n \cdot \rho_1 \cdot \text{Kvol} \cdot \text{hfg}}{3.14 \cdot (1 + n)} \right] \cdot \left[1 + n \cdot \text{rco}^{n+1} \cdot \text{rmax}^{-(n+1)} \right]}{\text{qt}(\text{rmax})} \text{drmax}$$

$$\tau_{\text{co}} = 0.046$$

APPENDIX D

MATCAD SOURCE PROGRAM IV DROP DEPARTURE RATE BETWEEN 0° TO 90°

hfg := 2257872

v := 0.475

qt_r := 1.14 · 10⁶

md := 1.268 · 10⁻⁶

Ddep := 0.0097

τco := 0.609

fd₀ := 32183

fd₁ := 27603

h := 0.002

$$x_1 := \frac{qt_r}{md \cdot hfg} \cdot \left[1 - \frac{3.14 \cdot Ddep^2}{4 \cdot v} \cdot \left(\frac{fd_1 + fd_0}{2} \right) \cdot h \right] \cdot \left[1 - \tau co \cdot Ddep \cdot \left(\frac{fd_1 + fd_0}{2} \right) \cdot h \right] - fd_1$$

x₁ → 227559.91740780206766

$$v1 := 0.483$$

$$qt_{r1} := 1.2 \cdot 10^6$$

$$md1 := 1.092 \cdot 10^{-5}$$

$$Ddep1 := 0.00835$$

$$\tau_{co1} := 0.581$$

$$h1 := 0.002$$

$$fd_2 := 23292$$

$$x_2 := \frac{qt_{r1}}{md1 \cdot hfg} \left[1 - \frac{3.14 \cdot Ddep1^2}{4 \cdot v1} \cdot \left(\frac{fd_0 + 2fd_1 + fd_2}{2} \right) \cdot h1 \right] \cdot \left[1 - \tau_{co1} \cdot Ddep1 \cdot \left(\frac{fd_0 + 2fd_1 + fd_2}{2} \right) \cdot h1 \right] - fd_2$$

$$x_2 \rightarrow -1038.226664613479248$$

$$v2 := 0.502$$

$$qt_{r2} := 1.239 \cdot 10^6$$

$$md2 := 9.477 \cdot 10^{-5}$$

$$Ddep2 := 0.00761$$

$$\tau_{co2} := 0.558$$

$$h_2 := 0.002$$

$$fd_3 := 19847$$

$$x_3 := \frac{qt_{r2}}{md2 \cdot hfg} \left[1 - \frac{3.14 \cdot Ddep2^2}{4 \cdot v2} \cdot \left(\frac{fd_0 + 2fd_1 + 2fd_2 + fd_3}{2} \right) \cdot h_2 \right] \cdot \left[1 - \tau_{co2} \cdot Ddep2 \cdot \left(\frac{fd_0 + 2fd_1 + 2fd_2 + fd_3}{2} \right) \cdot h_2 \right] - fd_3$$

$$x_3 \rightarrow -17866.771436682513603$$

$$v3 := 0.514$$

$$qt_{r3} := 1.297 \cdot 10^6$$

$$md3 := 8.226 \cdot 10^{-6}$$

$$Ddep3 := 0.006606$$

$$\tau_{co3} := 0.512$$

$$h_3 := 0.002$$

$$fd_4 := 17025$$

$$x_4 := \frac{qt_{r3}}{md3 \cdot hfg} \left[1 - \frac{3.14 \cdot Ddep3^2}{4 \cdot v3} \cdot \left(\frac{fd_0 + 2fd_1 + 2fd_2 + 2fd_3 + fd_4}{2} \right) \cdot h_3 \right] \cdot \left[1 - \tau_{co3} \cdot Ddep3 \cdot \left(\frac{fd_0 + 2fd_1 + 2fd_2 + 2fd_3 + fd_4}{2} \right) \cdot h_3 \right] - fd_4$$

$$x_4 \rightarrow 7452.069218283646402$$

$$v_4 := 0.31$$

$$qt_{r4} := 1.358 \cdot 10^6$$

$$md_4 := 5.655 \cdot 10^{-6}$$

$$Ddep_4 := 0.005726$$

$$\tau_{co4} := 7.385 \times 10^{-2}$$

$$h_4 := 0.002$$

$$fd_5 := 44932$$

$$x_5 := \frac{qt_{r4}}{md_4 \cdot hfg} \left[1 - \frac{3.14 \cdot Ddep_4^2}{4 \cdot v_4} \left(\frac{fd_0 + 2fd_1 + 2fd_2 + 2fd_3 + 2fd_4 + fd_5}{2} \right) \cdot h_4 \right] \left[1 - \tau_{co4} \cdot Ddep_4 \left[\left(\frac{fd_0 + 2fd_1 + 2fd_2 + 2fd_3 + 2fd_4 + fd_5}{2} \right) \cdot h_4 \right] \right] - fd_5$$

$$x_5 \rightarrow 48069.950249540873717$$

$$v_5 := 0.525$$

$$qt_{r5} := 1.358 \cdot 10^6$$

$$md_5 := 5.975 \cdot 10^{-6}$$

$$Ddep_5 := 0.005726$$

$$\tau_{co5} := 0.451$$

$$h_4 := 0.002$$

$$fd_5 := 44932$$

$$x_5 := \frac{qt_{r4}}{md_4 \cdot hfg} \left[1 - \frac{3.14 \cdot Ddep_4^2}{4 \cdot v_4} \left(\frac{fd_0 + 2fd_1 + 2fd_2 + 2fd_3 + 2fd_4 + fd_5}{2} \right) \cdot h_4 \right] \left[1 - \tau_{co4} \cdot Ddep_4 \left[\left(\frac{fd_0 + 2fd_1 + 2fd_2 + 2fd_3 + 2fd_4 + fd_5}{2} \right) \cdot h_4 \right] \right] - fd_5$$

$$x_5 \rightarrow 48069.950249540873717$$

$$v_5 := 0.525$$

$$qt_{r5} := 1.358 \cdot 10^6$$

$$md_5 := 5.975 \cdot 10^{-6}$$

$$Ddep_5 := 0.005726$$

$$\tau_{co5} := 0.451$$

$$h_5 := 0.002$$

$$fd_6 := 14714$$

$$x_6 := \frac{qt_{r5}}{md_5 \cdot hfg} \left[1 - \frac{3.14 \cdot Ddep_5^2}{4 \cdot v_5} \left(\frac{fd_0 + 2fd_1 + 2fd_2 + 2fd_3 + 2fd_4 + 2fd_5 + fd_6}{2} \right) \cdot h_5 \right] \left[1 - \tau_{co5} \cdot Ddep_5 \left[\left(\frac{fd_0 + 2fd_1 + 2fd_2 + 2fd_3 + 2fd_4 + 2fd_5 + fd_6}{2} \right) \cdot h_5 \right] \right] - fd_6$$

$$x_6 \rightarrow 4467.860832708919228$$

$$\begin{aligned}
v6 &:= 0.535 & \overline{q_{r6}} &:= 1.41 \cdot 10^6 \\
md6 &:= 5.173 \cdot 10^{-6} & Ddep6 &:= 0.00505 & \overline{\tau_{co6}} &:= 0.384 \\
h_6 &:= 0.002 & & & & \\
fl_7 &:= 12791 & & & & \\
x_7 &:= \frac{q_{r6}}{md6 \cdot h_6} \left[1 - \frac{3.14 \cdot Ddep6^2}{4 \cdot v6} \left(\frac{fl_0 + 2fl_1 + 2fl_2 + 2fl_3 + 2fl_4 + 2fl_5 + 2fl_6 + fl_7}{2} \right) h_6 \right] \left[1 - \tau_{co6} \cdot Ddep6 \left(\frac{fl_0 + 2fl_1 + 2fl_2 + 2fl_3 + 2fl_4 + 2fl_5 + 2fl_6 + fl_7}{2} \right) h_6 \right] - fl_7 \\
x_7 &\rightarrow 27858.046835149806790
\end{aligned}$$

$$\begin{aligned}
v7 &:= 0.554 & \overline{q_{r7}} &:= 1.46 \cdot 10^6 \\
md7 &:= 4.492 \cdot 10^{-6} & Ddep7 &:= 0.004457 & \overline{\tau_{co7}} &:= 0.315 \\
h_7 &:= 0.002 & & & & \\
fl_8 &:= 11176 & & & & \\
x_8 &:= \frac{q_{r7}}{md7 \cdot h_7} \left[1 - \frac{3.14 \cdot Ddep7^2}{4 \cdot v7} \left(\frac{fl_0 + 2fl_1 + 2fl_2 + 2fl_3 + 2fl_4 + 2fl_5 + 2fl_6 + 2fl_7 + fl_8}{2} \right) h_7 \right] \left[1 - \tau_{co7} \cdot Ddep7 \left(\frac{fl_0 + 2fl_1 + 2fl_2 + 2fl_3 + 2fl_4 + 2fl_5 + 2fl_6 + 2fl_7 + fl_8}{2} \right) h_7 \right] - fl_8 \\
x_8 &\rightarrow 58536.095358659821728
\end{aligned}$$

$$\begin{aligned}
v8 &:= 0.572 & \overline{q_{r8}} &:= 1.52 \cdot 10^6 \\
md8 &:= 4.092 \cdot 10^{-6} & Ddep8 &:= 0.004008 & \overline{\tau_{co8}} &:= 0.259 \\
h_8 &:= 0.002 & & & & \\
fl_9 &:= 9808 & & & & \\
x_9 &:= \frac{q_{r8}}{md8 \cdot h_8} \left[1 - \frac{3.14 \cdot Ddep8^2}{4 \cdot v8} \left(\frac{fl_0 + 2fl_1 + 2fl_2 + 2fl_3 + 2fl_4 + 2fl_5 + 2fl_6 + 2fl_7 + 2fl_8 + fl_9}{2} \right) h_8 \right] \left[1 - \tau_{co8} \cdot Ddep8 \left(\frac{fl_0 + 2fl_1 + 2fl_2 + 2fl_3 + 2fl_4 + 2fl_5 + 2fl_6 + 2fl_7 + 2fl_8 + fl_9}{2} \right) h_8 \right] - fl_9 \\
x_9 &\rightarrow 88162.434684947027270
\end{aligned}$$

$$\begin{aligned}
v9 &:= 0.6 & \overline{q_{r9}} &:= 1.57 \cdot 10^6 \\
md9 &:= 4.029 \cdot 10^{-6} & Ddep9 &:= 0.003595 & \overline{\tau_{co9}} &:= 0.21 \\
h_9 &:= 0.002 & & & & \\
fl_{10} &:= 8641 & & & & \\
x_{10} &:= \frac{q_{r9}}{md9 \cdot h_9} \left[1 - \frac{3.14 \cdot Ddep9^2}{4 \cdot v9} \left(\frac{fl_0 + 2fl_1 + 2fl_2 + 2fl_3 + 2fl_4 + 2fl_5 + 2fl_6 + 2fl_7 + 2fl_8 + 2fl_9 + fl_{10}}{2} \right) h_9 \right] \left[1 - \tau_{co9} \cdot Ddep9 \left(\frac{fl_0 + 2fl_1 + 2fl_2 + 2fl_3 + 2fl_4 + 2fl_5 + 2fl_6 + 2fl_7 + 2fl_8 + 2fl_9 + fl_{10}}{2} \right) h_9 \right] - fl_{10} \\
x_{10} &\rightarrow 110591.38107356477806
\end{aligned}$$